Cellulose Nanofibrils reinforced Castor oil based Polyurethane Shape Memory Nanocomposites for Medical Applications

File no. 42-402/2013 (SR)/ March 31, 2013

Final Completion Report

Submitted to

Principal Investigator: Prof. Anupama Sharma
SSB University Institute of Chemical Engineering and Technology,
Panjab University, Chandigarh

Final Completion Report

1. Project report — Final

2. UGC Reference No. — F. **42-402/2013 (SR)/ March 31, 2013**

3. Period of report: — **from April 2013 to March 31, 2017**

4. Title of research project — **Cellulose Nanofibrils reinforced Castor oil based Polyurethane Shape Memory Nanocomposites for Medical Applications**

5. (a) Name of the Principal Investigator — **Prof. Anupama Sharma**

(b) Deptt. — **SSB University Institute of Chemical Engineering and Technology, Panjab University, Chandigarh India-160014**

(c) College where work has progressed — **SSBUICET, Panjab University**

6. Effective date of starting of the project — **April 2013**

7. Grant approved and expenditure incurred during the period of the report:

a. Total amount approved — **Rs. 14,27,217/-**

b. Total expenditure — **Rs. 13,57,663/-**

c. Report of the work done: (Please attach a separate sheet) **Attached as Annexure 1**

i. Brief objective of the project

1. **Develop fundamental understanding of routes of synthesis of segmental polyurethanes from castor oil**
2. **Synthesizing biodegradable segmental polyurethanes with shape memory properties**

   Synthesize a series of biodegradable segmental polyurethane elastomers based on castor oil with tunable glass transition temperature and degradation rates and potential applications in biomedical implants.

Segmental Polyurethanes will also be synthesized using some largely available polyol (Poly(ε-caprolactone) diol) in order to compare the properties of Castor oil based and commercial polyol based polyurethanes.

These new polyurethanes will be characterized by FTIR, NMR, DSC, XRD, uniaxial tensile tests and DMA to evaluate chemical, physical, mechanical and structural properties. The required glass transition temperature (Tg) for these polymers is between 35-53^{o}C which is in the vicinity of body temperature and recovery ratio more than 95%.

3. **Study interfacial interactions between shape memory polyurethanes and nanocellulose fibers to achieve good dispersion and for reinforcement of polyurethanes. Study mechanism of polymer formation in the presence of nanocellulose fibers.**
4. **Reinforcing biodegradable polyurethanes with cellulose nanofibrils to improve the shape memory behavior and thermal properties**

   Mixing of cellulose nanofibrils in polyurethane matrix will be done during prepolymer stage by high shear mixing in an internal mixer so that the fillers are well dispersed in the matrix. The uniform distribution of the particles will be established using XRD (SAXS and WAXS) and microscopy (SEM and TEM). The improvement in shape memory will also be evaluated in terms of creep and thermal response (mechanical tests). Rheological behavior (plate-plate and cone-plate rheometers) of the materials will be evaluated to better understand the structure and processability of the nanocomposites.

5. **Establishing the biodegradability and biocompatibility of these biodegradable shape memory polyurethane composites by in vitro studies**

To undertake in-vitro (cell culture) studies for the new biomaterials; thus generating a strong biocompatibility knowledge base

6. **Comparison of developed biodegradable shape memory polyurethane composite with existing material used for biomedical implants**

ii. Work done so far and results achieved and publications, if any, resulting from the work

(Give details of the papers and names of the journals in which it has been published or accepted for publication)

Details of work done is given in Annexure 1

1. Gaurav Verma, Anupama Kaushik, Anup Ghosh, Nano-interfaces between clay platelets and polyurethane hard segments in spray coated automotive nanocomposites, Progress in Organic Coating, Vol 99, 2016; 282-294 (Impact Factor 6.2)
2. Mandeep Singh, Anupama Kaushik, Dheeraj Ahuja, Surface Functionalization of Nanofibrillated Cellulose Extracted From Wheat Straw: Effect of Process Parameters, Carbohydrate Polymers 150: 48-56, 2016 (Impact Factor 11.2)

3. Anupama Kaushik, R Kaur, Thermoplastic starch nanocomposites reinforced with cellulose nanocrystals: effect of plasticizer on properties, Composite Interfaces 23 (7), 701-717, 2016 (Impact Factor 2.6)
4. Sheetal Monga, A Kaushik, B Gupta, Optimization of Process Parameters for Controlled Ring Opening Polymerization of Lactide to Produce Poly (L-Lactide) Diols as Precursor for Polyurethanes, Polymer-Plastics Technology and Engineering, 55(17), 2016 (Impact Factor 2.7)
5. Sheetal Monga, A Kaushik, B Gupta, Synthesis of L-Lactide Based Segmented Polyurethanes, Polymer-Plastics Technology and Engineering, 55 (9), 943-948, 2016 (Impact Factor 2.7)
6. Sapana Kumari, Ghanshyam S. Chauhan, Sheetal Monga, Anupama Kaushik and Jou-Hyeon Ahn, New lignin-based polyurethane foam for wastewater treatment, RSC Advances, 6, 77768-76, 2016 (Impact Factor 3.9)
7. Anupama Kaushik, Jatinder Kumra, Morphology, thermal and barrier properties of green nanocomposites based on TPS and cellulose nanocrystals, Journal of Elastomers and Plastics, (3): 284-299, 2014 (Impact Factor 1.2)
8. Anupama Kaushik, Alka Garg, Castor Oil Based Polyurethane Nanocomposites with Cellulose Nanocrystallites Fillers, Advanced Materials Research 856, 309-313, 2014

iii. Has the progress been according to original plan of work and towards achieving the objective. if not, state reasons

Yes, it was according to the original plan.

iv. Please enclose a summary of the findings of the study. One bound copy of the final report of work done may also be sent to the concerned Regional Office of the UGC.
Attaches as Annexure 1

v. Any other information **Nil**

SIGNATURE OF THE PRINCIPAL INVESTIGATOR

PRINCIPAL (Seal)

Annexure 1

Summary of the findings

INTRODUCTION

Polyurethanes are the class of polymers that contain urethane groups in their backbone structures (Figure 1) [1]. These are generally obtained by condensation reaction of di-isocyanates and polyol compounds and consist of a two-phase structure: a hard segment and soft segment.

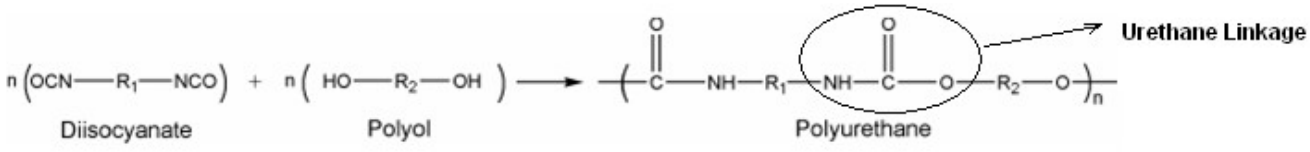

Illustration 1. Polyurethane synthesis process

Polyurethane structure is unique having segmented structure with semicrystalline and rigid 'hard segment'enriched domains that are dispersed in a matrix of crystallizable soft segments (figure 1) [2-4]. *Hard segment* clusters are generally of dimensions <1 μm formed by the phase separation process and these clusters have higher glass transition temperature or melting temperaturevalues than the ones of soft segment and act as multifunctional physical net-points. The amorphous matrix, with its low glass transition temperature, is called *soft segment*. The hard segments mainly consist of the diisocyanate; either aromatic or aliphatic and the chain extender while the soft segments are sequence of macroglycol moieties which are used to maintain the temporary shape [5]. The thermodynamically incompatible hard and soft segments are combined end-to-end through covalent urethane bonds making polyurethanes as multiblock copolymers. Soft segments are generally comprised of polyester, polycarbonate, or polyether macroglycols. Chain extenders may be low molecular weight diols or diamines used to further couple these pre-polymers [6, 7]. The differences in polarity between the hard and soft segments render these regions incompatible and the result is that they do not mix on a molecular level, producing a microphase separated structure.

Segmented polyurethanes are stimuli-responsive materials i.e. their temporary deformation can be eliminated or their permanent shape can be recovered at a critical stimulus value, also known

as shape memory materials having capability of changing their shape upon application of an external stimulus. This stimulus can be heat, stress, magnetic fields, electric fields, pH values, UV light, and even water [8, 9]. The segmented polymer is conventionally processed for its *permanent shape* followed by deformation to the intended *temporary shape*. Finally, the permanent shape is restored through the recovery process. If the change in shape is caused by a change in temperature is called a thermally induced shape memory effect or thermoresponsive shape memory behaviour. Large numbers of chemical and structural factors play important roles in microphase separation and thus response to the stimulus. These factors include Chemical structure, number average molecular weight and molecular weight distribution of soft segments, chemical structure and symmetry of the diisocyanate compound, chemical structure of the chain extender, average chain length and length distribution of hard segments, hard/soft segment ratio in the copolymer [10, 11], crystallizability of hard and soft segments [12], extent of competitive hydrogen bonding between hard–hard and hard–soft segments, inherent solubility between hard and soft segments [13, 14], method/polymerization procedure used during the synthesis and the nature of the interfacial region between the soft segment matrix and hard segment domains [15]. By adjusting the molecular weight of the macrodiol moiety and the molar ratio of the soft-to-hard segment, the shape recovery temperature of polyurethane can be successfully adjusted to 37-40 ^{0}C.

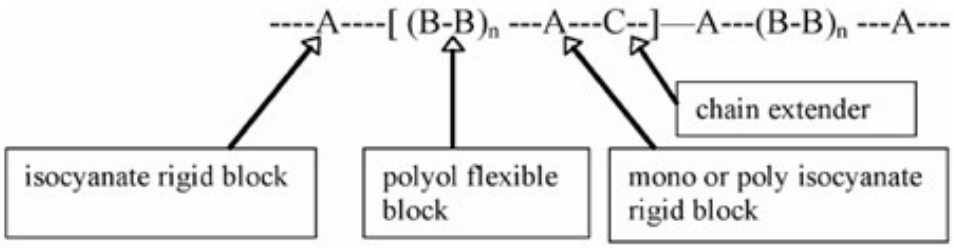

Figure 1: Polyurethane structure showing hard segment dispersed in soft crystallizable phase [16]

Segmented polyurethanes are extensively used polymers in biomedical applications because of their durability, elasticity, fatigue resistance, compliance, bio-stability, biodegradability and tailorable backbone structure from a wide range of available precursors. A thermo-responsive segmented polyurethane get deformed at a temperature above transition temperature (which can be glass transition or melting temperature) and suddenly cooled to a temperature below *transition temperature*, the deformed shape becomes frozen. When it is heated above *transition temperature*, the polymer recovers its original shape [17]. Because of the ability of thermo-responsive segmental polyurethanes to recover shape at critical temperature large bulky devices could thus potentially be introduced into the body in a compressed temporary shape by means of minimally invasive surgery and then expand to their permanent shape to fit as required [18]. This property is very useful in cardiovascular stents and sutures. Conventionally used alloys, like Nitinol, for cardiovascular stents exhibit outstanding features, such as small size and high strength, but show disadvantages like high manufacturing cost, limited recoverable deformation and complicated surgery process [19]. Moreover, metal stents being rigid compared to the surrounding vessel, cause abrupt change of compliance in the junction of the host artery and the stent, lead to an abnormal stress concentration which will initiate an adaptive response in the vascular tissue [20]. Therefore, shape memory polymers have come to the focal point over the last decade as proposed materials for stents [21, 22]. Potential Biodegradability is an additional functionality of shape memory polymers that can prevent a second surgery for device explanation. With good biodegradability, they would neither stay in the human body for a very long time nor require a second surgery to be removed from the human body. With shape-memory property and a recovery near body temperature, the handling of the corresponding medical devices would be easy.

Shape Memory Polyurethanes

Shape-memory materials, including shape-memory alloys, ceramics, hydrogels, and shape memory polymers, have found wide applications in various fields, such as sensors, transducers, actuators and medical implants.In order to qualify as a shape memory material it should possess shape memory effects. Shape memory effects are those in which a material can be deformed and

fixed into temporary shape and can return to original permanent shape under cyclic conditions of loading/unloading and thermal swings. Shape memory effect caused by thermal stimuli are more common as in this the recovery takes place with respect to a certain critical temperature. The first shape memory effect induced smart material was first discovered by Chang and Read in 1932 (Chang and Read 1951). Even though shape memory materials based on alloys possess excellent mechanical properties and have found a ample of technical applications, they have been replaced by ceramics and polymers because of the high manufacturing cost, narrow recoverable deformation and appreciable toxicity.

A great deal of attention is being focused towards shape memory polymers for the development of smart materials because of their varying mechanical properties and higher degree of deformation offered along with low cost, light weight and easy processibility. Further, an added advantage offered by polymers is that they may be resistant to chemical attack, non toxic, biocompatible and can be made biodegradable. Different kinds of shape memory polymers have been reported and developed after the development of “Polynorbornene” the first shape memory polymer developed by CDF Chimie company (France) in 1984.

Shape memory polymers are those that can adopt a new temporary shape and revert back to original shape under the influence of an external stimulus. In these cases, the shape memory performance not only depends on the molecular structure, but also on the mode of deformation and the programming of the stimulus application process. Obtaining a new shape is dependent on both the nature of stimulus and the mode of deformation. On the other hand, regaining the original shape is always dictated by how the stimulus is applied. The stimulus here refers to heat, light, chemical reaction, electricity, and magnetism. This may be applied independently, e.g. only heat or light, or in complex combinations (Beloshenko, Varyukhin, and Voznyak 2005). The process is shown in figure 2.

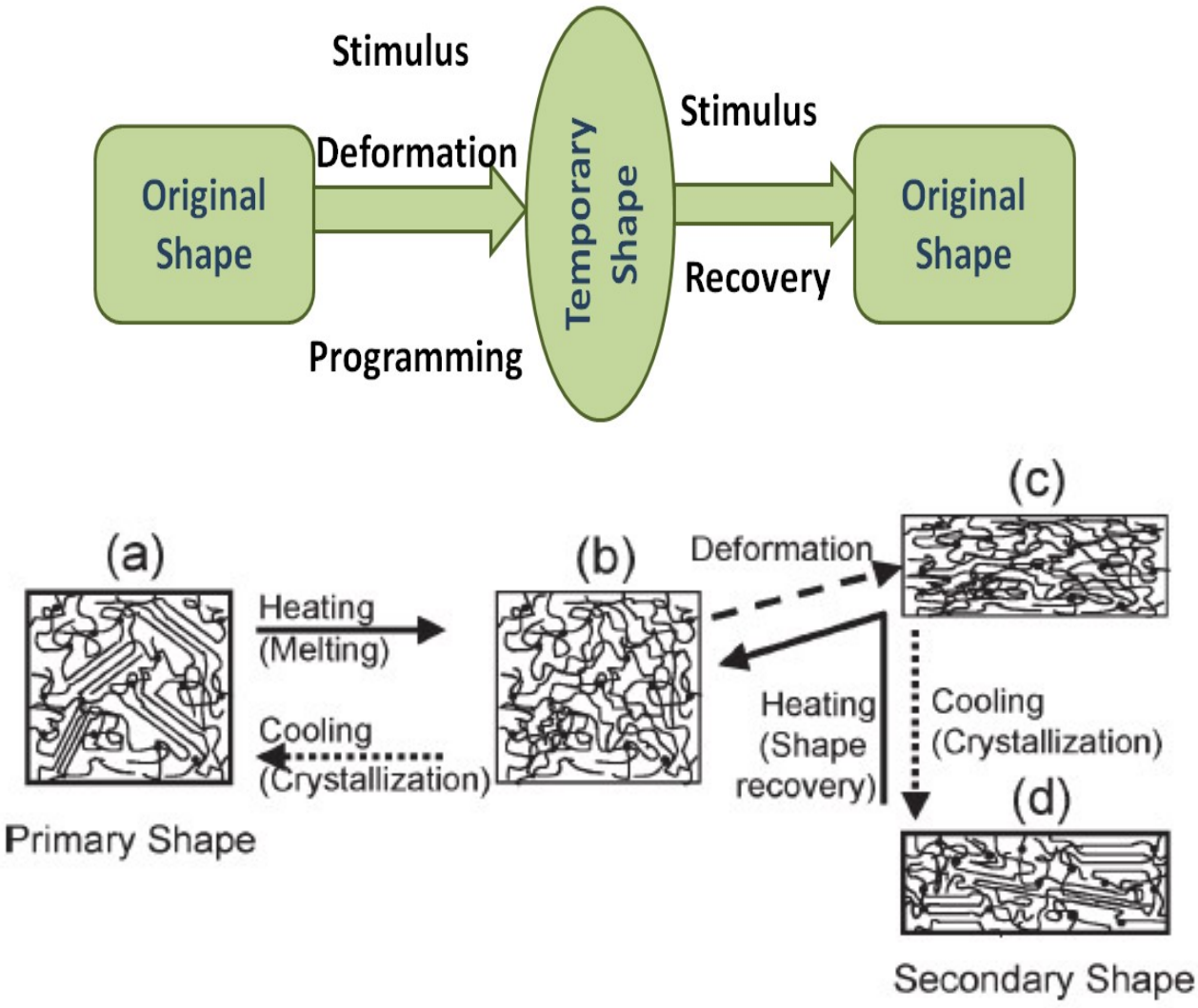

Figure 2: Process of Shape memory polymer

The material having shape memory effects should have atleast two independent or synergitically working phases, among which one phase should be reversible while the other shall be in the active range of the stimulus. Therfore, shape memory effects are accomplished during a transition stage i.e. where the reversible phase undergoes changes from temporary to permanent shape and a permanent shape can be acheieved by polymer chains on deformation during this transition state. However, it should be noted that on attainment of temporary shape stimulus should be taken away rapidly for achieving the desired form as if the stimulus takes longer time to return to the reference state, polymer chains can relax leading to the poorer shape memory performance. For example, low thermal conductivity of polymers in case of thermal gradients

leads to the slower cooling and heating where the elastically stored energy plays an important role in shape memory performances as the polymer chains store an important part of energy during deformation which is used to recover the original shape upon the application of the stimulus. The heat dissipation is another important factor. Further, an important factor that accounts for shape loss is heat dissipation during deformation and recovery in a single shape memory cycle. However, these types of loss depends on the rheological properties of the materials. Stretching/deformation temperature and extent of deformation/strain level along with rheological properties of polymer are the most critical conditions used to determine the recovery force and extent of shape useful in deciding suitable applications of the shape memory polymers. For example magnitude of recovery stress developed by polymers needs to be evaluated carefully while replacing shape memory alloys with shape memory polyurethanes.

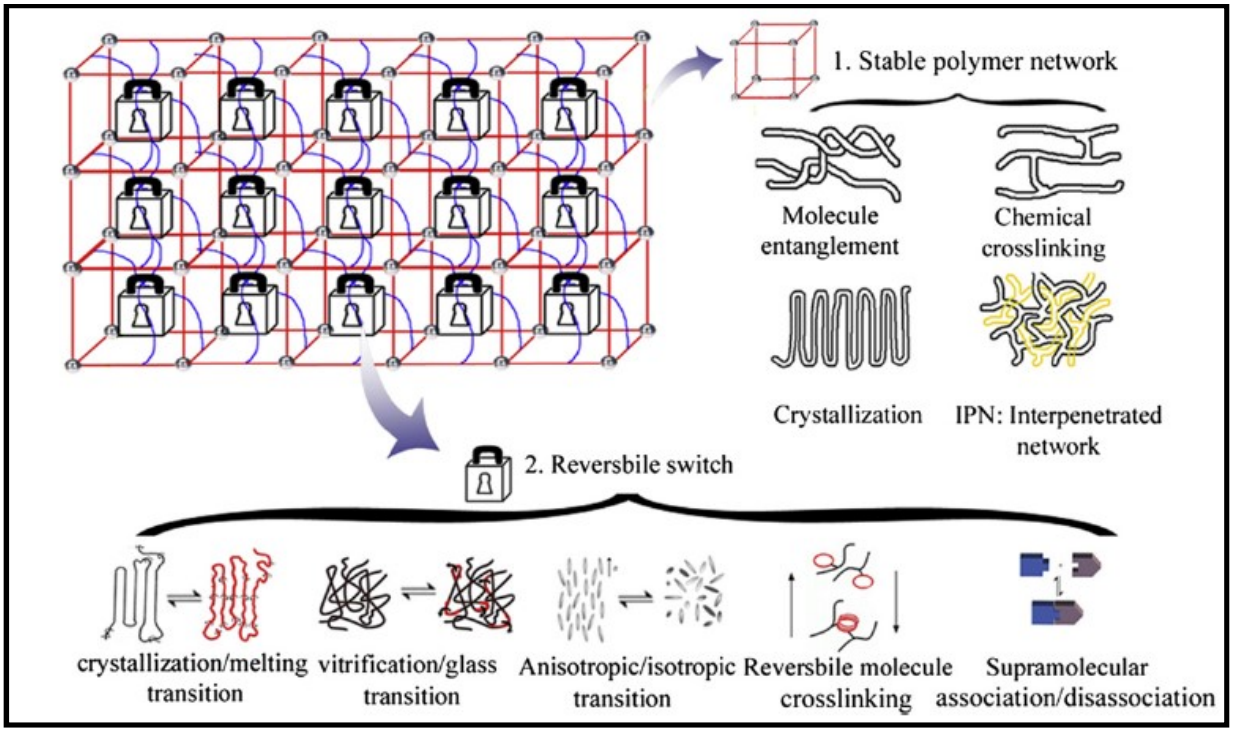

Figure 3. Molecular Structures of Polymers which gives shape memory effect

Shape memory effects are possessed by a variety of polymers such as theroplastics based on polyethylene and polystyrene copolymers and thermosets based on polyurethanes and polyepoxides. Polyurethanes with shape memory effects have become the most polpular among these polymers because of their unique properties such as high shape recoverability with a

maximum recoverable strain of >400%, wide range of shape recovery temperature from -30 to 70 °C, good processing ability and excellent biocompatibility. Some other characteristics of the shape memory polyurethanes (SMPU's) that make them prominent material as compared to other shape memory polymers are biodegradability, vast possibilities for synthesis and production from readily available commercial raw materials at affordable cost. Figure 3 elaborates the molecular structure of polymers which contributes to shape memory polymers

Shape memory polyurethanes (SMPU's) are one of the most popular groups of biomaterials applied for biomedical applications which may be attributed to their segmented block copolymeric character that endows them for a wide range of versatility in terms of tailoring their physical properties, blood and tissue compatibility. They are usually thermo-responsive, i.e., their temporary deformation can be eliminated and their permanent shape can be restored at a critical temperature (referred as transition temperature or switching temperature), which can be either the glass transition (T_g) or the melting temperature (T_m) of the materials. Singhal et al synthesiszed polyurethanes foams with shape memory effecs for embolic biomedical applications.

The usage of polyurethanes as SMPs suffers from several challengessuch as thermal degradation, hydrolytic degradation, low stiffness and a dimensional instability after processing leading to the insufficient recovery stress, long recovery time and in some cases low value of shape fixity.The low stiffness of SMPUs results in a relatively small recovery force under constraint (actuation force) compared to alternative active actuation materials or schemes. Thus, in some applications, SMPUs may not generate sufficient recovery force to be viable. This drawback can be overcome by use of high modulud organic or inorganic fillers such as glass fibers, ceramic filler, poly (D,L-lactide), silsequioxanes, celite, carbon nanotubes, carbon nanofibers, cellulose nanofibers and nanoclay particles to the polymer matrix.

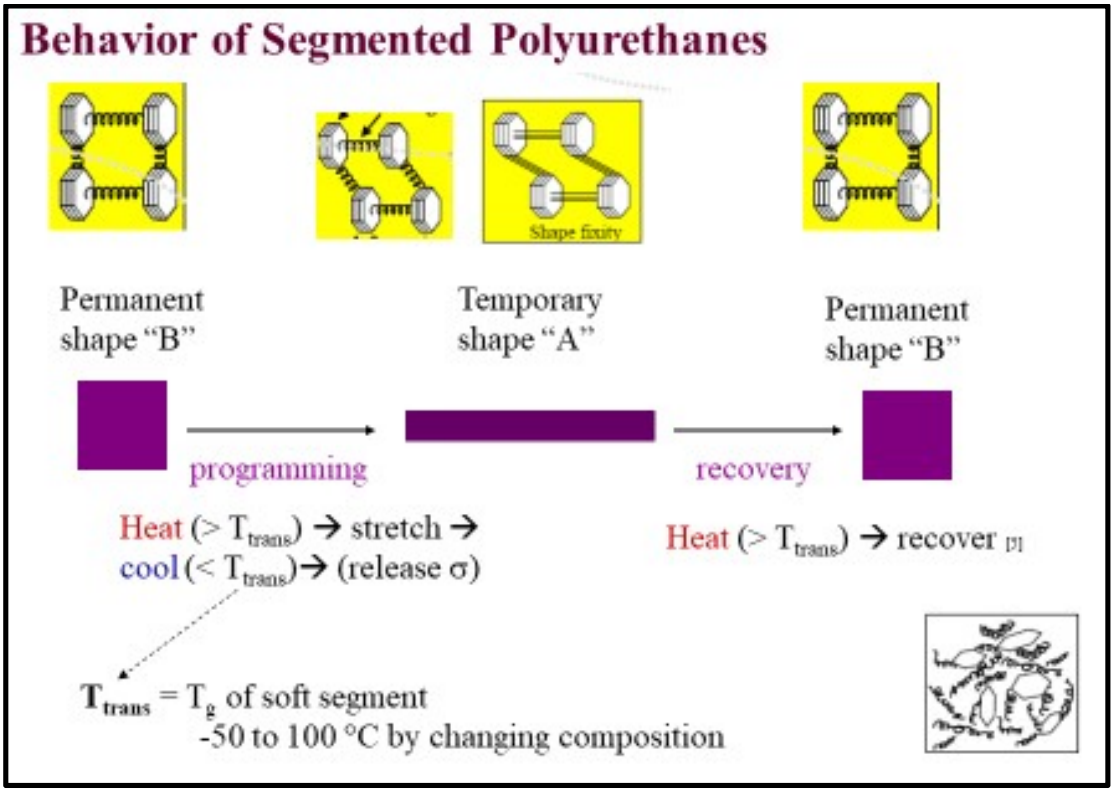

Figure 3. Behavior of shape memory polymers

Although shape memory polyurethanes have found extensive applications in biomedical filed, but limitations like relatively low recovery stress, which is usually 1–3 MPa compared to 0.5–1 GPa for shape memory metal alloys [23-25], prevent their widespread applications. The relatively low recovery stress becomes a limiting factor in many applications especially in cases where a large resisting stress during shape recovery is required. One of the best avenue to improve mechanical properties and to add multiple functionalities to the shape memory polyurethanes is to mix with high modulus fillers [26] like carbon nanotubes, clays and cellulose nanofibrils. However, it has been observed that there is a trade-off between modulus enhancement and recoverable strain ratio due to the effects of filler particle size, much higher stiffness of fillers, or potential infringement with the polymer networks especially at high filler loadings. These issues can be alleviated by reducing the size of filler and the loading content which reduces the soft segment crystallinity. The reduction of soft segment crystallinity causes an imbalance of Helmholtz free energy, which in turn, caused a reduction of SM properties [27]. Chopped and continuous, especially continuous, nanofibres are superior to nano-sized particles to improve the mechanical strength of shape memory polymers [28]. The use of cellulose

nanofibers in segmented polyurethane matrix may be advantageous over traditional fillers because of the strong interactions that are formed between adjacent nanofibrils due to the surface hydroxyl groups, high stiffness of nanofibrils that improves the stiffness and strength of polymer matrix, increased thermal stability [29, 30] and decreased thermal expansion [31] of the resulting nanocomposite. At the same time, if a transparent matrix is used, it is possible to maintain most of the transparency due to the fine scale of the fibrils, even at fiber contents as high as 70% with an added advantage of low cost and renewability [32-34]. Well established procedure will be used to isolate cellulose nanofibrils from biomass using steam explosion method to get fibers of diameter range 4-50 nm and length 200-250 nm [35].

2. EXPERIMENTAL

2.1. Fourier Transform Infrared Spectroscopy (FTIR)

The chemical structure of lignin obtained at various pH values and alkali concentrations, lignopolyol, lignopolyol based polyurethanes, cellulose microfibers (CMF), cellulose nanofibers (CNF) and polyurethane/cellulose nanofibers(PU-CNF) based nanocomposites (NPU) film was characterized by Fourier Transform Infrared Spectroscopy (FTIR) in Perkin Elmer model RZX-FTIR spectrophotometer (figure 5) using KBr technology i.e. by making pellets with KBr. FTIR spectra were recorded in a spectral range of 4000–450 cm^{-1} with a resolution of 2 cm^{-1} with two scans for each sample.

The relative level of cross linking in lignin can be calculated by absorbance ratios of peaks at1500 and 1600 cm^{-1} [130]. The higher is the ratio more condensed and cross linked is the lignin.

S/G ratio for lignin was calculated by the estimating the intensities of the bands around 1327 cm^{-1} (S units) and 1271 cm^{-1} (G units), after resolution enhancement (subtraction of × 1000 second derivative), moving-average smoothing (× 100) and baseline correction between valleys ca. 1401 and 1172 cm^{-1}[131].

2.2. ^{H}NMR

The chemical structure of castor oil was studied using Nuclear Magnetic Resonance (NMR) spectrometry.^{H}NMR spectra were recorded on a Bruker AV II 400 MHz spectrophotometer(figure 5). The ^{H}NMR spectrum was obtained at 400 MHz using 10 mg acid-insoluble lignin and castor oil/ polyol in 0.5 mL of dimethylsulfoxide-d6 (DMSO-d6). The chemical shifts of ^{H}NMR spectrum were calibrated with reference to DMSO, used as an internal standard, at 2.49 ppm. The acquisition time was 2.7 s, and relaxation time was 1.0 s.

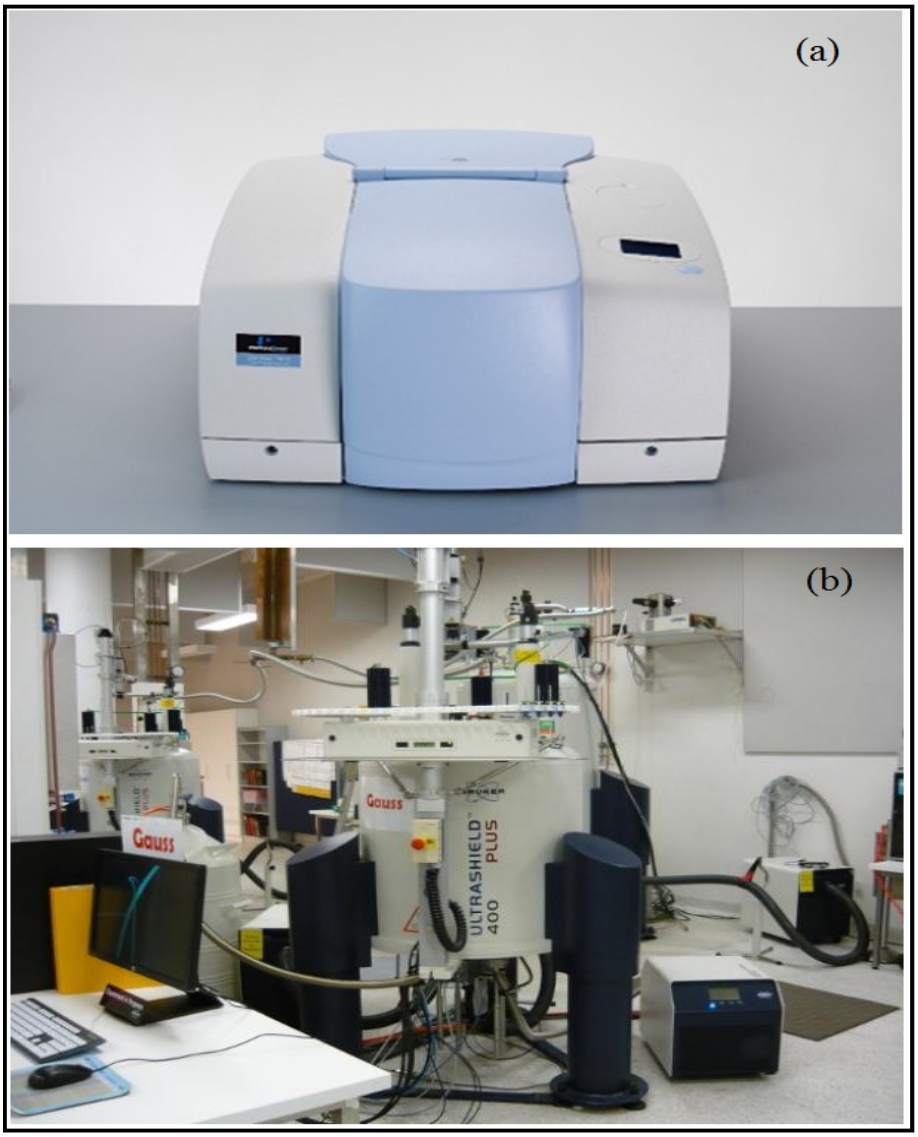

Figure 5: Photographic images of (a) Perkin elmer model RZX-FTIR spectrophotometer; (b) Bruker AV II 400 MHz NMR spectrophotometer

2.1. UV-Vis Spectrophotometer

UV-vis spectrophotometer is used to study the chemical structure and purity of lignin. For this a Shimadzu spectrophotometer model UV-1200 (figure 6) was used. Prior to the analysis, 5mg of sample was dissolved into 10 ml 90% (v/v) dioxane-water aliquot. 1 ml of aliquot was further diluted into 25 ml by using 50% (v/v) dioxane-water. The absorbance was measured for the range of 200 nm to 400 nm [189].

2.2. Elemental Analysis (C, H, N AND O)

Elemental analysis (C, H, and N) was performed on lignin, castor oil/ polyol, CMF and CNF samples using Thermo Finnigan Elemental Analyzer (figure 6) for CHN and the Oxygen content were calculated by difference. Prior to analysis samples were vacuum dried at 100^0C overnight, to remove traces of moisture.

Figure 6: Photographic images of (a) Shimadzu spectrophotometer model UV-1200; (b) Thermo Finnigan Elemental Analyzer

2.3. Estimation of Hydroxyl Value

The hydroxyl value is defined as the number of milligrams of potassium hydroxide equivalent to the hydroxyl content of one gram of the sample.

In spite of the numerous techniques that have been reported in the literature [374–377] for the determination of hydroxyl content, most widely used method is Phthalation and Acetylation. The

second method involves actylating the sample with acetic anhydride in pyridine (as solvent) and excess anhydride is estimated by titrating with alcoholic potassium hydroxide after it has been decomposed with water to generate acetic acid.

Different ratios of acetic anhydride in pyridine have been recommended. The ratios are important since they affect reaction time and therefore quantitative results. The total number of hydroxyl groups that can be quantitavely acetylated with a given volume of reagent and the ratios also have some effect on quantitative accuracy. The type and amounts of hydroxyl groups, such as primary and secondary hydroxyl groups also influence accuracy since they do not acetylate with same ease. Generally 1:3 ratio of acetic anhydride to pyridine is used.

The proposed mechanism for the catalyzed acetylation in pyridine is:

$$C_6H_5NH^+ + Ac_2O \leftrightarrow (C_5H_5NAc)^+ + AcOH$$

The pyridine acetylium ion then reacts with the alcohol to form ester and regenerate the pyridinium ion.

$$(C_5H_5Nac)^+ + ROH \rightarrow ROAc + C_5H_5NH^+$$

For estimation, a known quantity of dried sample was taken in an Erlenmeyer flask 10ml of acetylating reagent (containing 1:3 ratios of acetic anhydride and pyridine) was added, along with some pieces of non-porous (Carborundum) boiling chips or pumic stone. An air condenser was fixed vertically in the neck of the flask and heated to slow boil in water bath for one hour. Then the mixture was allowed to cool a bit, and 5 ml distilled water was added for decomposition of excess acetic anhydride. It was finally heated for 10-15 minutes more to ensure complete decomposition of acetic anhydride. On cooling, sides of the condenser were washed with little more water and the contents titrated as a whole against 1N standard alcoholic potassium hydroxide solution using phenolphthalein indicator. A blank experiment was also run simultaneously under same conditions. The hydroxyl value was calculated as:

$$OH_{No.} = \frac{56.1 \times NNaoH \times (mlblank - mlsample)}{weightofsample} \times 100 \qquad (2.3)$$

2.4. MALDI-Time-of-Flight Mass Spectrometry(MALDI-ToF)

Mass spectra of lignin and castor oil/ polyol was recorded on an Autoflex III MALDI time-of-flight mass spectrometer of BrukerDaltonics(figure 7) operating in the reflector and linear

positive or negative mode using a pulsed nitrogen laser (l337 nm, pulse rate of 10 Hz) as the ionization source. The analyzer was used at an acceleration voltage of ±20 kV. Laser light was focused on the sample using a 5.2 kV lens. A pulsed ion extraction was optimized to 200 ns. Lignin samples were dissolved in dimethylformamide (DMF) with a concentration of 10 mg/mL and DHB (2, 5-dihydroxybenzoic acid) used as matrix material was also dissolved in DMF. Overall, 2 µL of lignin and 2 µL of matrix were mixed together in a plate. 1 µL of sample was deposited on each well of the stainless steel multiple sample container and permitted to dry in air. The sample was completely dried in air before introducing in the mass spectrometer. A peptide calibration set was used as an external standard. A total of 300 shots were provided. Each sample preparation and analysis was duplicated.

Weight average molecular weight, number average molecular weight and polydispersity index of the EL and ML was calculated using equation 2.4 to 2.6 [378]:

$$Mn = \frac{\sum(NiMi)}{\sum Ni} \quad (2.4)$$

$$Mw = \frac{\sum(NiMi^2)}{\sum(NiMi)} \quad (2.5)$$

$$Pi = \frac{Mw}{Mn} \quad (2.6)$$

Where, M_n= Number average molecular weight.

M_w= Weight average molecular weight

N_i= Signal intensity of the i^{th} oligomers in the distribution.

M_i= Molecular weight of i^{th} oligomers in the distribution

Pi = Polydispersity Index

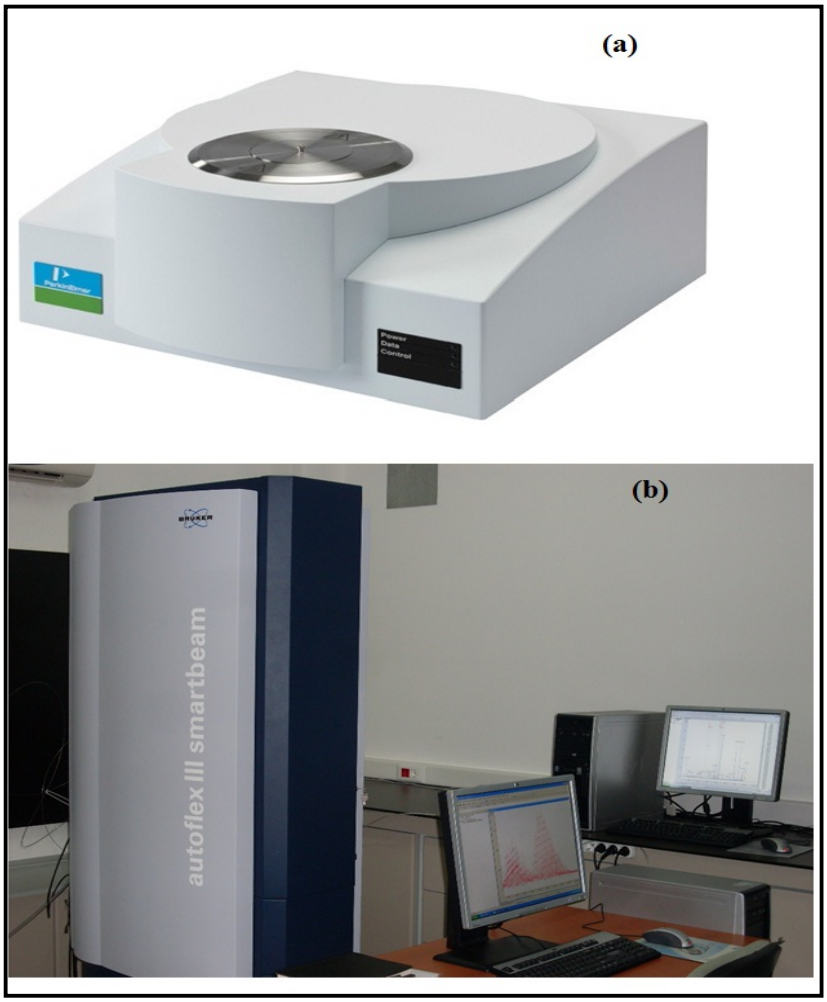

Figure 7: Photographic images of (a) Thermo gravimetric Analyzer (TGA) of Perkin Elmer STA-6000; (b) Autoflex III MALDI time-of-flight mass spectrometer of BrukerDaltonics

2.5. Thermal Gravimetric Analysis (TGA)

Thermal stability of lignin,castor oil/ polyol, castor oil/ polyol based polyurethanes, CMF,CNF and PU/CNF nanocomposites films was studied using a Thermo gravimetric Analyzer (TGA) of type Perkin Elmer STA-6000 (figure 7). Approximately 10 mg of sample was weighed in an aluminum pan and placed in thermo gravimetric analyzer (TGA). Heating was done at a rate of 10^0C min^{-1} from room temperature to 800^0C in nitrogen atmosphere at a flow rate of 15mL min^{-1}. Percent weight loss was plotted against temperature. A derivative of this curve, DTG was obtained to indicate the temperatures at which maximum rates of weight loss occurred.

2.6. Scanning Electron Microscopy (SEM)

Scanning Electron Microscope (SEM) model JSM JEOL-6490 (figure 8) was used for morphological analysis of lignin,castor oil/ polyol, castor oil/ polyol based polyurethanes CMF and PU/CNF nanocomposites films.For these analysis, all samples were mounted on a metal stub and platinum coated by using sputter coating technique for 20 s to make them conducting. Images were taken at 20 kV accelerating voltage at different magnifications.

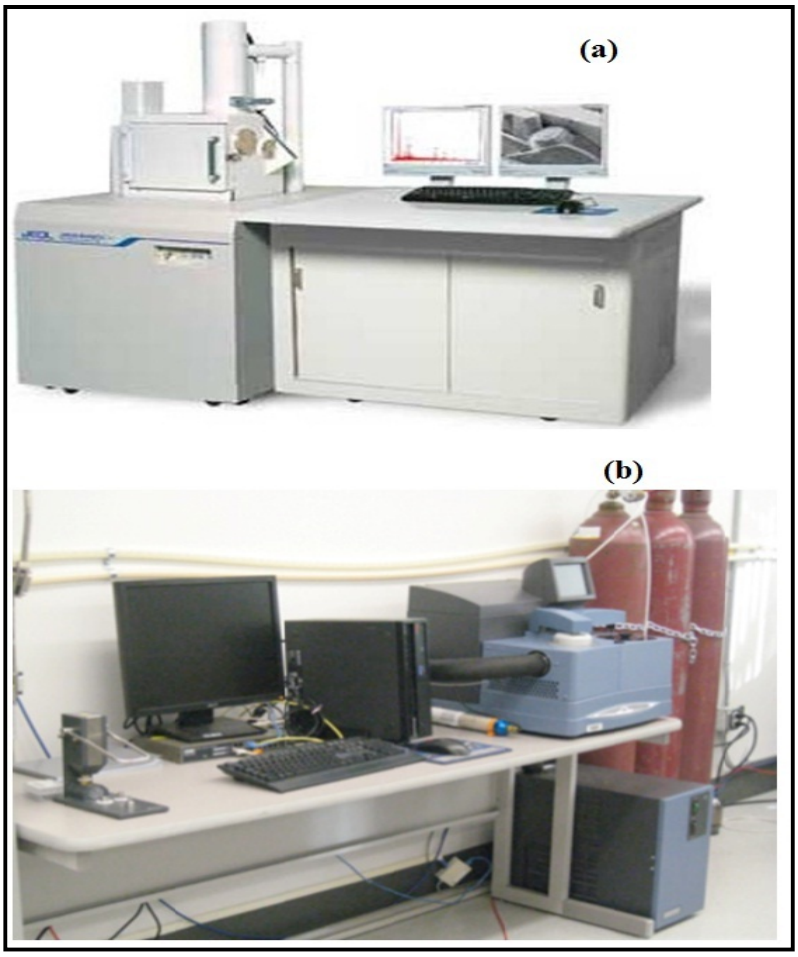

Figure 8: Photographic images of (a) SEM model JSM JEOL-6490; (b) DSC from TA Instruments Inc model no. Q2000

2.7. Differential Scanning Calorimeter (DSC)

DSC measurements of lignin castor oil/ polyol, castor oil/ polyol based polyurethanes,CMF, CNF and PU/CNF nanocomposites films were performed using Q2000 from TA Instruments Inc(figure 2.9 b). Approximately 5.0 ± 0.25mg samples were placed in a hermetic pan and

sealed. DSC scans were performed at a heating rate of 10°C/min from 30 to 400°C under nitrogen environment.

2.8. Transmission Electron Microscopy (TEM)

The network and surface topography of cellulose nanofibers was observed using Transmission Electron Microscopy (TEM) model Hitachi-2100 (figure 9). All the images were taken at 80 kV accelerating voltage. The sample for the test was prepared by depositing and drying a drop of dilute NFC suspension (prepared in de-ionized water) on a carbon coated grid.

The diameter and length of CNF were examined using TEM images of nanofibers. For this, TEM images of NFCs were loaded in UTHSCSA Image Tool analyzer program (IT version 3) and diameters of the fibers were measured using a two point measuring analysis. The scale of the software was calibrated using the scale bars on each TEM image. Approximately 300 measurements were taken to obtain fiber diameter distribution.

Figure 9: Photographic image Transmission Electron Microscope (TEM)

2.9. Wide Angle X-Ray Diffraction (WAXRD)

WAXRD of castor oil/ polyol based polyurethanes film, CMF, CNF and PU/CNF nanocomposites film was conducted by subjecting the samples to X-ray radiation at room temperature. The films were analyzed by using a Philips X'Pert Pro R-ray diffractometer system (figure 10). The radiation was Cu Kα (λ=1.54060 A^o) with 40 kV voltage and 40 mA intensity.

Crystallinity and crystallite size of the raw jute fibers, CMF, CNF was calculated using the following equations:

$$Crystallinity\ Index\ (CrI) = 100 \times \frac{I_{Total} - I_{Am}}{I_{Total}} \qquad (2.7)$$

Where, $I_{Total}$is the maximum intensity of the (002) lattice diffraction and I_{Am} is the intensity diffraction at 18° 2θ diffraction angle.

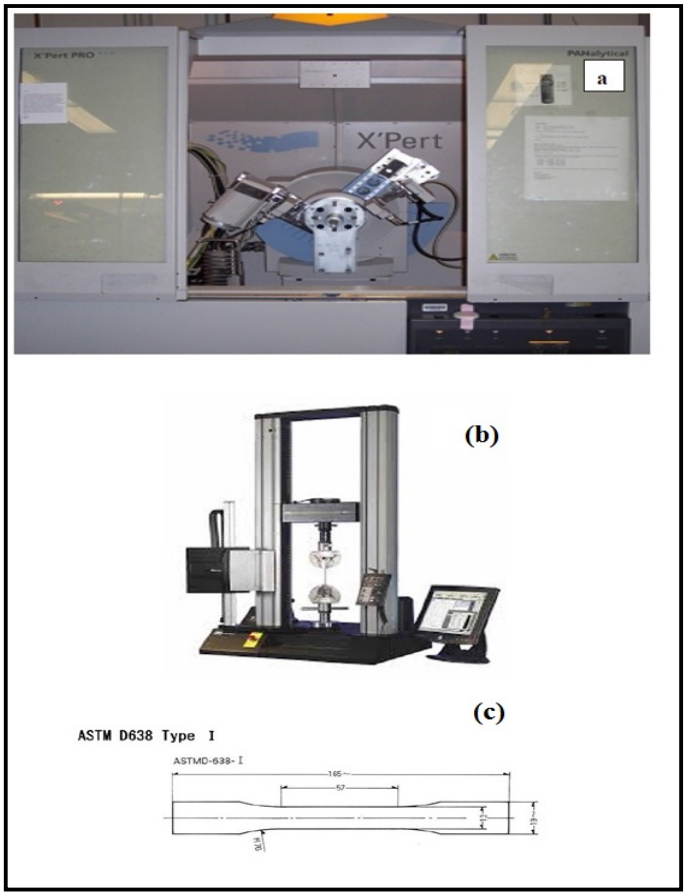

Figure 10: Photographic images of (a) X'PertPro X-ray diffractometer system; (b) and (c) Instron 4466 instrument; sample shape and its dimensions as per ASTM D638 standard

The crystallite size or the thickness of crystal in a direction perpendicular to its Miller planes was also estimated using Scherer's equation (2.8)

$$t_{hk} = \frac{K\lambda}{\beta_{hkl}cos\theta} \quad (2.8)$$

Where, $t_{hkl}$is takenas the thickness of crystallites at the (hkl) plane of diffraction , λis an X-ray wavelength (λ = 0.1542 nm for CuKa), θ is the Bragg angle of the reflection, β_{hkl} is the pure integral of width of the reflection at half maximum height, and *K* is the Scherrer constant that falls in the range 0.87-1.0.

2.10. Mechanical Analysis

Tensile testing of castor oil/ polyol based polyurethane samples and PU/CNF nanocomposite films was done using Universal Tensile Testing machine Instron 4466 (figure 2.11 b) upgraded with Blue Hill 2 software and assembly A564-229 version 2.0. The load cell of 10 kN was installed following ASTM D638 standards. For the test, crosshead speed was set to 2 mm/min and film samples were cut in a dumble shape (figure 10). Four to five specimens were tested for each sample and average value was taken. A stress vs. % strain curve was obtained from which the tensile strength and yield strength of castor oil/ polyol based polyurethanes films was calculated.

2.11. Antimicrobial Activity (Growth Conditions and Inhibition Analysis)

Antimicrobial activity of PU/CNF nanocomposites was examined by macrodilution method against *Staphylococcus aureus* (Gram-positive) and *Escherichia coli* (Gram-negative). For this the bacterial strains were grown overnight in Brain heart infusion broth at 37°C and 100µl of culture was added to the freshly prepared 10 ml Mueller hinton broth containing castor oil/ polyol based polyurethanes sheets (5 mm x 5 mm). PU/CNF nanocomposites free broth served as control. Inhibition of bacterial growth was visible as a clear broth and the presence of growth was detected by the presence of turbidity. Further, overnight growth was also monitored by measuring the optical density at 600 nm.

2.12. Biodegradation Study in PBS Solution

The PU/CNF nanocomposites films of about 10 x 10 mm^2 with weight 'W_o' were placed in a beaker with 25 mL of a PBS buffer solution with pH=7.4 and then incubated at 37°C. At specific time intervals, the specimen was taken out, washed with double distilled water and kept for

drying in vacuum oven for 2 days till constant weight was achieved. Then final dried weight (W_d) was determined. % Degradation was evaluated using Eq. (2.9):

$$\% \, Degradation = \frac{(W_o - W_d)}{W_o} \times 100 \qquad (2.9)$$

3. RESULTS AND DISCUSSION

Characterizations of Cellulose Nanofibers

Cellulose nanofibers were isolated using physical-chemical methods followed by high shear homogenization. The overall isolation of cellulose nanofibrils is a two-step process involving:

i. Extraction of cellulose micro fibers (CMF) aggregates using soda cooking and bleaching followed by acid hydrolysis of the raw jute fibers.

ii. Mechanical disintegration of microscopic cellulose fibers (CMF) aggregates into nanofibrillated cellulose (CNFs) using high shear homogenization.

Soda cooking, the first and the primary step which results in the defibrillation of large cellulose bundles in to microscopic cellulose fibers (CMF) with the removal of all the components like lignin, hemicelluloses, pectin leaving pristine cellulose. Microscopic cellulose fibers (CMF) aggregates in the second step are mechanically disintegrated into nanofibrillated cellulose (CNFs).

This section deals with the morphological, structural and thermal characterizations of raw jute fibers, microscopic cellulose fibers (CMF) and nanofibrillated cellulose (CNFs). The various analytical techniques like TEM, SEM, FT-IR, XRD, TGA DSC and elemental analysis were used at different stages of the isolation.

Yield of Cellulose Microfibers and Cellulose Nanofibers

Yield of the cellulose microfibers (CMF) and cellulose nanofibers (CNF) was calculated using equation 2.2 and found to be 55 and 53%, respectively. There was a slight decrease of 2% in the yield of cellulose nanofibers that may be due to wastage during processing of cellulose microfibers.

Fourier Transform Infrared Spectroscopic Analysis (FTIR)

Traces of lignin, hemicelluloses and pure cellulosic groups present in raw jute fibers, microscopic cellulose fibers (CMF) and nanofibrillated cellulose (CNFs) were identified using FTIR spectroscopy technique. Figure 11 shows the FTIR spectra of raw jute fibers, chemically treated microfibers (CMF) and mechanically treated cellulose nanofibers (CNF), while table 3.1 shows the prominent peaks of these spectra and their description.

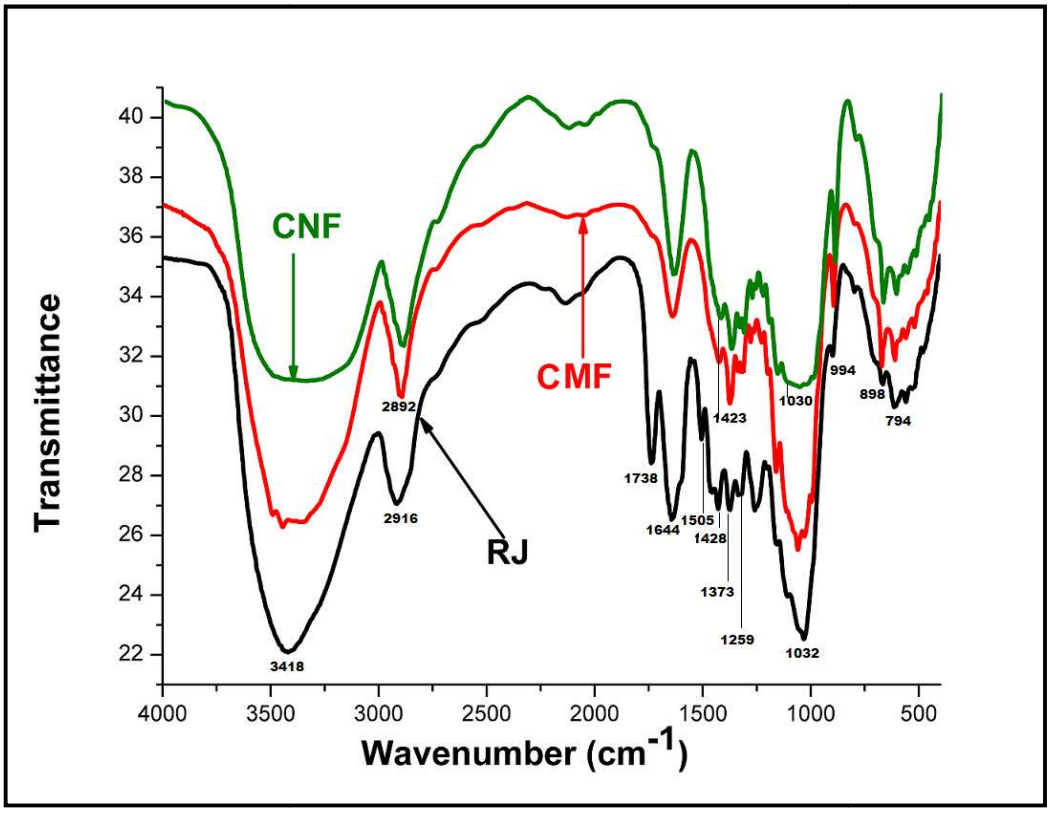

Figure 11: FTIR spectra of Raw Jute raw jute fibers, chemically treated microfibers (CMF) and mechanically shear treated cellulose nanofibers (CNF)

In the FTIR spectra a broad peak in the range of 3,200–3,500 cm^{-1} was due to O–H stretching vibration and bands at 2850-2930 cm^{-1}were due to methyl and methylene groups. Peak at 1732 cm^{-1} in the spectrum of raw jute fibers is either due to the acetyl and uronic ester groups of the hemicelluloses or the ester linkage of carboxylic group of the ferulic and p-courmeric acids of lignin and/or hemicelluloses. Bands around 1652 cm^{-1}maybe due to the bending mode of the absorbed water and some contributionsfrom carboxylate groups.The strong and sharp band around 897 cm^{-1} and 655 cm^{-1}corresponds to C-H deformation ring vibrations and C-OH out-of-plane, respectively. Bands at 1510 and 1425cm^{-1} correspond to aromatic ring vibrations of

phenyl propane groups of lignin seen in spectrum of raw jute whereas in case of chemically treated fibers the band around 1510 cm^{-1}vanished completely. The intensity of peak at 1426 cm^{-1}has significantly decreased in chemically treatedfibers attributing to partial removal of lignin. The peak at 1373cm^{-1} represents C-H asymmetric deformation seen in all the spectra whereas the peak at 1258 cm^{-1} corresponds to hemicelluloses which diminished completely in case of chemically and mechanically treated fibers thus indicating the complete removal of hemicellulose. Peak at 895 cm^{-1}in chemically and mechanically treated fibers relates to the crystalline regions of cellulose associated with cellulosic β-glycosidic linkages.

Table 1: Observed peaks with their band description for Raw Jute raw jute fibers, chemically treated microfibers (CMF) and mechanically shear treated cellulose nanofibers(CNF)

Band Description	**Observed peaks/bands**		
	RJ	**CMF**	**CNF**
-OH Stretching	3418	3366	3335
C-H Vibration	2916	2892	2892
C=O stretching due to hemicellulose	1738	-	-
Absorbed water	1644	1639	1644
Aromatic C=C vibration of lignin	1609	-	-
	1505	-	-
	1428	1423	1423
C-H stretching	1373	1373	1373
Hemicellulose	1259	-	-
C-O-C stretching	1163	1160	1160
C-C stretching	1032	1031	1030
C-H Rock vibration of cellulose	994	996	996

	898	894	894
	794	796	-

Wide Angle X-Ray Diffraction (WAXRD) Analysis

WAXRD analysis is performed for studying the crystalline behavior and for determining structure-property relation of the fibers. In all natural fibers, cellulose is highly crystalline by nature but its binding components lignin, hemicellulose and other components are amorphous which results in decrease in overall crystallinity of the natural fibers. Hence, the crystallinity of fibers is enhanced after chemical treatments as it removes lignin and other components [66,306]. Figure 12 shows the XRD patters of raw jute fibers, CMFs and CNFs. From the XRD patterns, it was inferred that the chemical treatment resulted in the transformation of native cellulose I to cellulose II. It can be confirmed from the shifting of peak from 16.8° to 12.5° 2θ angle and evolution of new peak at 2θ 20.5° corresponding to cellulose II. It may be due to penetration of liquor in cellulose fibers during soda cooking causing a rearrangement of the crystal packing of chains from native cellulose I to cellulose II. Also a sharp intensity peak for native cellulose I was observed at 22.6° thus confirming the coalescenceof cellulose I and II. The nanostructure obtained resulted in increase in specific surface area of the fiber, making the hydroxyl groups of cellulose macromolecules more accessible. Similar results were observed for CNF.From figure 12 it was also observed that crystallinity of fibers increasedwith the chemical treatment as indicated by increase in the intensity of peak at 2θ = 22.6° corresponding to 002 lattice plane and further increases sharply with high shear mechanical treatment.

Table 2 shows that the crystallinity and crystallite size of raw jute fibers, CMF and CNF. The crystallite size decreased from 13.57 nm for chemically treated to 2.84 nm for cellulose nanofibers whereas crystallinity increase from 44.99% for untreated to 94% for mechanically/high shear treated cellulose nanofibers. This increase in crystallinity could also be attributed to reorganization of amorphous and para-crystalline region of cellulose at higher temperature during soda cooking process which may have accumulated during the crystallization

phase of cellulose biosynthesis and interaction of the cellulose with hemicellulose and lignin in cell wall formation.

Table 2: Crystallinity and crystallite size Raw Jute raw jute fibers, chemically treated microfibers (CMF) and mechanically shear treated cellulose nanofibers (CNF)

Sample ID	% Crystallinity	Crystallite Size
RJX	45	-
MFC	84	13.57
CNF	98	2.48

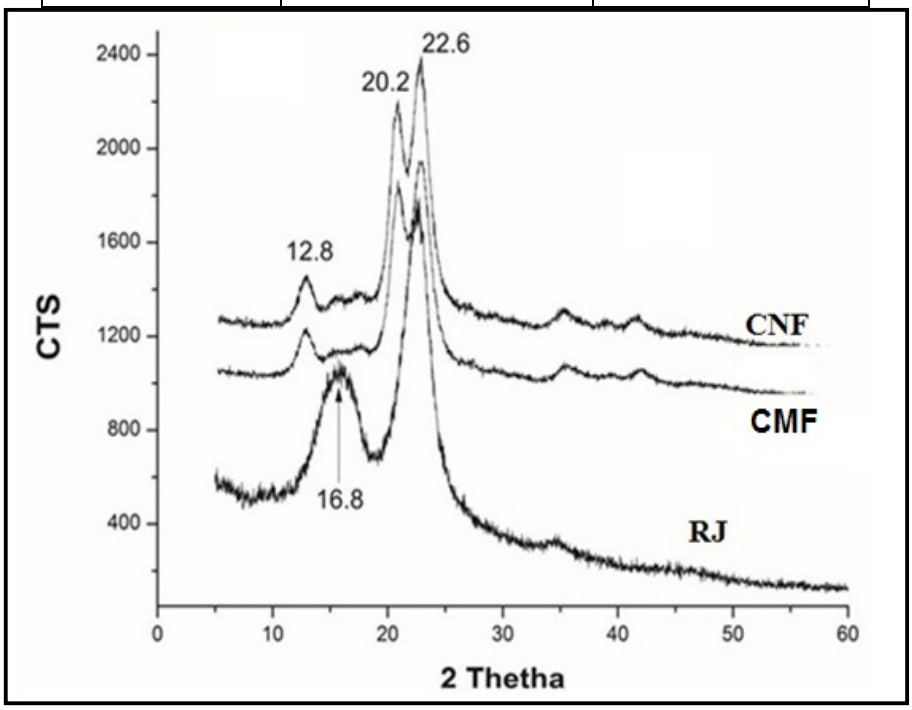

Figure 12: XRD patterns of Raw Jute raw jute fibers, chemically treated Microfibers (CMF)

and mechanically shear treated cellulose nanofibers (CNF)

Scanning Electron Microscope (SEM)

Scanning electron microscopic images of raw jute fibers and chemically treated microfibers CMF obtained after acid hydrolysis were taken to determine the microstructure of cellulosic

fibers. Structural as well as chemical changes were observed after soda cooking process as it results in the fragmentation of bonds of lignin, hemicellulose in the cell wall.

Surface morphology of raw jute fibers and chemically treated CMFs are shown in Figure 13(i) and 13 (ii) at different magnifications, respectively.SEM micrographs shown in Figure 13 (ii) (a-d), clearly show individual fibers with an average diameters of about 10–15 μm, lower than the average size of fiber bundles which get disrupted with the removal of hemicelluloses, lignin, and pectin during chemical treatment. This reduction of size may be attributed to the disintegration of hemicellulose and lignin corroborated by FTIR results. SEM images also show that the obtained fibers are cylindrical in shape.Further, SEM images clearly show the effect of physicochemical treatments i.e. soda cooking, bleaching and acid hydrolysis. Isolation of cellulose microfibers bundles that are major component of ligno-cellulosic material was also confirmed from SEM images.

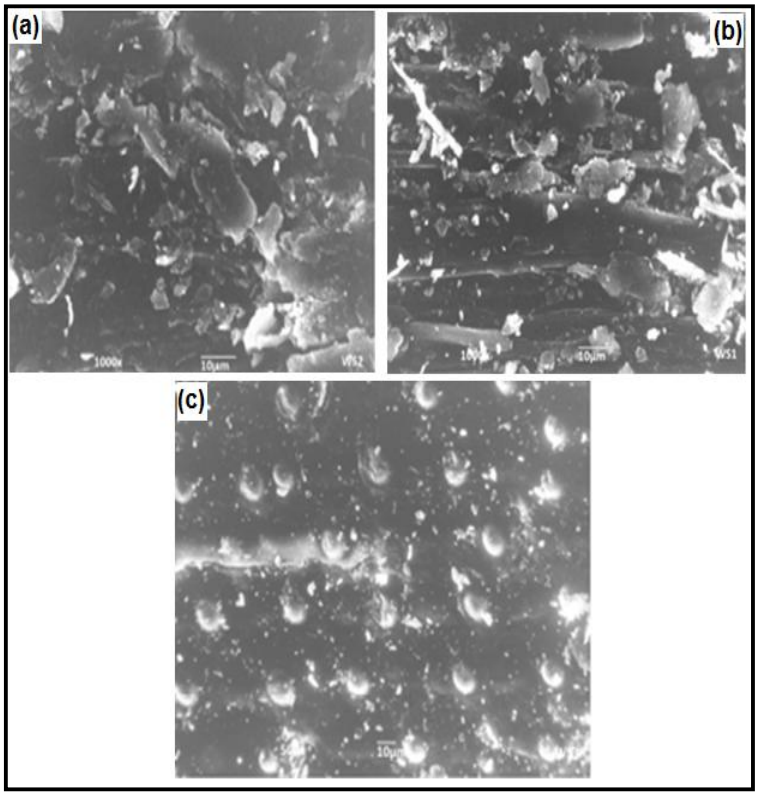

Figure 13 (i): SEM images of Raw Jute fibers at different magnifications

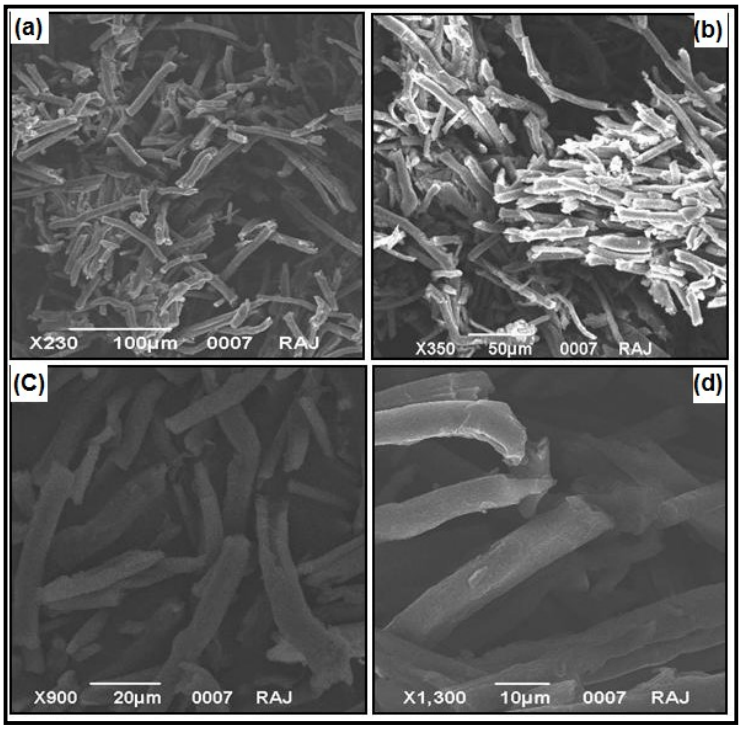

Figure 13 (ii): SEM images of chemically treated cellulose microfibers (CMFs) at different magnifications

Transmission Electron Microscope (TEM)

Figure 14(i) shows TEM images of the CNFs after the chemical and mechanical treatments. Mechanical treatment resulted in defibrillation of the cellulose nanofibrils from the cell bundle and thus TEM images reveal the disintegrated nanofibers from the micro sizes fiber bundles. The diameter of the fibers was found in the range of 5–60 nm. A tendency of agglomeration can also be observed in TEM images. It is not clear whether this was due to drying of the suspension onto the carbon film covering the carbon grids or if it reflected the state of the suspension.

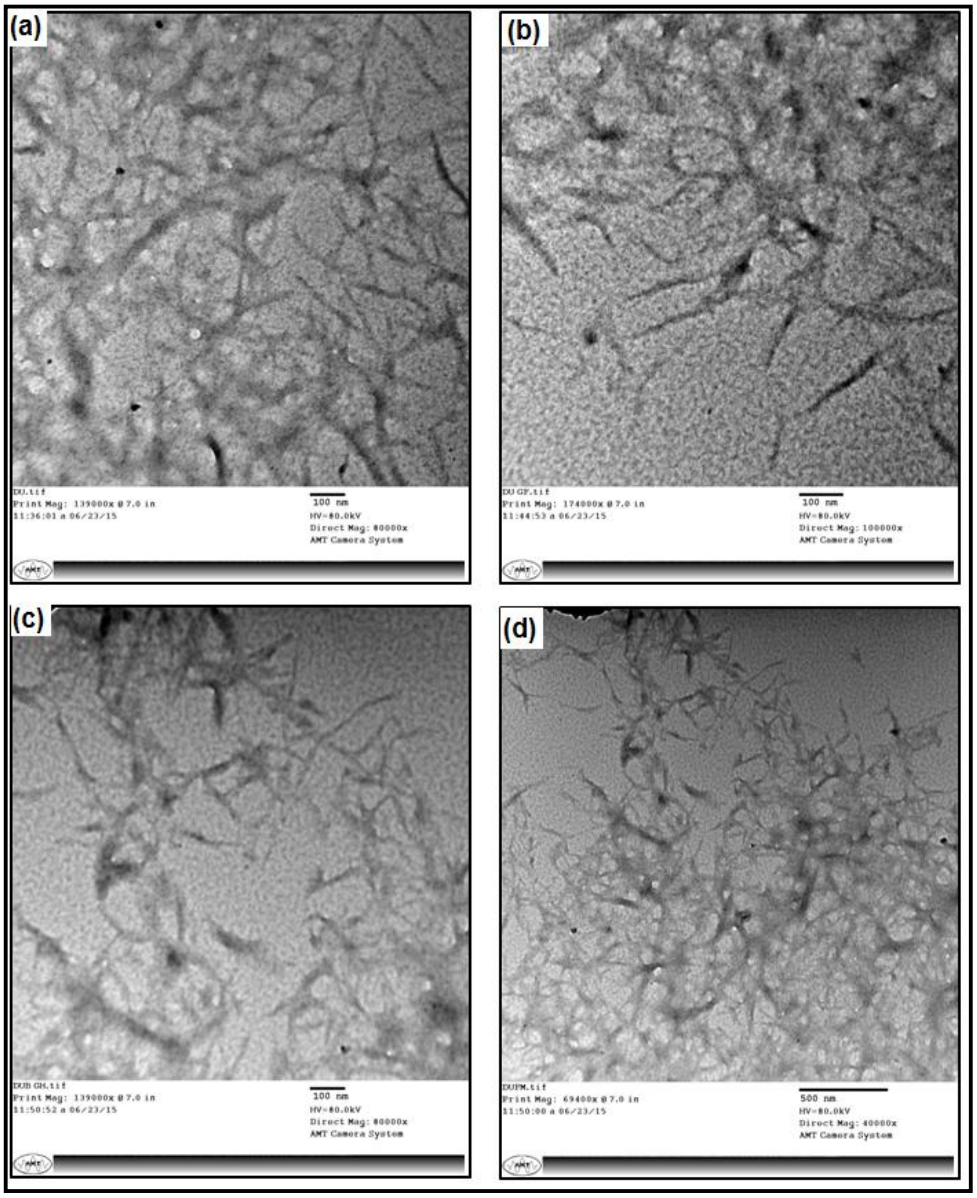

Figure 14 (i) a-d: TEM images of mechanically treated cellulose nano fibers (CNFs) at different magnifications

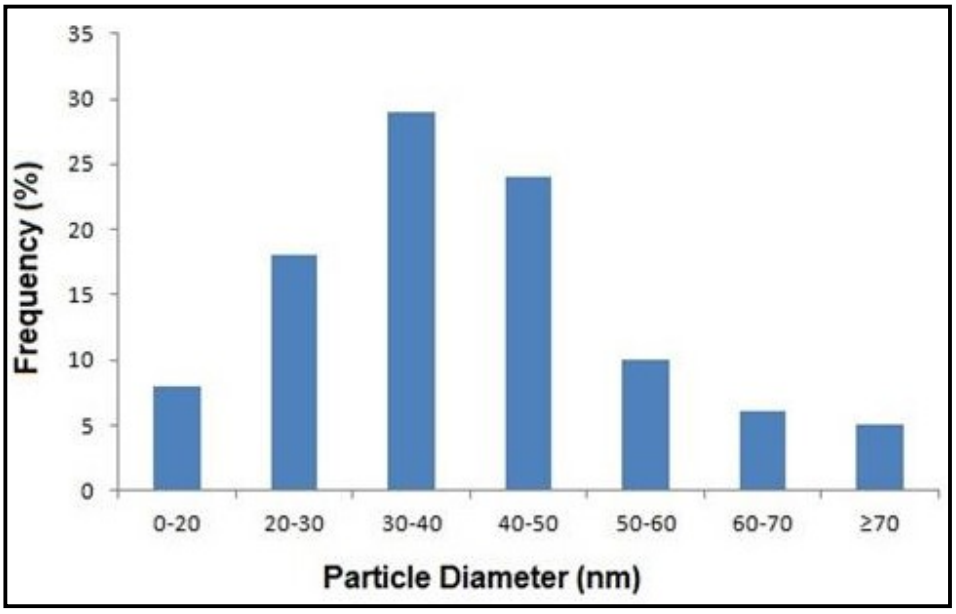

Figure 14(ii). Particle size distribution using image tool analyzer (UTHSCSA).

UTHSCSA digital image analysis software was used to calculate the average diameter from the electron micrographs. Diameter was found to be in the range of 30–50 nm for most of the particles. Figure 14(ii) shows the distribution of nanofibers diameter after final treatment from which it was revealed that only 5% of fibers have diameter >70 nm. Almost 62% of fibers have diameter between 30–50 nm and 18% of the fibers have a diameter less than 30 nm.

Thermal Analysis of Raw, Chemically (CMFs) and Mechanically (CNFs) treated Jute Fibers

The main objective behind isolation of cellulose nanofibers is to synthesize polyurethane nanocomposites by reinforcing them into polyurethane matrix. It also gives an idea about purity of cellulose. Therefore, thermal analysis of nanofibrils becomes important for their processing. TGA curves gives information about the percentage weight loss with respect to temperature while (DTG) demonstrate the corresponding rate of weight loss. The point at which maximum rate of thermal decomposition occurs is predicted from the peak of DTG curves and is termed as DTG_{max} and is used for comparing thermal stability of various samples.

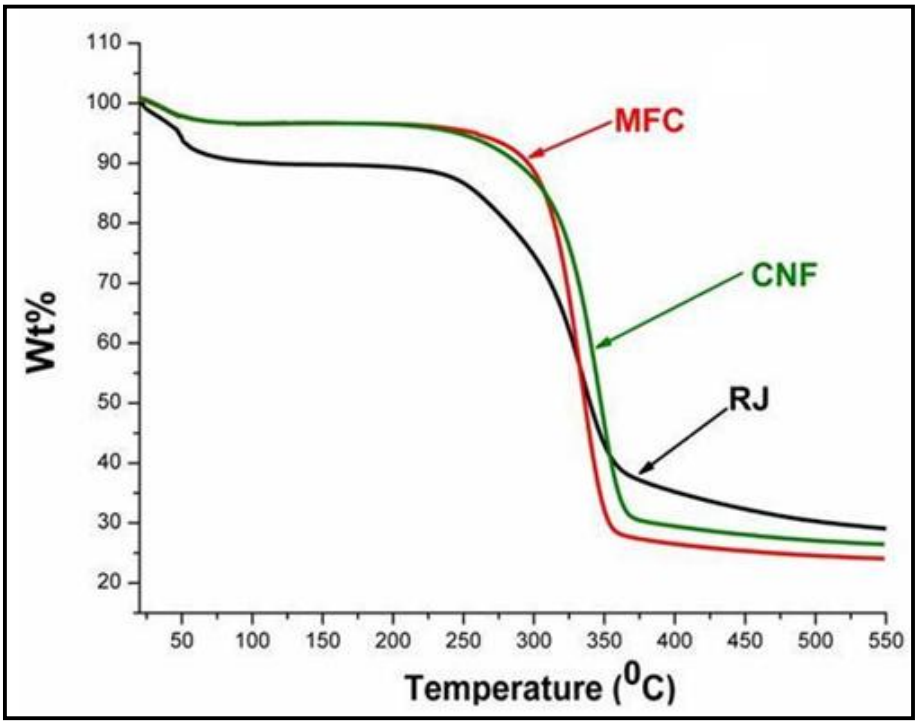

Figure 15 (i): TGA curves of Raw Jute raw jute fibers, chemically treated Microfibers (CMF) and mechanically shear treated cellulose nanofibers (CNF)

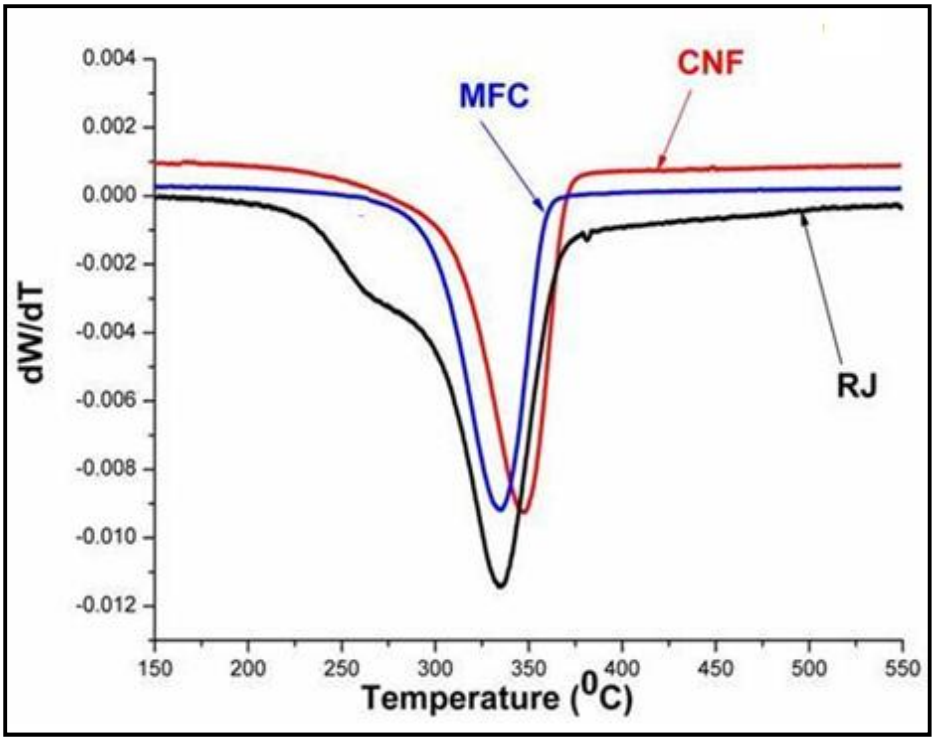

Figure 15 (ii): DTGA curves of Raw Jute raw jute fibers, chemically treated Microfibers (CMF) and mechanically shear treated cellulose nanofibers (CNF)

TGA and DTG curve of raw jute fibers, CMFs and CNFs are shown in figures15(i) and 15(ii), respectively. From the TGA of raw jute, it is apparent that degradation occurs between a broad range of 120 to 550°C. The initial weight loss around 100°C was due to the evaporation of absorbed moisture. Second and third degradation stage at 230 and350°C corresponds to degradation of hemicellulose and cellulose. The last stage of degradation above 370°C corresponds to degradation of lignin. It was observed that in case of chemically and mechanically treated fibers, the thermal stability T_{onset} is higher which may be due to complete removal of amorphous non-cellulosic material resulting in higher degree of ordered structure of crystalline cellulose.

From DTG results shown in figure 15(ii) three major degradation peaks were observed in case of raw jute. First decomposition shoulder peak at 250°C relates to the thermal depolymerization of hemicelluloses or pectin, the second major peak due to degradation of cellulose was seen at 338 °C and finally a small tail at 370 °C relates to the degradation of lignin. In case of chemically and mechanically treated fibers, only a sharp second peak around 335-350°C appears which corresponds to decomposition of highly crystalline cellulose, whereas 1stand 3rdpeak disappeared showing the complete removal of lignin and hemicellulose as also confirmed from other results.

The thermal degradation characteristics like T_{onset}, T_{max} and their corresponding % mass loss and % mass residue at 550 °C of raw jute, CMFs and CNFs are tabulated in table 3. Where T_{onset} relates to the temperature at which degradation starts, T_{max} to the temperature where maximum degradation takes place. From the results, it was observed that the T_{onset}, T_{max} and % mass loss at T_{max} for CNFs is higher than raw jute fibers, confirming their higher thermal stability. The higher thermal stability of CNFs may be attributed either to the presence of organic compounds or may be due to complete removal of amorphous non cellulosic material resulting in higher degree of ordered structure of crystalline cellulose as substantiated by FTIR and XRD results.

Table 3: Thermal degradation characteristics of Raw Jute raw jute fibers, chemically treated microfibers (CMF) and mechanically shear treated cellulose nanofibers (CNF)

Sample ID	T_{onset}(^{o}C)	%Mass loss at T_{onset}	T_{max} (^{o}C)	%Mass lossat T_{max}	% Mass Residue at 550^{o}C

RJ	288	23.70	332	42.62	29.30
CMF	300	15.59	340	58.17	15.44
CNF	311	18.13	348	64.68	11.94

Differential Scanning Calorimeter (DSC) is another important technique for the analysis of thermal properties. It provides important information regarding transition temperature i.e. the temperature at which the material morphology changes from crystalline to amorphous and about the degradation whether it is endothermic or exothermic.

DSC curves of raw jute fibers, MFCs and CNFs are shown in figure 16. From the figure a peak below 150°C is observed in case of raw, MFCs and CNFs, this may be due to the evaporation of moisture from the sample on heating. Further, in case of raw jute fibers, two more degradation peaks were seen in the range of 290-310°C and 340-360°C similar to TGA, that may be due to the degradation of hemicellulose and α-cellulose. However, in case MFCs and CNFs only one degradation around 320°C was observed corresponding to the degradation of crystalline cellulose which further reaffirms the observation of TGA results.

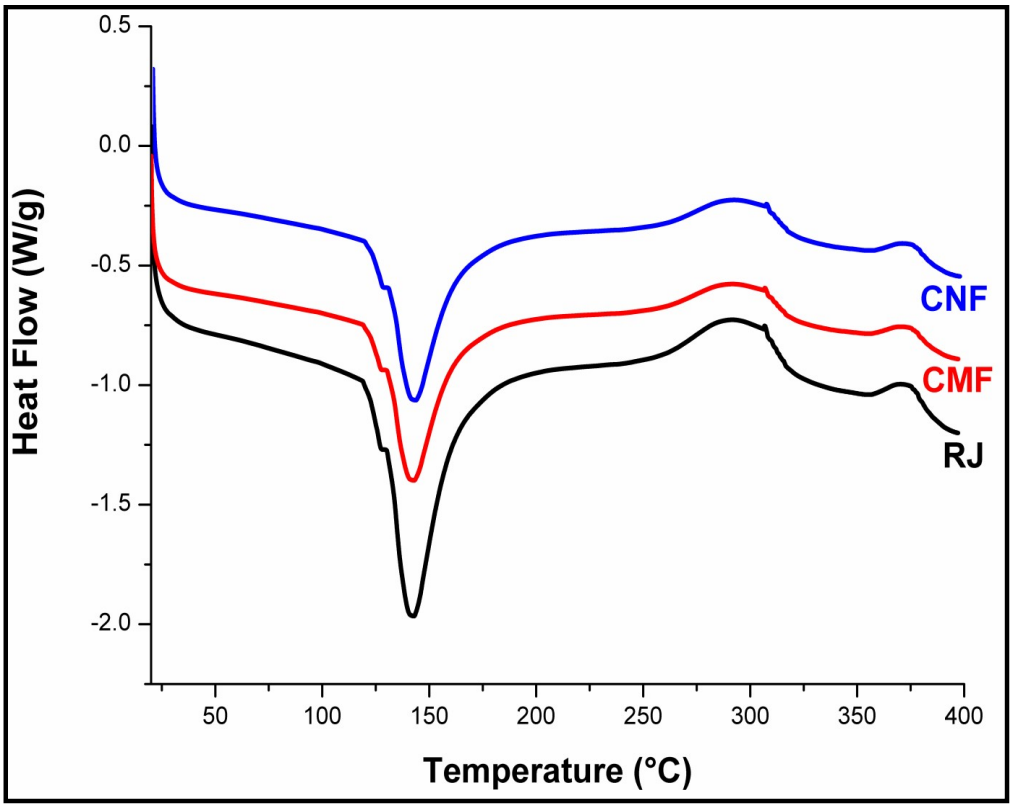

Figure 16: DSC curves of Raw Jute raw jute fibers, chemically treated Microfibers (CMF) and mechanically shear treated cellulose nanofibers (CNF)

Table 4: Degradation temperatures and their corresponding enthalpies from DSC results

Sample	First degradation temperature (°C)	Enthalpy at first degradation (J/g)	Second degradation temperature (°C)	Enthalpy at Second degradation (J/g)
CMF	**137.47**	**82.03**	**348.14.**	**56.32**
CNF	**137.65**	**58.51**	**357.31**	**35.60**

Elemental Analysis of Raw, chemically (CMFs) and mechanically (CNFs) treated fibers

The elemental analysis results i.e. C, H, O, N, S wt% and O/C and H/C ratios of the MFC and cellulose nanofibers (CNF) are shown in table 5.

Table 5: Elemental analysis depicting C, H, O, N, S wt%

Sample ID	%C	%H	%O	%N	%S	O/C	H/C
MFC	50.56	7.38	41.76	0	0	0.82	0.14
CNF	51.12	7.59	42.18	0	0	0.83	0.15

From the results, it is revealed that no sulphur was present in the chemically and mechanically treated fibers and the core structure of cellulose was intact as it contained carbon, oxygen and hydrogen. Further no nitrogen was present in the heated fibers which may be due to absence of proteins. Proteins are completely removed during soda cooking process due to their solubility in alkali.It was also observed that the content of carbon decreased whereas the content of oxygen increased indicating large structural differences. The O/C ratio for is 0.83 for cellulose which is in the typical range of cellulose (0.83) indicating that the samples consisting of only carbon and hydrogen are mainly carbohydrates i.e. showing absence of nitrogen.

Characterization of Synthesized polyol based Polyurethane with varying Hard to Soft Segment Ratio

In the preceding section the focus was on the isolation of CNFs and optimization of lignin extraction from waste jute bags using soda cooking process and further modification of extracted soda lignin to lignopolyol by oxypropylation mechanism. Various physicochemical, morphological and compositional characteristics of cellulose nanofibrils, lignin and lignopolyol were discussed.

In this section the focus is on the study of numerous properties of the lignopolyol based polyurethane synthesized using solvent evaporation method resulting from reaction of PO, BDO and MDI with varying hard to soft segment ratio. The methodology has been explained in section 2.2.6**.** Various analytical techniques like FTIR, XRD, TGA, DSC and tensile testing were used for the study of structure, morphological, thermal and mechanical properties of synthesized polyurethane. Also the ratios of hard to soft segment were optimized to obtain best thermal and mechanical properties. Polyurethane samples with varying hard to soft segment ratios are indicated as PU1, PU2, PU3 and PU4; their detailed nomenclature has been indicated in table 2.3, 2.2.6.

FTIR Analysis

FTIR spectra of Lignopolyol, MDI and lignopolyol based polyurethanes with varying hard to soft segment ratio is shown in figure 17 (i) and 17 (ii), respectively. Also, the observed prominent peaks with their band descriptions are tabulated in table 6.

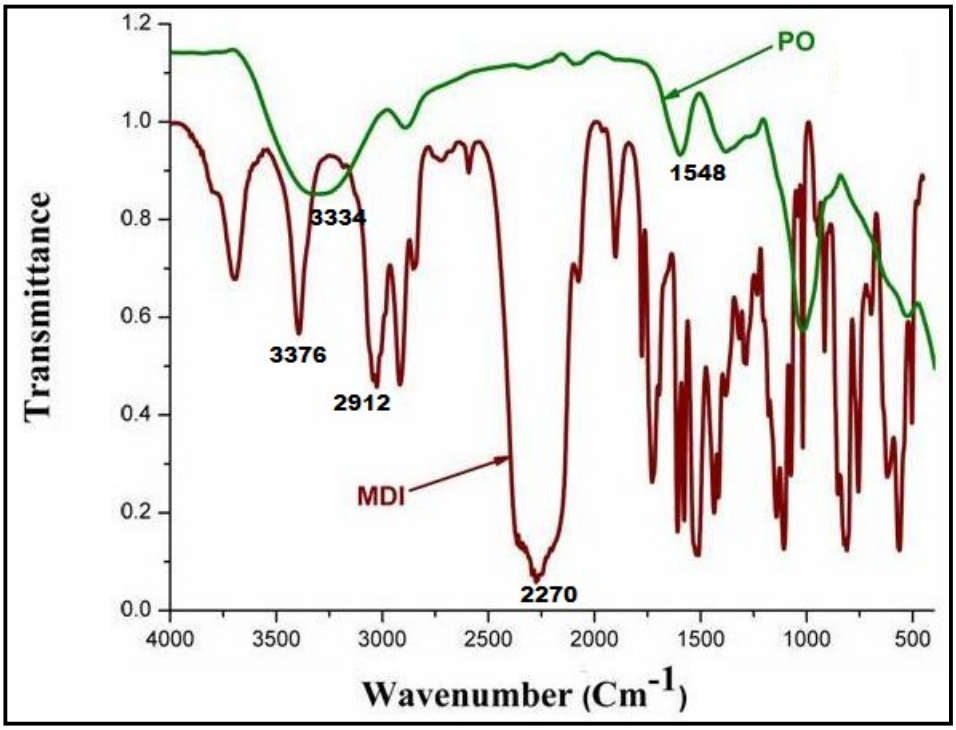

Figure 17 (i): FTIR spectra of Lignopolyol and MDI

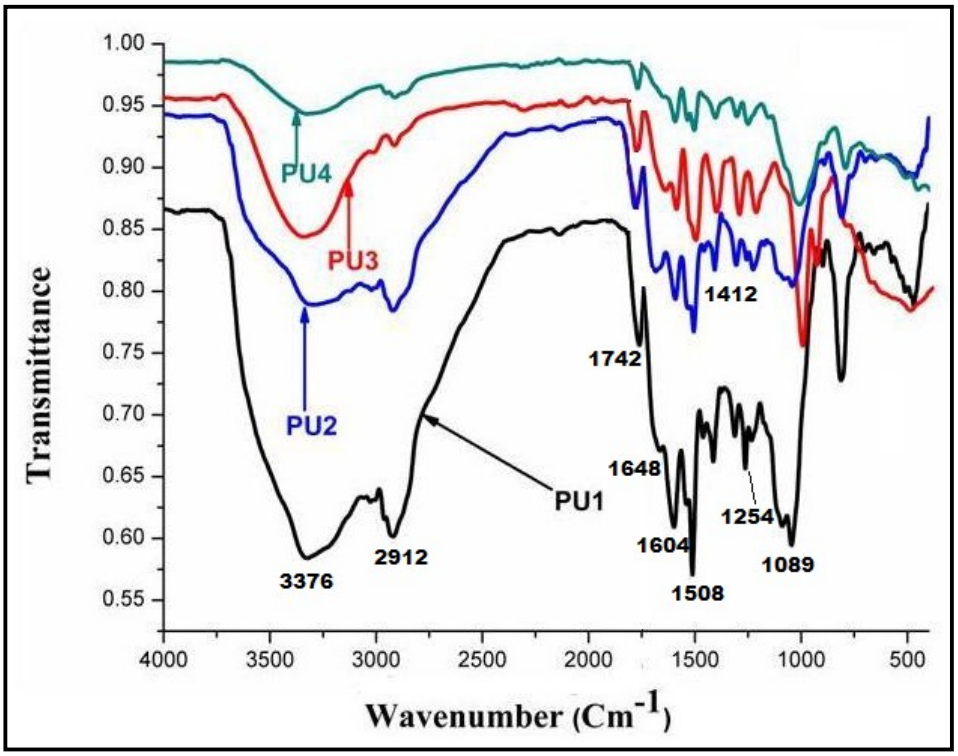

Figure 17(ii): FTIR spectra lignopolyol based polyurethanes with varying hard to soft segment ratio

Table 6: Prominent peaks with their corresponding band description of lignopolyol based polyurethanes with varying hard to soft segment ratios

Observed Peaks	Bands/Peaks Description
3334-3376	Hydrogen-bonded N-H stretching vibration [416]
2912-2914	C–O–C stretching vibrations [417]
1742	-NHCOO stretching combined with ester -COO stretching [417].
1648	Hydrogen bonded carbonyl group of urethane linkage [418,419]
1604	–C=C stretching due to aromatic ring of MDI [417]
1508	
1410-1413	C–O–C bending vibrations [417]
1304-1312	C–O–C wagging vibrations [417]
1254	–C–O–C stretching vibration in hard and soft segments [417]
1089	C–O–C stretching vibration of ether group [417]

Broad Hydroxyl peaks are observed in the spectra of lignopolyol and MDI due to the presence of moisture seen at 3454, 3100and 3450 cm^{-1}, respectively. A characteristic peak of isocyanate is seen at 2270 cm^{-1} in the spectra of MDI. A narrow peak for carbonyl group is observed at 1548 cm^{-1} in FTIR spectra of lignopolyol.

Important feature of PU polymer is hydrogen bonding between urethane linkages that has a significant effect on its properties. Polyurethanes include different hydrogen bonds such as N-H bonds of the amide group as the donor and the urethane carbonyl, the ether oxygen, or the carbonyl group in the lignopolyol as the acceptor. Single stretching band at ~3334-3376 cm^{-1}, corresponds to the hydrogen-bonded N-H stretching vibrations. Absence of peak between 3400 - 3500 cm^{-1} indicate that the all amide groups present in polyurethane films are involved in hydrogen bonding.Peak due to urethane carbonyl group (C=O) and ester groups i.e. NHCOO stretching combined with ester -COO stretching is seen around 1742cm^{-1}.Peak near 1648 cm^{-1} represents ordered/crystalline region hydrogen bonded carbonyl in urethane groups that can be

seen in all the spectra but for PU2 this peaks is broadest which may be due to higher hard segment content.

Further, it was also observed that the intensity ratio of peaks corresponding to the hydrogen-bonded and the non-hydrogen-bonded carbonyl groups increases with increase in BDO content suggesting increased intermolecular interaction of hard and soft segment.This may be attributed to increased OH functionality resulting in the higher crosslinking and an increased urethane content.Bands at 2912-2914 cm^{-1}, 1410-1413 $cm^{-1}$and 1304-1312 cm^{-1}, respectively, are attributed to stretching, bending and wagging vibrations of $–CH_2$ group, along with bands at 1508 cm^{-1} and 1604 cm^{-1} due to –C=C stretching in aromatic ring of MDI. Peaks at 1089 cm^{-1} is due to the ether group C–O–C stretching vibration. Avery strong band at 1254 cm^{-} is assigned to –C–O–C stretching vibration in hard and soft segments. Disappearance of peak around 2270 cm^{-1} signifies the complete curing and reaction of soft and hard segment with the successful synthesis of PU. Also, C–O–C stretching absorption band corresponding to the chemical linkage between OH and NCO groups to form urethane bond also provide strong evidence for the formation of PU.

3.4.2 XRD Analysis

X-ray diffraction patterns of the lignopolyol based polyurethane (LPU)with varying soft to hard segment ratios are shown in Figure 18.From the figure, it is observed that the XRD diffractograms exhibits broad peaks at 2θ angles around 9°, 12.5°, 20° and 26.8º, respectively indicating moderate degree of crystallinity. Effect of variation in PO and BDO concentrations on degree of crystallinity was studied as it relates to the interaction of hydrogen bonding between the soft and hard segment. Further, from the figure, it was observed that the LPU with same molar concentration of PO and BDO i.e. 1:1 and 0.45:0.55 shows the maximum crystallinity as evidenced from high intensity peaks at 2θ angles, 20° and 26.8º, which may be due to trifunctional active sites that increases the degree of crystallinity. With the change in the molar ratio of PO and BDO to 0.25:0.75 and 0.75:0.25, respectively, peaks located at 2θ angles 20° and 26.8º become broader showing a decrease of crystallinity in the sample. From these results it can be concluded that the crystallinity is controlled by the variation in hard and soft segment which may be attributed to the degree of cross linking of polyurethane controlled by the hydroxyl group existing in the lignopolyol. Thus, increasing the molar ratio of lignopolyol to butanediol decreases the urethane cross linking.

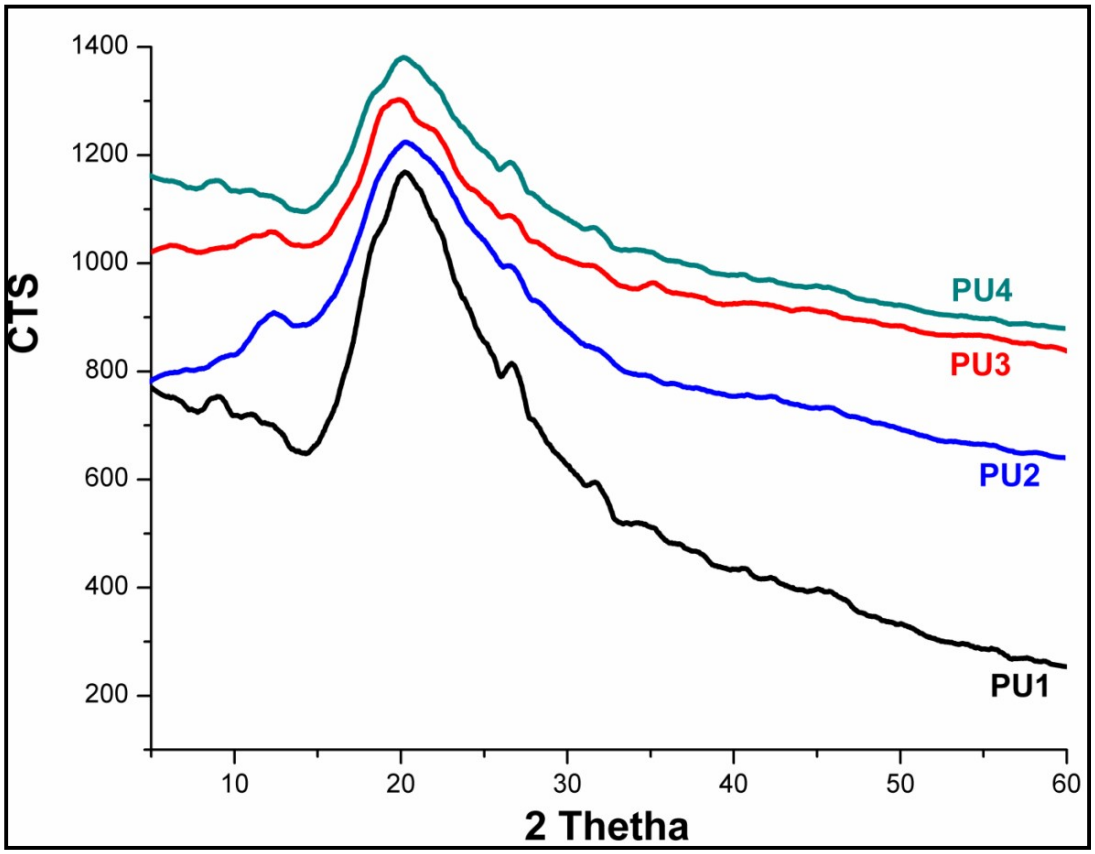

Figure 18: XRD of lignopolyol based polyurethanes with varying hard to soft segment ratio

TGA Analysis

TGA determines the amount of weight loss of a material as a function of temperature or time in a controlled atmosphere. As materialis heated, they can lose weight by simple processes such as drying, oxidation and chemical changes that liberate gases and lighter fragments. Some materials can gain weight by reacting with the atmosphere in the testing environment. Since weight loss and gain completely destroy the material, knowledge of the magnitude and temperature range of related reactions are necessary in order to design adequate thermal ramps and holds during those critical reaction periods. The technique is best suited to characterize the materials that exhibit weight loss or gain due to decomposition, oxidation, or dehydration. The first derivative (DTG) of TGA indicates the corresponding rate of weight loss. The peak of DTG curves i.e. DTG_{max} gives the highest rate of thermal decomposition and can be used as a means to compare thermal stability characteristics of different materials.

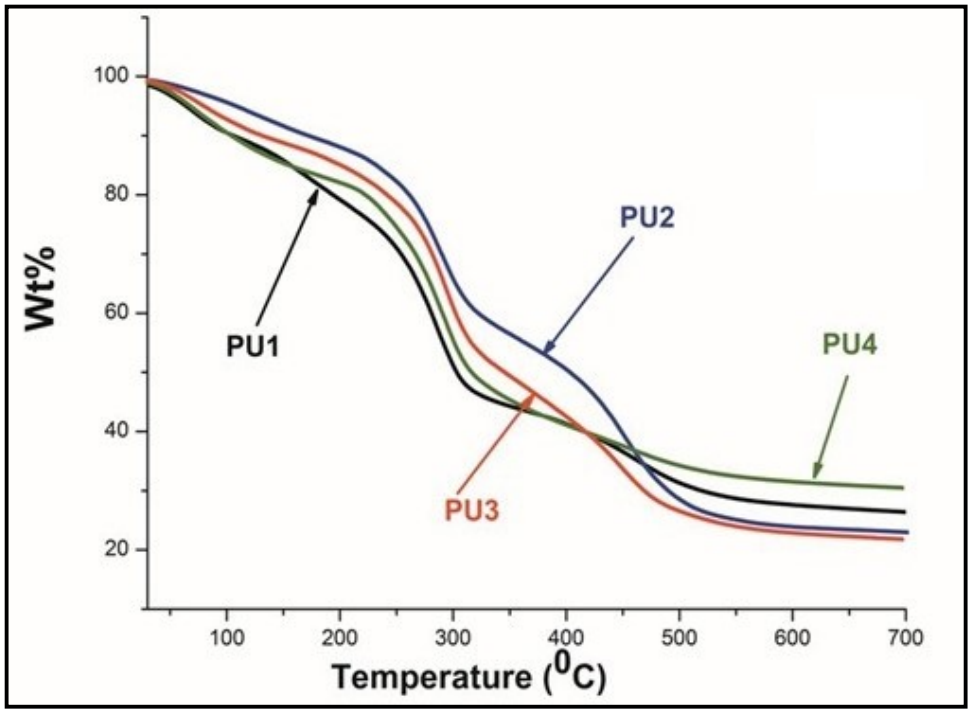

Figure 19 (i): TGA curves of lignopolyol based polyurethanes with varying hard to soft segment ratio

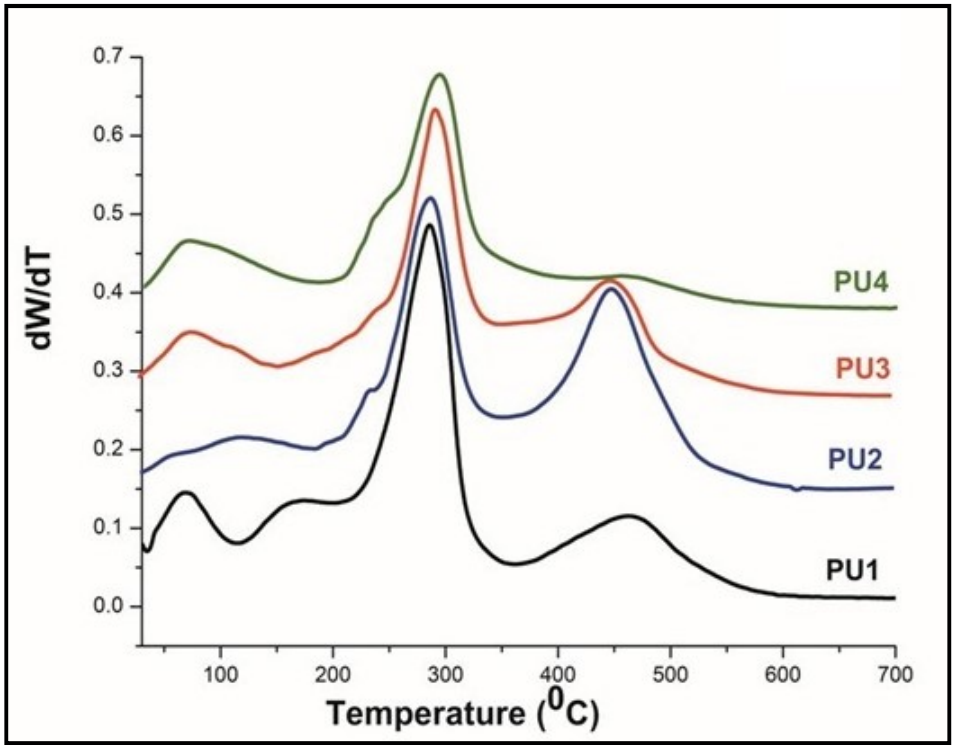

Figure 19 (ii): DTGA curves of lignopolyol based polyurethanes with varying hard to soft segment ratio

Figure 19 (i) and figure 19 (ii), respectively shows the TGA and DTG curves of LPU synthesized with different hard to soft segment ratios. Also the percent mass loss at different degradation temperatures, DTG_{max} and T_{onset} are summarized in table 3.17. From the figure, it was observed that the polyurethane degradation takes place in three steps. The first degradation below 100 °C may be due to traces of moisture in the LPU films while the second degradation observed between 200 to 300 °C corresponds to urethane bond decomposition either due to isocyanate and polyol dissociation or the due to the amines or olefins formation. The third degradation that takes place from 400-500 ºC may be due to lignopolyol scission and hence in case of PU3 the % mass loss in this region is maximum.

Hence, three step degradation was observed for all LPU films; in the first step degradation is due to moisture in the all LPU films, while in the second step urethane degradation temperature and % mass loss for PU1 and PU4 was higher than the PU2 and PU3 and maximum for PU1 which may be due the same composition of the hard and soft segment resulting in higher degree of crosslinking, crystallinity and hydrogen bonding interaction that was also confirmed by FTIR and XRD results, while in the second step, % mass loss was less for PU1 and PU4 which may be due to presence of large quantity of free hydroxyl groups.

Table 7: Thermal decomposition characteristics of lignopolyol based polyurethanes with varying hard to soft segment ratios

	1st Thermal event			**2nd Thermal event**			
Sample ID	**T_{onset} (^oC)**	**T_{max} (^oC)**	**%Mass loss at T_{max}**	**T_{onset} (^oC)**	**T_{max} (^oC)**	**%Mass loss at T_{max}**	**% Mass Residue at 700 ^oC**
PU1	260	300	41.42	422	462	10.50	27.50
PU2	240	286	33.29	420	444	32.30	19.71
PU3	246	288	32.30	425	445	31.51	18.55
PU4	256	298	40.30	419	460	16.60	22.98

The overall thermal degradation was determined from TGA curves using onset degradation method. From the data in table1 it can be seen that for LPU films with varying hard to soft segment ratio, the T_{max} for urethane bonds decreases from 300 to 286 ºC with decrease in molar ratio of lignopolyol and BDO from 1 to 0.75 and 0.25. This may be attributed to the decreased crystallinity as it controls the crosslinking of urethane groups. Also from the table it was observed that onset thermal degradation temperature i.e. T_{onset} increases with increase in hard segment and is maximum for the sample PU1. Similar trends were seen for percent mass residue at 700ºC. The percent mass residue increase from 18.55 to 27.50 for PU3 to PU1 thereby suggesting that the PU1 is thermally most stable out of all the samples. Also, the thermal stability of lignopolyol based polyurethane was found to be similar or higher than the commercially available polyurethanes such as polyethylene glycol, polypropylene glycol, castor oil and vegetable oil based polyurethanes.

Tensile Testing

Tensile measurements give important information regarding tensile strength, Young's modulus, %elongation and toughness of a material. The important structural parameters that control tensile strength and Young's modulus of segmented polyurethane are degree of crystallinity, crosslinking and intermolecular interaction. The tensile strength, Young's modulus and % elongation of lignopolyol based polyurethanes with varying hard to soft segments ratios were obtained from the stress strain curve (figure 20(a)) and are tabulated in table 8.

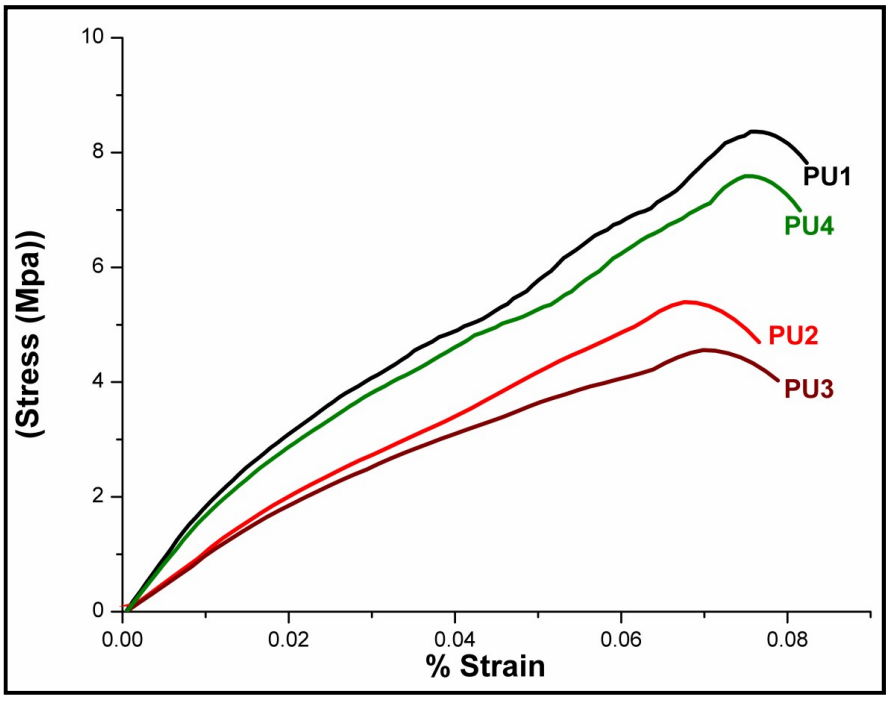

Figure 20 (i): Stress vs. Strain curves of lignopolyol based polyurethanes with varying hard to soft segment ratios

Table 8:Mechanical properties of polyurethanes with varying hard to soft segment ratios

Sample	Tensile Strength(MPa)	% Elongation	Young's Modulus (MPa)
PU1	8.4 ± 0.4	144 ± 4.3	247.06 ± 8.7
PU2	5.1 ± 0.3	320 ± 14.2	175.86 ± 5.3
PU3	4.7 ± 0.5	288 ± 9.2	142.42 ± 4.5
PU4	7.7 ± 0.4	192 ± 6.8	220.00 ± 6.4

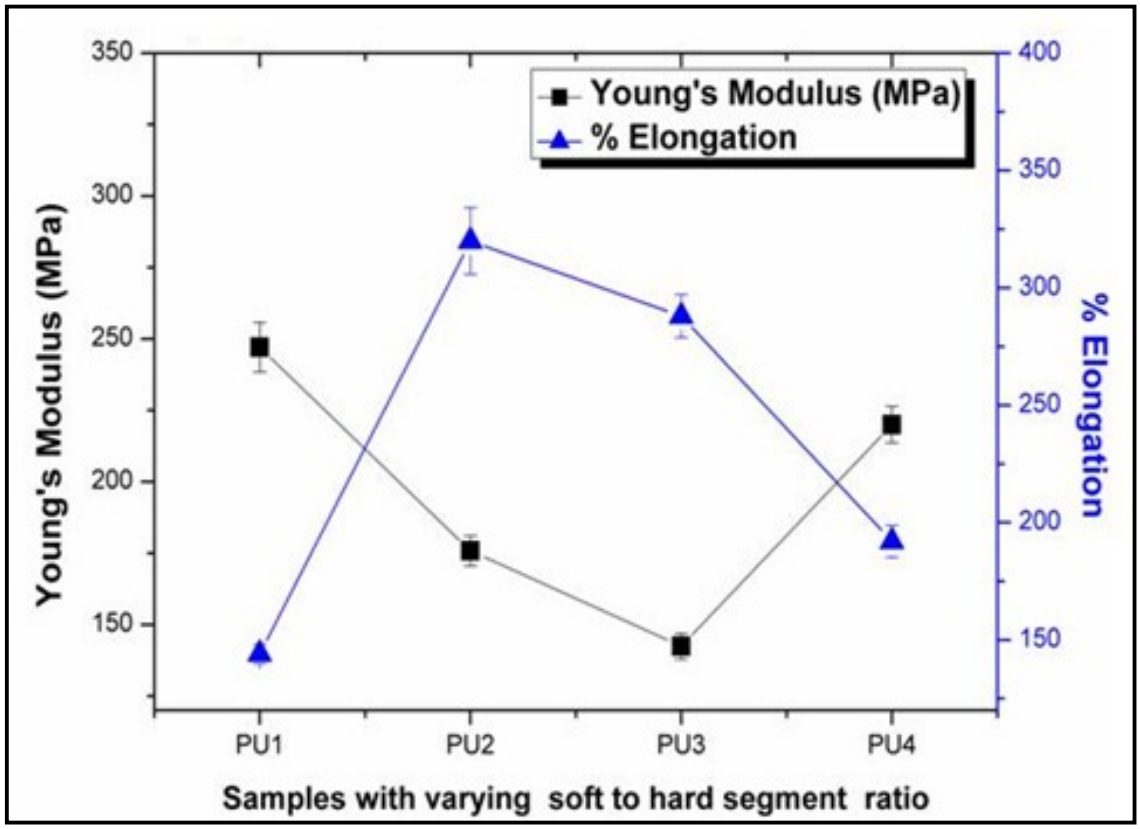

Figure 20 (ii): Young's modulus and % elongation of lignopolyol based polyurethanes with varying hard to soft segment ratios

From the results, it was observed that tensile strength and Young's modulus increases from 4.7 to 8.4 MPa and 142.42 to 247.06 MPa, respectively, with increase in hard segment content. It wasmaximum for the sample with equal composition of the hard and soft segment. The increase in Young's modulus and tensile strength may be attributed to increase in intermolecular bonding, degree of interconnectivity of hard and soft segment and degree of crystallinity of hard domains with the increase in concentration of hard segment as also confirmed by results of FTIR and XRD.

Further, the effect of filler content on percent elongation is shown in figure 20 (ii). It exhibits that increase in hard segment content results in decrease in % elongation and increase in Young's modulus i.e. polyurethanes with higher soft segment have elastomeric behavior whereas those with higher hard segment show an opposite trend which could be either because of soft segment potential to crystallize under strain or due to possibility of higher crystalline region formation with higher hard segment content. These results are in coherence with that reported in

literature.Further Young's modulus and tensile strength of lignopolyol based polyurethanes was found to be comparable with polyurethane synthesized using other polyols[429–432].Hence, these polyurethanes were further used for synthesizing nanocomposites with varying amount of CNFs.

Characterization of Synthesized Lignopolyol Based Polyurethane/Cellulose Nanofibers (PU/CNF) Nanocomposites

Lignopolyol/cellulose nanofibrils based polyurethane nanocomposites with varying weight percentage of CNF i.e.2.5, 5, 10 &15% were synthesized by incorporating them to lignopolyol based polyurethanes with equal amount of hard and soft segment i.e. PU1 using solvent evaporation method. Prepared nanocomposites were characterized for structural and morphological characteristics using FTIR, WD-XRD and SEM. Further, the effect of reinforcement on enhancement of thermal and mechanical properties was evaluated using TGA, DSC and tensile testing, respectively. Lignopolyol based polyurethane/cellulose nanofibers (PU/CNF) nanocomposites with varying weight percentage of cellulose nanofibrils are designated as PU, NPU1, NPU2, NPU3 and NPU4, respectively.

3.5.1 FTIR Analysis

Fourier transform infrared spectroscopy is used to analyze the chemical structure of polyurethane and its nanocomposites. FTIR spectra and various prominent peaks of lignopolyol based polyurethane and its nanocomposites are shown in Figure 21 and table 9, respectively. A broad band at 3320-3324 cm^{-1} can be related to the hydrogen bonded -NH stretching vibrations of urethane linkage or due to O-H stretching vibration of cellulose seen in all the spectra except for NPU4 which may be due to agglomeration of fibers at higher concentration resulting in the decreased interaction of hard and soft segment.

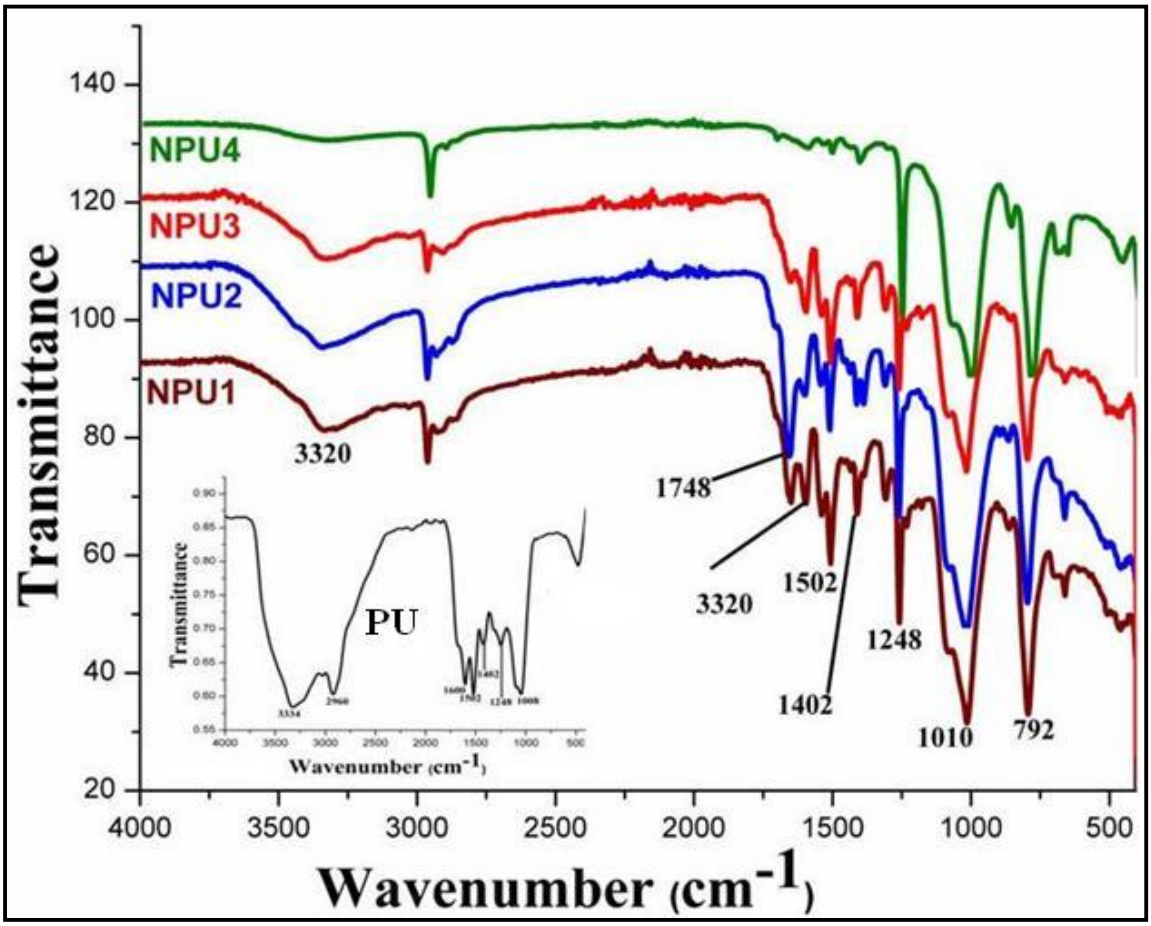

Figure 21: FTIR spectra's of lignopolyol based polyurethane and its nanocomposites with varying filler concentration

The peak at 2960-2970 cm^{-1} is due to asymmetric stretching vibrations of $–CH_2$. Peaks at 1734-1748 cm^{-1} correspond to urethane and ester stretching vibrations that corroborate the infusion of hard and soft segment in polyurethane matrix. Further as the filler concentration increase from 2.5 to 15% the carbonyl stretching peaks are displaced from 1734 to 1748 cm^{-1} suggesting that the reinforcement of CNF in PU matrix resulted in distortion of NH and C=O hydrogen bonding and improved micro phase separation between hard and soft segments because of increased interaction of CNF and PU matrix. Peaks between 1600-1648cm^{-1} and 1502-1510cm^{-1} are due to C=O stretching vibration of urea and C-N stretching or N-H out of plane bending.

The peak at 1402 -1404 cm^{-1} seen only in case of PU/CNF nanocomposites correspond to skewing of C-H bond thereby exhibiting the crystalline behavior of reinforced cellulose nanofibers. Bands at 1248-1252 cm^{-1} and 1008-1010 cm^{-1} relate to the stretching vibration of C-

N and C-O, respectively thereby affirming the formation of urethane linkages between lignopolyol hydroxyl and NCO group of isocyanates. Further, the disappearance of isocyanate peak at 2270 cm^{-1} confirmed the completion of reaction. The PU/CNF nanocomposites showed similar peaks but with the varying intensities. The intensity of the peak at 3320 cm^{-1}due to cellulose O-H stretching vibrations and N-H stretching vibrations decreases with increase in filler concentration and almost disappeared for nanocomposites with 15% CNF concentration that may be due to hydroxyl groups on cellulose reacting with isocyanate during PU synthesis. Overall, it was observed from the FTIR spectra that CNF reinforcement does not affect the structure and hydrogen bonding between NH and C=O of polyurethane till 10% CNF concentration beyond which the intensity of urethane linkage starts decreasing.

Table 9: Prominent peaks with their corresponding band description of lignopolyol based polyurethane/cellulose nanofibers (PU/CNF) nanocomposites

Observed Peaks/Bands	**Bands Descriptions**
3320-3324	-NH stretching vibrations of Urethane or O-H stretching vibration of cellulose [438,439]
2960-2970	Asymmetric $–CH_2$ stretching vibrations [440]
1734-1748	Urethane and ester stretching vibrations [441]
1600-1648	C=O urea stretching [443]
1502-1510	C-N stretching or N-H out of plane bending [443]
1402 -1404	C-H bond deformation [441]
1248-1252	Stretching vibration of C-N [438]
1008-1010	C-O stretching vibration [439]

XRD Analysis

X-ray diffraction techniquewas used to get information regarding crystalline behavior of PU/CNF nanocomposites films. Figure 22 shows the XRD patterns of cellulose nanofibers and lignopolyol based polyurethane nanocomposites.From the figure, it was observed that cellulose nanofibers show three peaks at 12.5°, 20.5° and 22.6° 2θ angle, respectively. Where peak at 12.5° and 20.5° 2θ angles correspond to cellulose II, peak at 22.6° 2θ angle corresponds to native cellulose I revealing the coalescenceof cellulose I and II that has already been explained. For lignopolyol/cellulose nanofibers based polyurethane nanocomposites only a broad hump was observed between 20-23° 2θ till 10% CNF concentration beyond which a single peak at 22.6° 2θ angle was seen, confirming that the cellulose nanofibers were well dispersed in PU matrix up to 10% filler concentration.This may be due to the strong interaction between carbonyl group of PU matrix and hydroxyl group of CNF originating from hydrogen bonding. But beyond 10% filler concentration CNFs started agglomeratingas also confirmed from SEM results. This agglomeration may be either due to the high surface energyof cellulose or due to the hydrophilic character of the cellulose that causes the irreversible agglomeration because of the formation of additional hydrogen bonds between the amorphous parts of the CNFs.

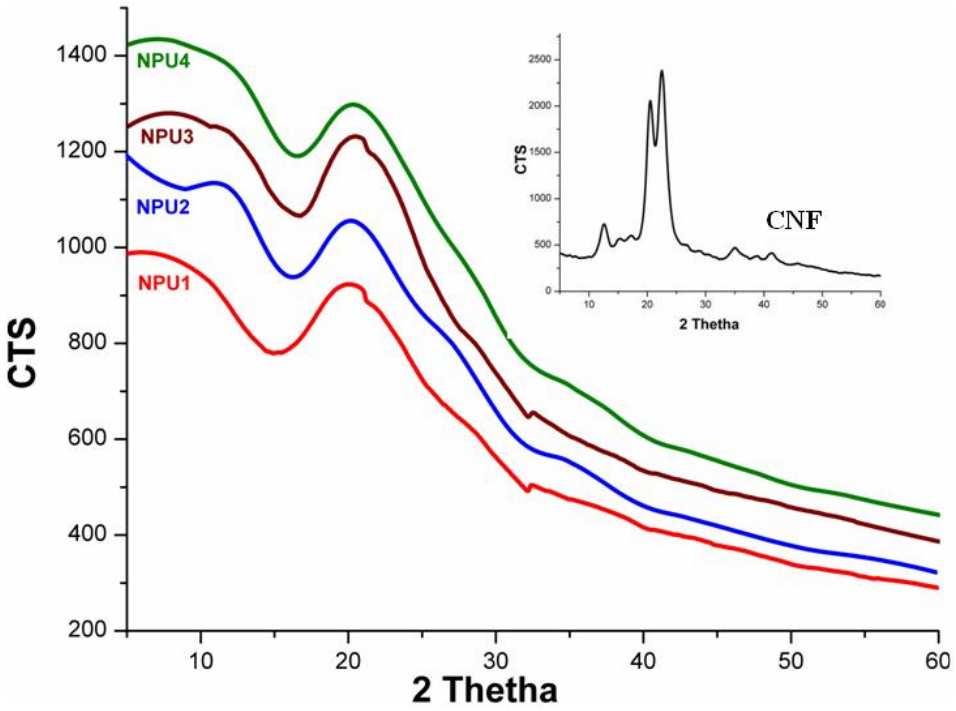

Figure 22: X-ray diffractograms of lignopolyol based polyurethane and its nanocomposite with varying filler concentration

SEM Analysis

The various properties of polyurethane nanocomposites not only depend on the interactionsbetween soft and hard segments or the interaction of PU matrix with fillers but also on the micro phase structure and level of dispersion of nanofibers that can be well studied by SEM analysis.SEM images of CNF, neat PU and (PU/CNF)nanocompositeswith varying filler concentrations are shown in figure 23. From SEM images of PU/CNF nanocomposites (figure 23 (c-f), it was observed that CNFs are homogeneously dispersed in polyurethane matrix. PU is visible as amorphous phase in the background and CNFs are seen as fibers. The structure is intact and there is a good adhesion between PU and CNF as seen in SEM images.

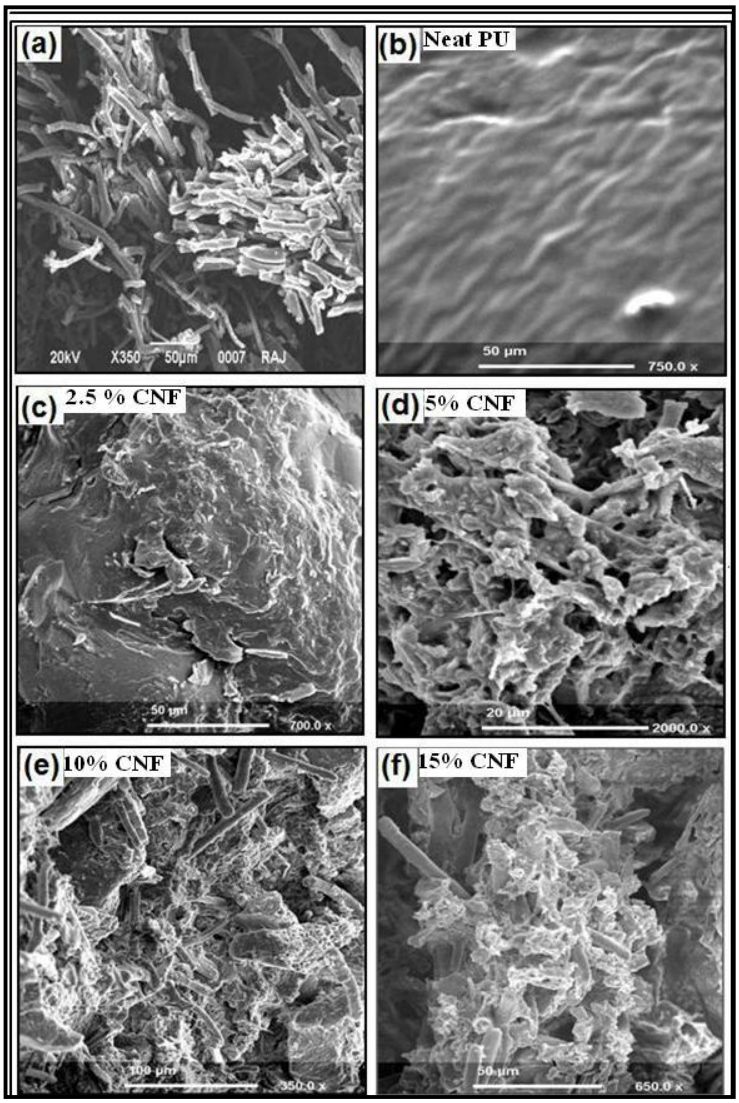

Figure 23: SEM micrographs of lignopolyol based polyurethane and its nanocomposites with varying filler concentration

It was also observed that the structure of fractured PU/CNF nanocomposites with 2.5 wt% (figure 25 (c)) filler concentration was not much affected with the incorporation of cellulose nanofibers and only small white dots were seen on the overall surface. This is due to the fact that at lower filler concentration cellulose nanofibers are uniformly dispersed in the polyurethane matrix because of the strong hydrogen bonding that results in good adhesion of CNF with PU matrix. However, fibers bundles were observed for PU/CNF nanocomposites with 5, 10 and 15% filler concentration. Moreover, cellulose nanofibers were uniformly dispersed throughout the surface of polyurethane matrix up to 10% filler concentration beyond which complete agglomerated fibers were seen. This agglomeration may be attributed to the weak interaction of polymer matrix and cellulose nanofibers at higher filler loading. These results are in coherence with XRD results.

Overall, from SEM results, it was concluded that the morphology of PU/CNF nanocomposites was influenced by crystalline structure of cellulose nanofibers and presence of surface hydroxyl groups that has lead an excellent interaction between CNF and polymer matrix. This homogenous dispersion and good interaction results in enhanced physical, thermal and mechanical properties of the nanocomposites.

Tensile Testing Analysis

The mechanical properties of the neat PU and PU nanocomposite films were measured under tensile stress at room temperature. Stress vs. Strain curve of neat and polyurethane nanocomposites with varying filler content is shown in figure 24 (i). Tensile strength, Young's modulus and % elongations obtained from tensile measurements are summarized in table 10. Also the variation in Young's modulus and % elongation with varying filler concentration is shown in figure 24(ii). From these results it was observed that the cellulose nanofibers have profound effect on the mechanical properties of polyurethane nanocomposites. From the results, it is clearly seen that the tensile strength and Young's modulus increases while the percent elongation decreases with incorporation of cellulose nanofibers into PU matrix. The increase in tensile properties may be attributed to the formation of new interconnected cellulosic network facilitated by their flexibility due to high aspect ratio and the presence of amorphous domain along the nanofibrils. Nevertheless, other important parameters that explain the better mechanical properties of CNF based nanocomposites are network structure of lignopolyol

structure and high tensile strength (0.3-22 GPa) of cellulose nanofibers. However, it was observed that tensile properties of CNF reinforced polyurethane nanocomposites showed an improvement up to 10% filler concentration beyond which a slight decrease was observed. This decrease in tensile properties may attributed to aggregation of the nanofibers, driven by their high affinity for each other [457]. As, the agglomeration may result in commencement and proliferation of cracks thereby reducing the strength of nanocomposites. The factors important for enhanced tensile strength and Young's modulus are aspect ratio, fiber interaction between filler and polymer matrix and dispersion of filler. The mechanical properties of PU/CNF were found to be comparable with nanocomposite synthesized using other fibers such as kenaf fibers.

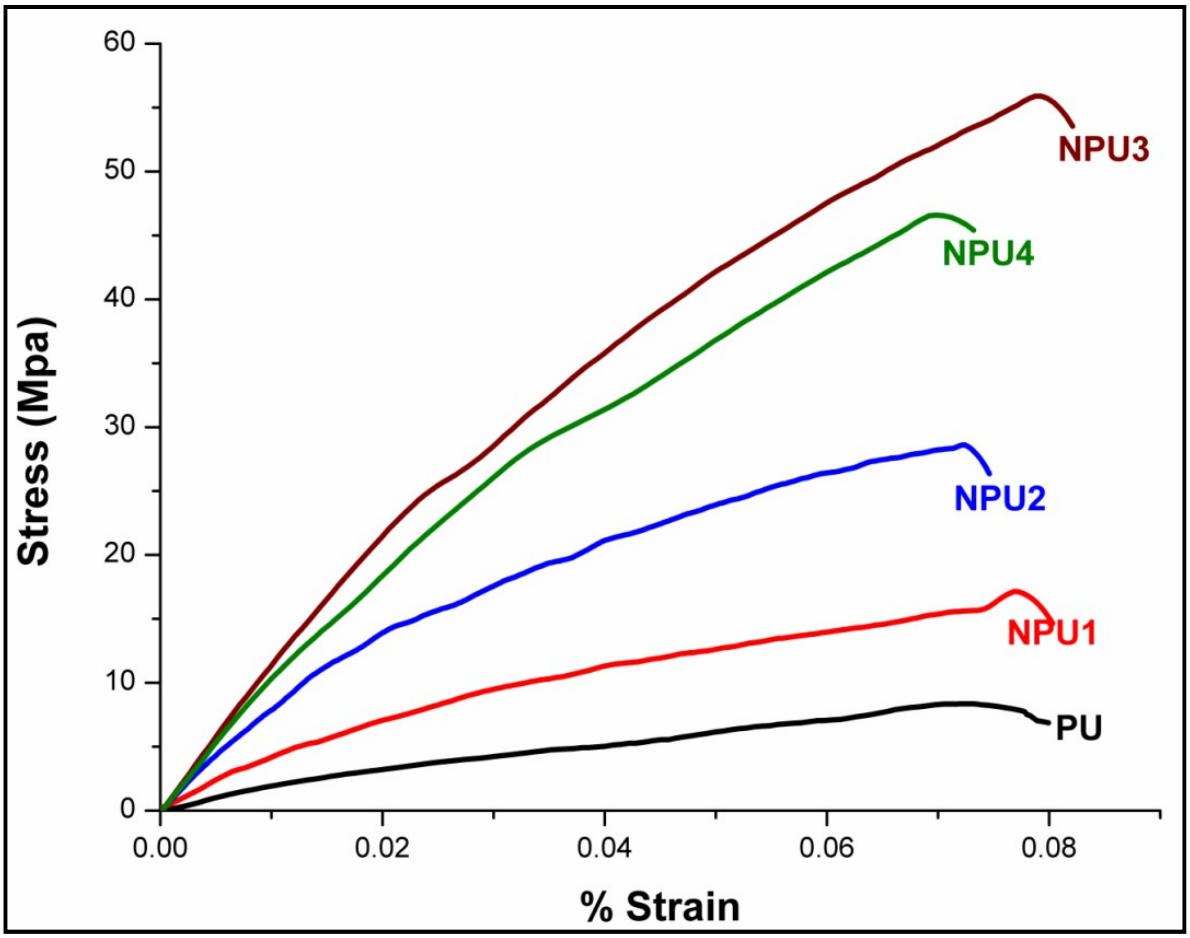

Figure 24(i): Stress vs. Strain curve of lignopolyol based polyurethane and its nanocomposites with varying filler concentration

Table 10: Tensile Strength, % elongation and Young's modulus of lignopolyol based polyurethane/cellulose nanofibers (PU/CNF) nanocomposites

Sample	Tensile Strength(MPa)	% Elongation	Young's Modulus (MPa)
PU1	8.4± 0.4	144±4.2	247.06±8.7
NPU1	16.5± 0.3	136±6.8	402.44±18.2
NPU2	27.9± 0.5	123.2±9.2	429.23±20.6
NPU3	54.5± 0.4	97.6±14.2	801.47±21.8
NPU4	46.8± 0.3	110.4±16.6	557.14±23.2

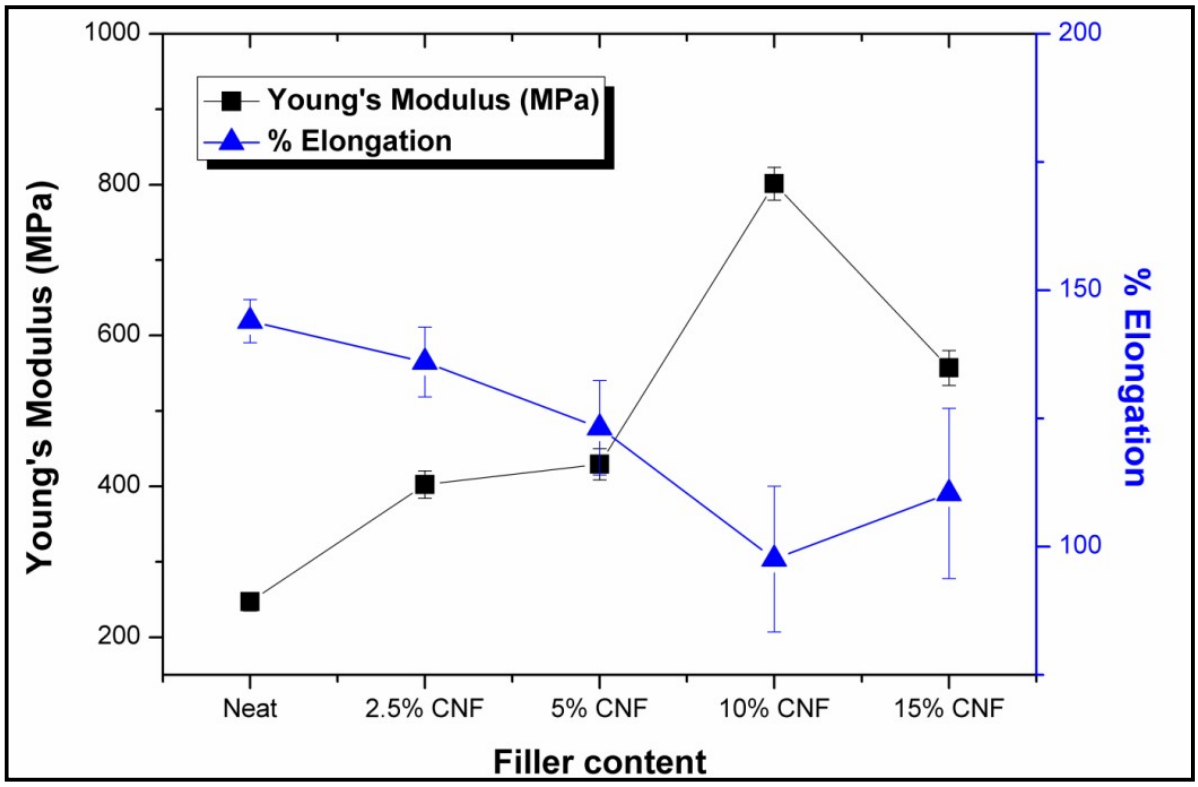

Figure 24(ii): Young's modulus and % elongation vs. filler content of lignopolyol based polyurethane and its nanocomposites with varying filler concentration

TGA Analysis

Thermogravimetric analysis (TGA) is a powerful technique for the measurement of thermal stability of materials including polymers. In this method, changes in the weight of a specimen are measured while its temperature is increased. Moisture and volatile contents of a sample can be measured by TGA. Thermo gravimetric analysis (TGA) was performed on the neat and cellulose nanofibers reinforced lignopolyol based polyurethanes nanocomposites and the % mass loss due to valorization of the products was monitored.

Figure 25 (i) and 25 (ii) show the TGA and DTGA curves of lignopolyol/CNF based polyurethane nanocomposites films with varying filler concentration. The thermal degradation parameters such as T_{onset}, T_{max}, their corresponding mass loss and % mass residue at 700 °C are given in table 11.

From the figures, two stage thermal decomposition was observed for neat and CNF reinforced polyurethanes, where the first decomposition at a T_{max} of 282-300 °C corresponds to the urethane linkage and the second at a T_{max} of 460-500 °C may be either due to chain scission at the β-position to the carbon-carbon double bond of polyurethane matrix or may be due to the formation of new bonds by the reaction of MDI and hydroxyl groups of cellulose nanofibers.

From the results it was seen that for the 1st degradation stage, the T_{max} varies from 282-300 °C and T_{onset} temperature increases with increase in filler concentration up to 10% CNF, beyond which it decreases. The increase in thermal stability up to 10% that may be due to enhanced molecular interaction of polyurethane matrix with cellulose nanofibers because of the polar nature of both cellulose nanofibers and polyurethane matrix and also due to the strong hydrogen bonding of PU/CNF nanocomposites generated because of the hydroxyl groups of cellulose thereby resulting in uniform and homogeneous dispersion of cellulose nanofibers in polyurethane matrix as also evidenced from earlier results.

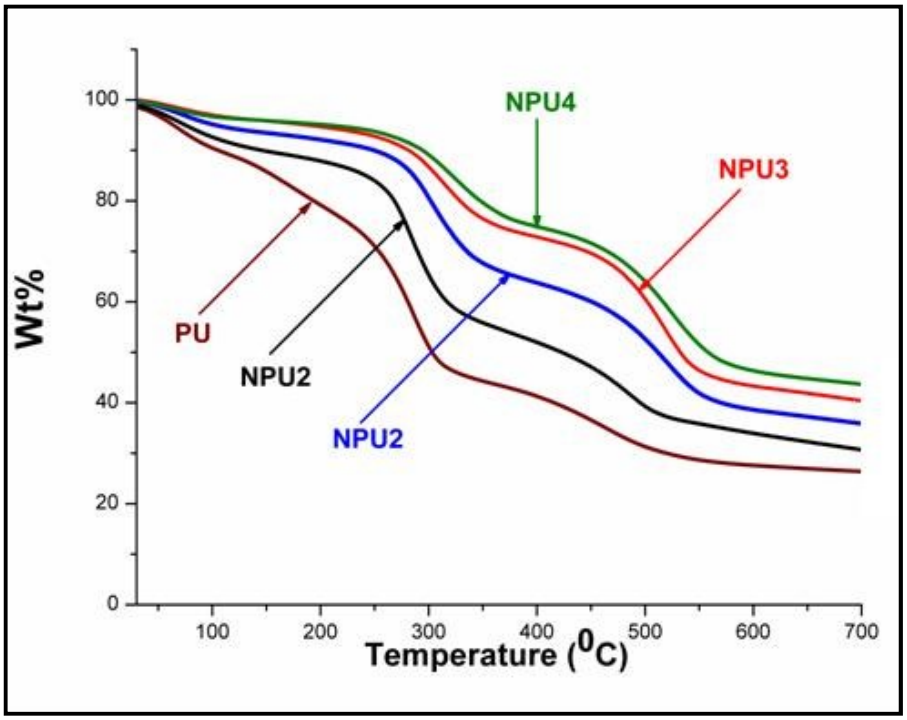

Figure 25(i): TGA curves of lignopolyol based polyurethane and its nanocomposites with varying filler concentration

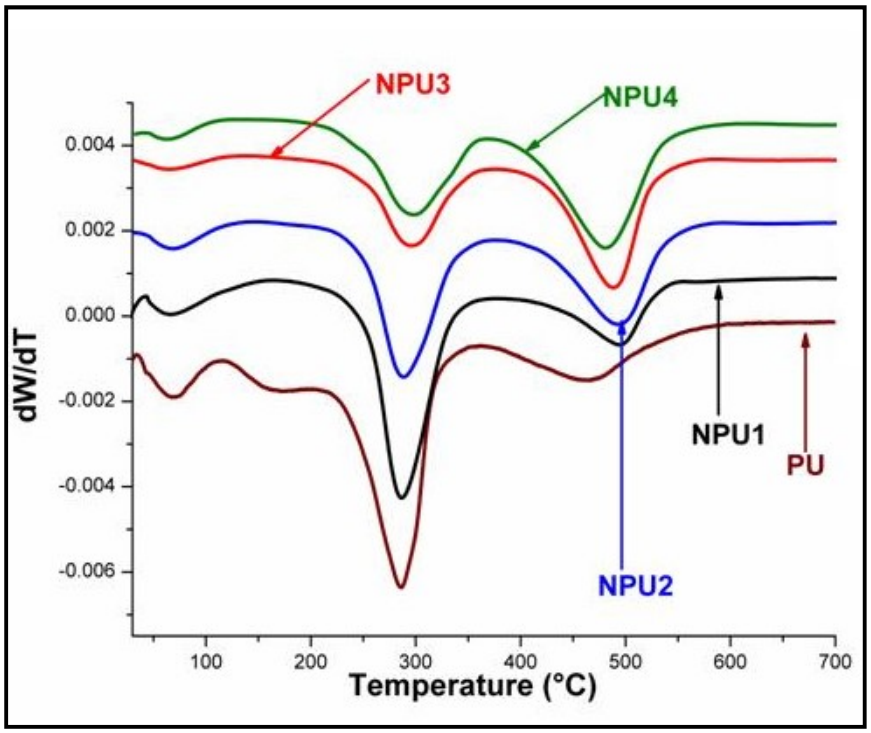

Figure 25(ii): DTGA curves of lignopolyol based polyurethane and its nanocomposites with varying filler concentration

Table 11: Thermal degradation characteristics of lignopolyol based polyurethane/cellulose nanofibers (PU/CNF) nanocomposites

	1st Thermal event			2nd Thermal event			
Sample ID	**T_{onset} (^oC)**	**T_{max} (^oC)**	**%Mass loss at T_{max}**	**T_{onset} (^oC)**	**T_{max} (^oC)**	**%Mass loss at T_{max}**	**% Mass Residue at 700 ^oC**
PU	220	282	40.96	380	460	66.52	27.50
NPU1	240	290	36.31	430	495	64.65	30.58
NPU2	248	296	24.40	440	500	58.24	34.95
NPU3	276	300	34.71	450	506	49.06	38.76
NPU4	262	294	19.92	438	483	53.31	44.81

The decrease in thermal stability beyond 10% may be attributed to aggregation of cellulose nanofibrils at higher filler loading. The same trend was observed for the 2nd degradation stage which may be due to due to increase of cellulose concentration that results in the formation of new bonds and increase in hydrogen bonding which enhances the thermal stability. Further, % mass residue at 700 ^oC also increased with increase in filler concentration indicating the higher thermal stability of PU/CNF nanocomposites as higher is the %mass residue higher is the thermal stability. Results are in coherence with those reported in the literature.Thermal stability of PU/CNF nanocomposites was found to either higher or similar as compared to PU nanocomposites with other nanofillers such as grapheme, carbon nanotubes and nanoclay.

Hydrolytic Degradation of Polyurethane Nanocomposites in Phosphate Buffer Saline (PBS) with pH =7.4

Biodegradable polymer nanocomposites are important class of materials for biomedical application. All biodegradable polymers contain hydrolysable bonds and hence primarily they are easily degraded by adopting the hydrolytic and enzymatic degradation mechanism. To a lesser extent, they can also be degraded by oxidation that leads to the crack formation and propagation. Some of the important parameters affecting the biodegradability of polymers

include type of chemical bond, polymer crystallinity, hydrophilicity, composition, pH value, molecular weight, morphology and glass transition temperature. Among these type of chemical bond and time dependent molecular weight are the two most commonly used parameters to determine the degradation rate as the type of chemical bond determines the rate of hydrolysis.

Depending on the application, the degradation behavior of polyurethane can be tailored by altering ratio of hard to soft segments. However, the soft segment contents are considered as the degradation rate controlling parameters as it leads to the formation of degradable chemical bonds. These chemical bonds along with fragments containing urethane and urea with acid terminal groups are degraded by the presence of acids or alkaline compounds. Further, degradation of urethane groups to free polyamines can occur depending on the type of diisocyanate used. Generally,the degradation of polyurethane takes place in several steps. Initially, the non-crystalline regions react with water molecules resulting in increase in chain mobility that reconstructs them into new and more defective crystals. Thereafter, the rate of degradation is increased due to the autocatalytic effect arising from the acidic nature of carboxyl/hydroxyl end groups. Finally, the complete hydrolysis occurs at the crystalline region.

Hydrolytic degradation of polyurethane started with the diffusion of water in the amorphous or semicrystalline regions that leads to the breakage of ester bonds. Mobility of polymer chains within the amorphous regions increased after chain scission. No appreciable reduction in the sample weight takes place indicating they could remain inside the polyurethane network structure as reported in the literature. Thereafter,an increase in weight loss was observed due to increase of -COOH/-OH end-groups which act as auto catalyst and accelerate the degradation process, resulting in shorter and more number of polymeric chains. Finally, the crystalline regions become susceptible to hydrolysis. Further, the incorporation of cellulose nanofibers also had a significant effect on the biodegradability as the reinforcement of cellulose nanofibers in polyurethane affects the microphase separation structure. In fact, the nanofiller consist of rigid domains that establish physical interactions with the polymer chains of the polyurethane by mean of their surface chains and entities. It was observed that with increase in % CNF loading, % weight loss increases. The amount of weight loss of polyurethane nanocomposite in phosphate buffer saline (pH≈7.4) in 1, 2, 4, 6 and 8 weeks was obtained as explained earlier section and is shown in figure 26.

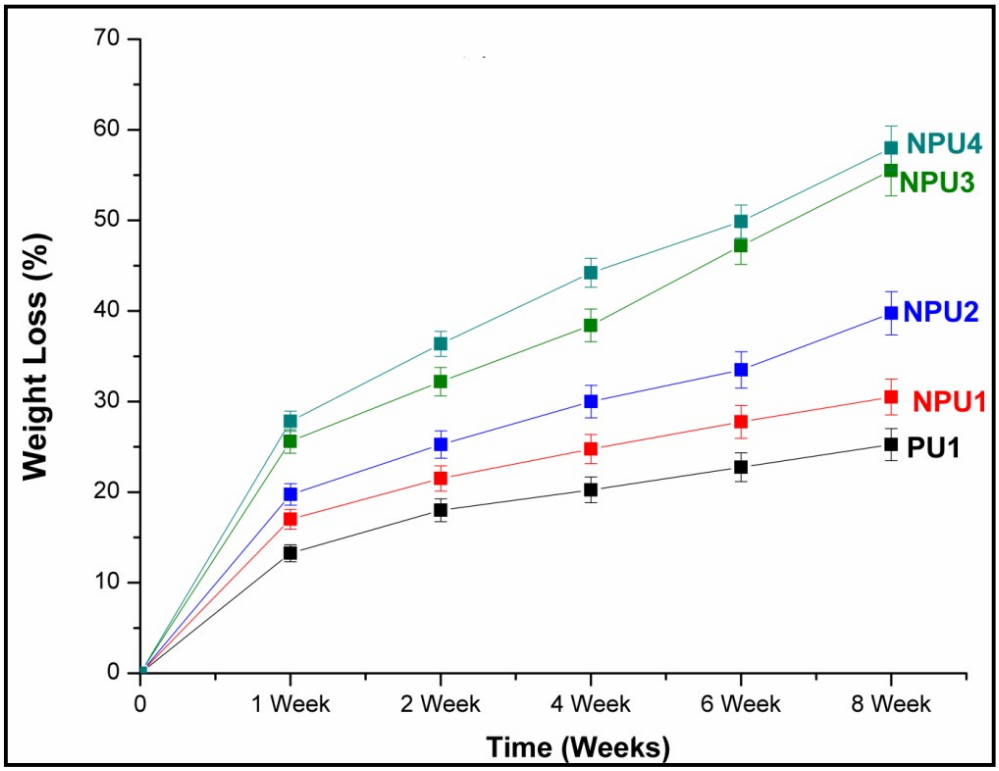

Figure 26: Percent Weight loss Vs. Time of lignopolyol based polyurethane nanocomposite with varying filler concentration from 0-15%

From the figure 3.26, it was observed that % weight loss after 8 weeks for neat polyurethane was 25.12%. With increase in filer content from 0 to 15% (w/w), % weight loss increased from 25.12 to 57.58%. This increase in weight loss may be attributed to the hydrophilic nature of cellulose nanofibers. Incorporation of hydrophilic component in polymer matrix can enhance water sorption and that might result in improved rate of hydrolysis of ester bonds present in polyurethane structure. Further, no decrease in the biodegradability was seen beyond 10% CNF concentration which may be also be due to the fact that with increasing amount of highly hydrophilic material in the nanocomposite film, possible infiltration of water molecules in the interfacial filler/matrix zone takes place. The higher the cellulose nanofiller content higher is the interfacial area and thus the possible interfacial water infiltration increases, which leads to higher chain scission rate and therefore, results in increase in % weight loss of polymer. Moreover, it was seen that the increase in percent weight loss was not much pronounced beyond 10% filler concentration thus PU nanocomposite with 10% CNF composition can be regarded as the suitable material for further applications.For this composition, the mechanical and thermal properties were also better than other nanocomposites.

Furthermore, the effects of degradation products on the pH value of the medium were also evaluatedwithout refreshing the medium during the biodegradation period. It was observed that during the 8 weeks' degradation, value of pH decreased to 7.1 from 7.4. This decrease in pH value may be due to acidic groups released during the degradation of lignopolyol or 1, 4-butanediol.

Overall, it was concluded that hydrolytic degradation of lignopolyol based polyurethane is greatly influenced by the incorporation of cellulose nanofibers.

Antimicrobial Activities of Lignopolyol/CNF based Polyurethane Nanocomposites

Polymers and its nanocomposite being used for biomedical applications must possess antimicrobial activity and protection against biofilm formation by microorganism. Staphylococcus aureus (*S. Aureus*) and Escherichia Coli (*E.coli*) are among the most common pathogens and are related to many infections including wounds, postoperative infections and prosthetic infections taking place using the use of catheters, endotracheal tubes and other biomaterials.

In the present study the antimicrobial activity of lignopolyol based polyurethane nanocomposite films containing cellulose nanofibers as nanofiller was determined against Gram-positive *S. aureus* and Gram-negative *E. coli* microorganisms. It is well known fact that polyurethane inherently does not possess any antimicrobial activity and can be induced by addition of a compound with antimicrobial activities. Cellulose nanofibers with a three dimensional non-woven network an highly hydrophilic nature exhibits excellent physical and mechanical properties such as high water absorption capacity, tensile strength, good permeability, crystallinity and biocompatibility that make them suitable for various biomedical applications. Hence cellulose nanofibers can also be explored for antimicrobial activity.The antimicrobial activities of polyurethane nanocomposite studies as explained in section 2.8.14 and are shown in figure 27(i) and 27(ii). From the figures no change in the color of the suspension containing films was observed which shows that all the nanocomposites films were capable of inhibiting the growth of the colonies of *E. coli* and *S. aureus*. However, the nanocomposite films were found to be more effective in inhibiting the growth of *E. coli* than *S. aureus*. Further, it was also seen that with increase in % CNF loading in polyurethane, appreciable increase in antimicrobial activity towards *S. aureus*and*E. Coli*whichcan be clearly seen from the images as the suspension containing film with 15% CNF loading was more clear. This increase in antimicrobial activity

may be attributed to the porous network structure if nanocellulose that promotes the transfer of antibiotics or other medicines serving as efficient physical barrier against any external infection [476].

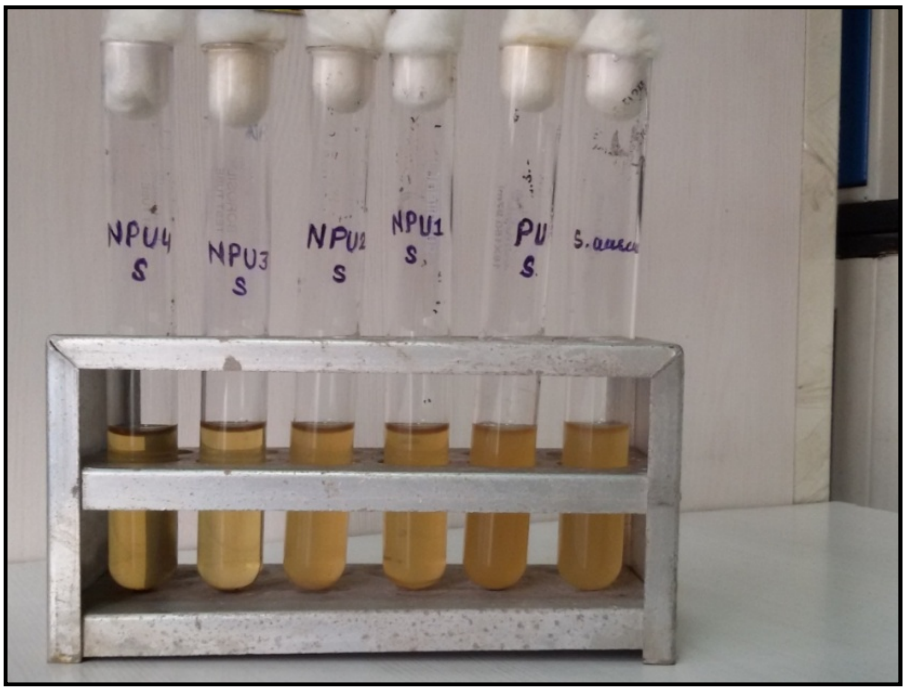

Figure 27 (i): Antimicrobial activity of lignopolyol based polyurethane nanocomposite with varying filler concentration from 0-15% against *S.aureus*

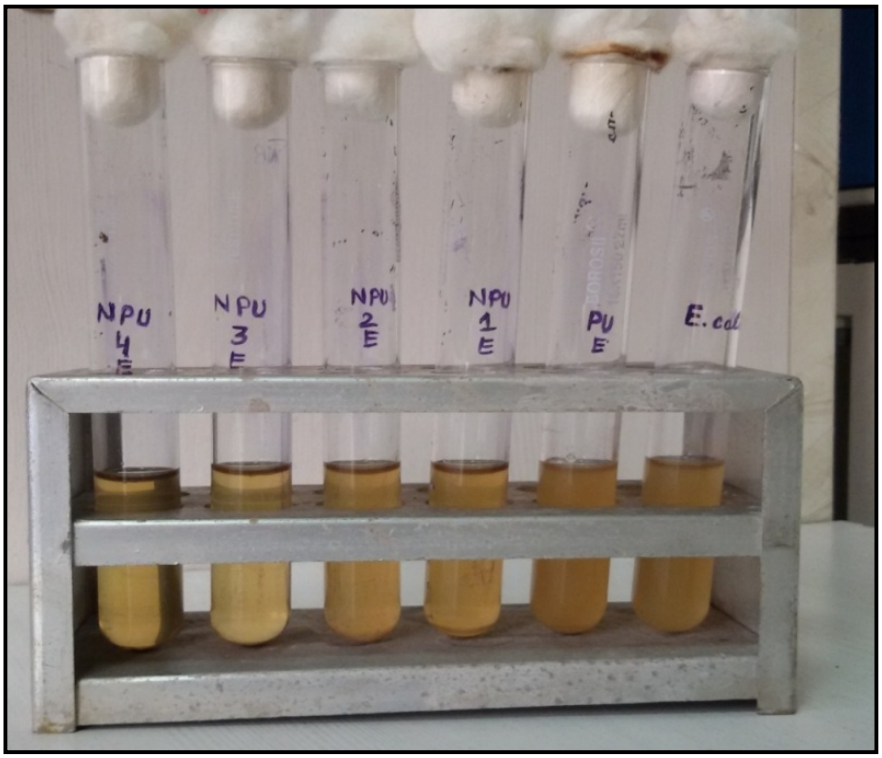

Figure 3.27 (ii): Antimicrobial activity of lignopolyol based polyurethane nanocomposite with varying filler concentration from 0-15% against *E.coli*

Further, it was also observed that with increase in % CNF loading in polyurethane, appreciable increase in activity towards *S. aureus* was observed than that of *E. coli*. The difference may be attributed to the difference in the bacterium cell structures and result of surrounding environmental factors.

Overall it was concluded that the lignopolyol based polyurethane nanocomposite films can inhibit the bacterial growth, thus can be optimally utilized in biomedical field.

REFERENCES

[1] D.J. David, H.B. Staley, Analytical chemistry of the polyurethanes, Wiley-Interscience Publications1969.

[2] M.A. Hood, B. Wang, J.M. Sands, J.J. La Scala, F.L. Beyer, C.Y. Li, Morphology control of segmented polyurethanes by crystallization of hard and soft segments, Polymer 51(10) (2010) 2191-2198.

[3] K. Nakamae, T. Nishino, S. Asaoka, Sudaryanto, Microphase separation and surface properties of segmented polyurethane; Effect of hard segment content, International Journal of Adhesion and Adhesives 16(4) (1996) 233-239.

[4] M. Xu, W.J. MacKnight, C.H.Y. Chen, E.L. Thomas, Structure and morphology of segmented polyurethanes: 1. Influence of incompatability on hard-segment sequence length, Polymer 24(10) (1983) 1327-1332.

[5] S. Mondal, D. Martin, Hydrolytic degradation of segmented polyurethane copolymers for biomedical applications, Polymer Degradation and Stability 97(8) (2012) 1553-1561.

[6] P.C. Caracciolo, A.A.A. de Queiroz, O.Z. Higa, F. Buffa, G.A. Abraham, Segmented poly(esterurethane urea)s from novel urea-diol chain extenders: Synthesis, characterization and in vitro biological properties, Acta Biomaterialia 4(4) (2008) 976-988.

[7] L.H. Chan-Chan, R. Solis-Correa, R.F. Vargas-Coronado, J.M. Cervantes-Uc, J.V. Cauich-Rodriguez, P. Quintana, P. Bartolo-Perez, Degradation studies on segmented polyurethanes prepared with HMDI, PCL and different chain extenders, Acta Biomaterialia 6(6) (2010) 2035-2044.

[8] M. Behl, A. Lendlein, Shape-memory polymers, Materials Today 10(4) (2007) 20-28.

[9] C. Liu, H. Qin, P.T. Mather, Review of progress in shape-memory polymers, Journal of Materials Chemistry 17(16) (2007) 1543-1558.

[10] J.T. Garrett, J. Runt, J.S. Lin, Microphase Separation of Segmented Poly(urethane urea) Block Copolymers, Macromolecules 33(17) (2000) 6353-6359.

[11] L. Ning, W. De-Ning, Y. Sheng-Kang, Crystallinity and hydrogen bonding of hard segments in segmented poly(urethane urea) copolymers, Polymer 37(16) (1996) 3577-3583.

[12] A. Saiani, W.A. Daunch, H. Verbeke, J.W. Leenslag, J.S. Higgins, Origin of Multiple Melting Endotherms in a High Hard Block Content Polyurethane. 1. Thermodynamic Investigation, Macromolecules 34(26) (2001) 9059-9068.

[13] A. Noshay, J.E. McGrath, Block copolymers: Overview and Critical survey., Academic Press, New York, 1977.

[14] V.P. Privalko, V.P. Azarenkov, A.V. Baibak, A.A. Usenko, Thermodynamic characterization of segmented polyurethanes, Thermochimica Acta 285(1) (1996) 155-165.

[15] E. Yılgör, İ. Yılgör, E. Yurtsever, Hydrogen bonding and polyurethane morphology. I. Quantum mechanical calculations of hydrogen bond energies and vibrational spectroscopy of model compounds, Polymer 43(24) (2002) 6551-6559.

[16] C. Li, J. Liu, J. Li, F. Shen, Q. Huang, H. Xu, Studies of 4,4-diphenylmethane diisocyanate (MDI)/1,4-butanediol (BDO) based TPUs by in situ and moving-window two-dimensional correlation infrared spectroscopy: Understanding of multiple DSC endotherms from intermolecular interactions and motions level, Polymer 53(23) (2012) 5423-5435.

[17] F. Khan, J.-H. Koo, D. Monk, E. Eisbrenner, Characterization of shear deformation and strain recovery behavior in shape memory polymers, Polymer Testing 27(4) (2008) 498-503.

[18] A. Lendlein, R. Langer, Biodegradable, elastic shape-memory polymers for potential biomedical applications, Science 296(5573) (2002) 1673–1676.

[19] P. Ping, W. Wang, X. Chen, X. Jing, Poly (e-caprolactone) Polyurethane and Its Shape-Memory Property Biomacromolecules 6(2) (2005) 587-592.

[20] I. Surovtsova, Effects of compliance mismatch on blood flow in an artery with endovascular prosthesis, Journal of Biomechanics 38(10) (2005) 2078-2086.

[21] O.F. Bertrand, R. Sipehia, R. Mongrain, J. Rodes, J.C. Tardif, L. Bilodeau, G. Cote, M.G. Bourassa, Biocompatibility aspects of new stent technology, Journal of the American College of Cardiology 32(3) (1998) 562-371.

[22] P. Tao, P. Gibula, Y. Kang-de, M.F.A. Goosen, Role of polymers in improving the results of stenting in coronary arteries, Biomaterials 17(7) (1996) 685-694.

[23] A. Lendlein, S. Kelch, Shape-Memory Polymers, Angewandte Chemie International Edition 41(12) (2002) 2034-2057.

[24] B. Yan, S. Gu, Y. Zhang, Polylactide-based thermoplastic shape memory polymer nanocomposites, European Polymer Journal (In Press).

[25] J. Leng, X. Lan, Y. Liu, S. Du, Shape-memory polymers and their composites: Stimulus methods and applications, Progress in Materials Science 56(7) (2011) 1077-1135.

[26] K. Gall, M.L. Dunn, Y. Liu, D. Finch, M. Lake, N.A. Munshi, Shape memory polymer nanocomposites, Acta Materialia 50(20) (2002) 5115-5126.

[27] I.S. Gunes, C. Perez-Bolivar, F. Cao, G.A. Jimenez, P. Anzenbacher, S.C. Jana, Analysis of non-covalent interactions between the nanoparticulate fillers and the matrix polymer as applied to shape memory performance, Journal of Materials Chemistry 20(17) (2010) 3467-3474.

[28] Q. Meng, J. Hu, A review of shape memory polymer composites and blends, Composites Part A: Applied Science and Manufacturing 40(11) (2009) 1661-1672.

[29] V. Favier, G.R. Canova, J.Y. Cavaillé, H. Chanzy, A. Dufresne, C. Gauthier, Nanocomposite materials from latex and cellulose whiskers, Polymers for Advanced Technologies 6(5) (1995) 351-355.

[30] V. Favier, H. Chanzy, J.Y. Cavaille, Polymer Nanocomposites Reinforced by Cellulose Whiskers, Macromolecules 28(18) (1995) 6365-6367.

[31] H. Yano, J. Sugiyama, A.N. Nakagaito, M. Nogi, T. Matsuura, M. Hikita, K. Handa, Optically Transparent Composites Reinforced with Networks of Bacterial Nanofibers, Advanced Materials 17(2) (2005) 153-155.

[32] M.A.S. Azizi Samir, F. Alloin, A. Dufresne, Review of Recent Research into Cellulosic Whiskers, Their Properties and Their Application in Nanocomposite Field, Biomacromolecules 6(2) (2005) 612-626.

[33] K.G. Satyanarayana, G.G.C. Arizaga, F. Wypych, Biodegradable composites based on lignocellulosic fibers; An overview, Progress in Polymer Science 34(9) (2009) 982-1021.

[34] I. Siro, D. Plackett, Microfibrillated cellulose and new nanocomposite materials: A Review, Cellulose 17(3) (2010) 459-494.

[35] A. Kaushik, M. Singh, Isolation and characterization of cellulose nanofibrils from wheat straw using steam explosion coupled with high shear homogenization, Carbohydrate research 346(1) (2011) 76-85.

[36] M.A.S. Azizi Samir, F. Alloin, J.-Y. Sanchez, N. El Kissi, A. Dufresne, Preparation of cellulose whiskers reinforced nanocomposites from an organic medium suspension, Macromolecules. 37 (2004) 1386–1393.

[37] A. Šturcová, G.R. Davies, S.J. Eichhorn, Elastic modulus and stress-transfer properties of tunicate cellulose whiskers, Biomacromolecules. 6 (2005) 1055–1061.

[38] X. Cao, H. Dong, C.M. Li, New nanocomposite materials reinforced with flax cellulose nanocrystals in waterborne polyurethane, Biomacromolecules. 8 (2007) 899–904.

[39] F.G. Calvo-Flores, J.A. Dobado, Lignin as renewable raw material, ChemSusChem. 3 (2010) 1227–1235.

[40] R.W. Thring, M.N. Vanderlaan, S.L. Griffin, Polyurethanes from Alcell® lignin, Biomass and Bioenergy. 13 (1997) 125–132.

[41] R.J.A. Gosselink, E. De Jong, B. Guran, A. Abächerli, Co-ordination network for lignin—standardisation, production and applications adapted to market requirements (EUROLIGNIN), Ind. Crops Prod. 20 (2004) 121–129.

[42] C.A. Cateto, M.F. Barreiro, A.E. Rodrigues, Monitoring of lignin-based polyurethane synthesis by FTIR-ATR, Ind. Crops Prod. 27 (2008) 168–174.

[43] S. Sarkar, B. Adhikari, Synthesis and characterization of lignin–HTPB copolyurethane, Eur. Polym. J. 37 (2001) 1391–1401.

[44] D. Stewart, Lignin as a base material for materials applications: Chemistry, application and economics, Ind. Crops Prod. 27 (2008) 202–207.

[45] E. Sjöström, Wood polysaccharides, Wood Chem. Fundam. Appl. (1993) 51–70.

[46] K.V. Sarkanen, C.H. Ludwig, Liguins. Occurrence, formation, structure, and reactions, New York.; Wiley-Interscience, 1971.

[47] F. Schulze, Beitrage zur Kenntniss des lignins, Chem Zentr. 21 (1857) 321–325.

[48] E.A.B. da Silva, M. Zabkova, J.D. Araújo, C.A. Cateto, M.F. Barreiro, M.N. Belgacem, A.E. Rodrigues, An integrated process to produce vanillin and lignin-based polyurethanes from Kraft lignin, Chem. Eng. Res. Des. 87 (2009) 1276–1292.

[49] J. Zakzeski, P.C.A. Bruijnincx, A.L. Jongerius, B.M. Weckhuysen, The catalytic valorization of lignin for the production of renewable chemicals, Chem. Rev. 110 (2010) 3552–3599.

[50] R. Benedikt, M. Bamberger, Über eine quantitative Reaction des Lignins, Monatshefte Für Chemie/Chemical Mon. 11 (1890) 260–267.

[51] E. Adler, Lignin chemistry—past, present and future, Wood Sci. Technol. 11 (1977) 169–218.

[52] K. Freudenberg, Biosynthesis and constitution of lignin, Nature. 183 (1959) 1152–1155.

[53] K. Freudenberg, Zur Kenntnis der Cellulose, Eur. J. Inorg. Chem. 54 (1921) 767–772.

[54] F.S. Chakar, A.J. Ragauskas, Review of current and future softwood kraft lignin process chemistry, Ind. Crops Prod. 20 (2004) 131–141.

[55] K. Freudenberg, Lignin: its constitution and formation from p-hydroxycinnamyl alcohols, Science (80-.). 148 (1965) 595–600.

[56] C.H. Ludwig, B.J. Nist, J.L. McCarthy, Lignin. XII. 1 The High Resolution Nuclear Magnetic Resonance Spectroscopy of Protons in Compounds Related to Lignin, J. Am. Chem. Soc. 86 (1964) 1186–1196.

[57] H. Nimz, Beech lignin—proposal of a constitutional scheme, Angew. Chemie Int. Ed. 13 (1974) 313–321.

[58] J. Marton, Lignin structure and reactions, ACS Publications, 1966.

[59] J.L. McCarthy, A. Islam, Lignin chemistry, technology, and utilization: a brief history, in: ACS Publications, 2000.

[60] G. Brunow, Methods to reveal the structure of lignin, Biopolym. Online. (2005).

[61] J.H. Lora, W.G. Glasser, Recent industrial applications of lignin: a sustainable alternative to nonrenewable materials, J. Polym. Environ. 10 (2002) 39–48.

[62] H. Hatakeyama, T. Hatakeyama, Lignin structure, properties, and applications, in:

Biopolymers, Springer, 2009: pp. 1–63.

[63] C.L. Chen, S.Y. Lin, C.W. Dence, Methods in lignin chemistry, Springer-Verlag, Berlin Heidelb. (1992) 301–321.

[64] Luc Averous, Peter J. Halley, Biocomposites based on plasticized starch, Biofuels, Bioprod. Biorefining. 3 (2009) 329–343.

[65] A. Bismarck, S. Mishra, T. Lampke, Plant fibers as reinforcement for green composites, Nat. Fibers, Biopolym. Biocomposites. (2005) 37–97.

[66] M.J. John, S. Thomas, Biofibres and biocomposites, Carbohydr. Polym. 71 (2008) 343–364.

[67] W. Boerjan, J. Ralph, M. Baucher, Lignin biosynthesis, Annu. Rev. Plant Biol. 54 (2003) 519–546.

[68] E. Dorrestijn, L.J.J. Laarhoven, I.W.C.E. Arends, P. Mulder, The occurrence and reactivity of phenoxyl linkages in lignin and low rank coal, J. Anal. Appl. Pyrolysis. 54 (2000) 153–192.

[69] T. Hatakeyama, Y. Izuta, S. Hirose, H. Hatakeyama, Phase transitions of lignin-based polycaprolactones and their polyurethane derivatives, Polymer (Guildf). 43 (2002) 1177–1182.

[70] D.P. Koullas, E.G. Koukios, E. Avgerinos, A. Abaecherli, R. Gosselink, C. Vasile, R. Lehnen, B. Saake, J. Suren, Analytical methods for lignin characterization-Differential scanning calorimetry, Cellul. Chem. Technol. 40 (2006) 719–725.

[71] C.G. Boeriu, D. Bravo, R.J.A. Gosselink, J.E.G. van Dam, Characterisation of structure-dependent functional properties of lignin with infrared spectroscopy, Ind. Crops Prod. 20 (2004) 205–218.

[72] Y. Chen, S. Sarkanen, Macromolecular lignin replication: A mechanistic working hypothesis, Phytochem. Rev. 2 (2003) 235–255.

[73] J. Ralph, K. Lundquist, G. Brunow, F. Lu, H. Kim, P.F. Schatz, J.M. Marita, R.D. Hatfield, S.A. Ralph, J.H. Christensen, Lignins: natural polymers from oxidative coupling of 4-hydroxyphenyl-propanoids, Phytochem. Rev. 3 (2004) 29–60.

[74] K. Freudenberg, A.C. Neish, Constitution and biosynthesis of lignin., Const. Biosynth. Lignin. (1968).

[75] G. Henriksson, In Ljungberg textbook, Pulp Pap. Chem. Technol. Ek M, Gellerstedt G, Henriksson G Fibre Polym. Technol. KTH, Stock. (2007) 125–148.

[76] M. Nagy, Biofuels from lignin and novel biodiesel analysis. Georgia Institute of Technology, (2009).

[77] E. Sjostrom, Wood chemistry: fundamentals and applications, Elsevier, 2013.

[78] E. Windeisen, G. Wegener, Lignin as Building Unit for Polymers-10.15, (2012).

[79] J. Grāvitis, J. Ābolinš, R. Tupčiauskas, A. Vēveris, Lignin from steam-exploded wood as binder in wood composites, J. Environ. Eng. Landsc. Manag. 18 (2010) 75–84.

[80] W.O.S. Doherty, P. Mousavioun, C.M. Fellows, Value-adding to cellulosic ethanol: Lignin polymers, Ind. Crops Prod. 33 (2011) 259–276. doi:10.1016/j.indcrop.2010.10.022.

[81] L. V Kanitskaya, A. V Rokhin, D.F. Kushnarev, G.A. Kalabin, Chemical structure of wheat dioxane lignin: 1H and 13C NMR study, Vysokomol. Soedin. 40 (1998) 800–805.

[82] A. Guerra, I. Filpponen, L.A. Lucia, D.S. Argyropoulos, Comparative evaluation of three lignin isolation protocols for various wood species, J. Agric. Food Chem. 54 (2006) 9696–9705.

[83] E.A. Capanema, M.Y. Balakshin, J.F. Kadla, A comprehensive approach for quantitative lignin characterization by NMR spectroscopy, J. Agric. Food Chem. 52 (2004) 1850–1860.

[84] J.-W. Choi, O. Faix, Characterization of Residual Lignins from Chemical Pulps of Spruce (Picea abies) and Beech (Fagus sylvatica) by $ KMnO_4 $ Oxidation, J. Korean Wood Sci. Technol. 31 (2003) 31–39.

[85] P.C. Pinto, D. V Evtuguin, C.P. Neto, Effect of structural features of wood biopolymers on hardwood pulping and bleaching performance, Ind. Eng. Chem. Res. 44 (2005) 9777–9784.

[86] R. Samuel, Y. Pu, B. Raman, A.J. Ragauskas, Structural characterization and comparison of switchgrass ball-milled lignin before and after dilute acid pretreatment, Appl. Biochem. Biotechnol. 162 (2010) 62–74.

[87] F. Lu, J. Ralph, DFRC method for lignin analysis. 1. New method for β-aryl ether cleavage: lignin model studies, J. Agric. Food Chem. 45 (1997) 4655–4660.

[88] K. Lundquist, K. Hedlund, ACID DEGRADATION OF LIGNIN. I. FORMATION OF KETONES OF GUAIACYLPROPANE SERIES, ACTA Chem. Scand. 21 (1967) 1750–+.

[89] K. Lundquist, T.K. Kirk, Acid Degradation of Lignin IV. Analysis of Lignin Acidolysis

Products by Gas Chromatography Using Trimethylsilyl Derivatives, Acta Chem. Scand. 25 (1971) 889–894.

[90] S. Li, O. Karlsson, K. Lundquist, R. Stomberg, Acid reactions of the lignin model 1, 2-bis (3, 4-dimethoxyphenyl)-1, 3-propanediol, Acta Chem. Scand. 51 (1997) 431–437.

[91] C. Lapierre, C. Rolando, B. Monties, Characterization of poplar lignins acidolysis products: capillary gas-liquid and liquid-liquid chromatography of monomeric compounds, Holzforschung-International J. Biol. Chem. Phys. Technol. Wood. 37 (1983) 189–198.

[92] C. Lapierre, B. Monties, C. Rolando, L. de Chirale, Thioacidolysis of lignin: comparison with acidolysis, J. Wood Chem. Technol. 5 (1985) 277–292.

[93] C. Rolando, B. Monties, C. Lapierre, Thioacidolysis, in: Methods Lignin Chem., Springer, 1992: pp. 334–349.

[94] T. Yokoyama, Y. Matsumoto, Revisiting the mechanism of β-O-4 bond cleavage during acidolysis of lignin. Part 1: Kinetics of the formation of enol ether from non-phenolic C6-C2 type model compounds, Holzforschung. 62 (2008) 164–168.

[95] C. Lapierre, C. Rolando, Thioacidolyses of pre-methylated lignin samples from pine compression and poplar woods, Holzforschung-International J. Biol. Chem. Phys. Technol. Wood. 42 (1988) 1–4.

[96] C. Lapierre, B. Pollet, B. Monties, C. Rolando, Thioacidolysis of spruce lignin: GC-MS analysis of the main dimers recovered after Raney nickel desulphuration, Holzforschung-International J. Biol. Chem. Phys. Technol. Wood. 45 (1991) 61–68.

[97] H. Önnerud, G. Gellerstedt, Inhomogeneities in the chemical structure of spruce lignin, Holzforschung. 57 (2003) 165–170.

[98] D. Fournand, I. Mila, C. Lapierre, Capillary zone electrophoresis of syringyl and guaiacyl monomers resulting from lignin thioacidolysis, Phytochem. Anal. 13 (2002) 338–342.

[99] H. Önnerud, Lignin structures in normal and compression wood. Evaluation by thioacidolysis using ethanethiol and methanethiol, Holzforschung. 57 (2003) 377–384.

[100] B. Leopold, Aromatic keto-and hydroxy-polyethers as lignin models. III, Acta Chem. Scand. 4 (1950) 1523–1537.

[101] B. Leopold, I.L. Malmstrom, Constitution of resin phenols and their biogenetic relations. 15. Nitrobenzene oxidation of compounds of the lignan type, Acta Chem. Scand. 5 (1951)

936–940.

[102] K. Freudenberg, A. Janson, E. Knopf, A. Haag, Zur kenntnis des lignins (15. mitteil.), Eur. J. Inorg. Chem. 69 (1936) 1415–1425.

[103] T.P. Schultz, M.C. Templeton, Proposed mechanism for the nitrobenzene oxidation of lignin, Holzforschung-International J. Biol. Chem. Phys. Technol. Wood. 40 (1986) 93–97.

[104] H.M. Chang, G.G. Allan, Lignins; Sarkaren, KW, Ludwig, CH, Eds, (1971).

[105] C.-L. Chen, Nitrobenzene and cupric oxide oxidations, in: Methods Lignin Chem., Springer, 1992: pp. 301–321.

[106] R. Katahira, F. Nakatsubo, Determination of nitrobenzene oxidation products by GC and 1 H-NMR spectroscopy using 5-iodovanillin as a new internal standard, J. Wood Sci. 47 (2001) 378–382.

[107] G.C. Galletti, R. Piccaglia, G. Chiavari, V. Concialini, HPLC/electrochemical detection of lignin phenolics from wheat straw by direct injection of nitrobenzene hydrolysates, J. Agric. Food Chem. 37 (1989) 985–987.

[108] K. Freudenberg, F. Sohns, W. Dürr, C.H.R. Niemann, Über Lignin, Coniferylalkohol und Saligenin, Cellulosechemie. 12 (1931) 263–275.

[109] M.N. Belgacem, A. Gandini, Monomers, polymers and composites from renewable resources, Elsevier, 2011.

[110] C.A.B. Cateto, Lignin-based polyurethanes: Synthesis, characterisation and applications, (2008).

[111] T. Javor, W. Buchberger, O. Faix, Capillary electrophoretic determination of lignin degradation products obtained by permanganate oxidation, Anal. Chim. Acta. 484 (2003) 181–187.

[112] J.C. Del Río, G. Marques, J. Rencoret, Á.T. Martínez, A. Gutiérrez, Occurrence of naturally acetylated lignin units, J. Agric. Food Chem. 55 (2007) 5461–5468.

[113] S. Tohmura, D.S. Argyropoulos, Determination of arylglycerol-β-aryl ethers and other linkages in lignins using DFRC/31P NMR, J. Agric. Food Chem. 49 (2001) 536–542.

[114] T. Ikeda, K. Holtman, J.F. Kadla, H. Chang, H. Jameel, Studies on the effect of ball milling on lignin structure using a modified DFRC method, J. Agric. Food Chem. 50 (2002) 129–135.

[115] D. FOURNAND, B. POLLET, C. LAPIERRE, Lignin evaluation by chemical degradative

methods: Relative performances of the DFEC and thioacidolysis techniques, in: Eur. Work. Lignocellul. Pulp, 2000: pp. 313–316.

[116] K.M. Holtman, H.-M. Chang, H. Jameel, J.F. Kadla, Elucidation of lignin structure through degradative methods: Comparison of modified DFRC and thioacidolysis, J. Agric. Food Chem. 51 (2003) 3535–3540.

[117] D.S. Argyropoulos, L. Zhang, Semiquantitative determination of quinonoid structures in isolated lignins by 31P nuclear magnetic resonance, J. Agric. Food Chem. 46 (1998) 4628–4634.

[118] S.Y. Lin, Ultraviolet spectrophotometry, in: Methods Lignin Chem., Springer, 1992: pp. 217–232.

[119] G.F. Zakis, Functional analysis of lignins and their derivatives, Tappi Press, 1994.

[120] A. Gartner, G. Gellerstedt, T. Tamminen, Determination of phenolic hydroxyl groups in residual lignin using a modified UV-method, Nord. Pulp Pap. Res. J. 14 (1999) 163–170.

[121] O. Goldschmid, Determination of phenolic hydroxyl content of lignin preparations by ultraviolet spectrophotometry, Anal. Chem. 26 (1954) 1421–1423.

[122] G. Aulin-Erdtman, R. Sanden, Spectrographic contributions to lignin chemistry, Acta Chem. Scan. 22 (1968) 1187–1209.

[123] E. Tiainen, T. Drakenberg, T. Tamminen, K. Kataja, A. Hase, Determination of phenolic hydroxyl groups in lignin by combined use of 1H NMR and UV spectroscopy, Holzforschung. 53 (1999) 529–533.

[124] A.S. Wexler, Characterization of lignosulfonates by ultraviolet spectrometry. Direct and difference spectrograms, Anal. Chem. 36 (1964) 213–221.

[125] T.A. Milne, H.L. Chum, F. Agblevor, D.K. Johnson, Standardized analytical methods, Biomass and Bioenergy. 2 (1992) 341–366.

[126] O. Faix, C. Grünwald, O. Beinhoff, Determination of phenolic hydroxyl group content of milled wood lignins (MWL's) from different botanical origins using selective aminolysis, FTIR, 1H-NMR, and UV spectroscopy, Holzforschung-International J. Biol. Chem. Phys. Technol. Wood. 46 (1992) 425–432.

[127] O. Faix, J.H. Böttcher, Determination of phenolic hydroxyl group contents in milled wood lignins by FTIR spectroscopy applying partial least-squares (PLS) and principal components regression (PCR), Holzforschung-International J. Biol. Chem. Phys. Technol. Wood. 47 (1993) 45–49.

[128] B. Hortling, T. Tamminen, E. Kenttä, Determination of carboxyl and non-conjugated carbonyl groups in dissolved and residual lignins by IR spectroscopy, Holzforschung-International J. Biol. Chem. Phys. Technol. Wood. 51 (1997) 405–410.

[129] M.A. Gilarranz, F. Rodríguez, M. Oliet, J. García, V. Alonso, Phenolic OH group estimation by FTIR and UV spectroscopy. Application to organosolv lignins, J. Wood Chem. Technol. 21 (2001) 387–395.

[130] D. Stewart, N. Yahiaoui, G.J. McDougall, K. Myton, C. Marque, A.M. Boudet, J. Haigh, Fourier-transform infrared and Raman spectroscopic evidence for the incorporation of cinnamaldehydes into the lignin of transgenic tobacco (Nicotiana tabacum L.) plants with reduced expression of cinnamyl alcohol dehydrogenase, Planta. 201 (1997) 311–318.

[131] J.C. del Río, A. Gutiérrez, I.M. Rodríguez, D. Ibarra, Á.T. Martínez, Composition of non-woody plant lignins and cinnamic acids by Py-GC/MS, Py/TMAH and FT-IR, J. Anal. Appl. Pyrolysis. 79 (2007) 39–46. doi:10.1016/j.jaap.2006.09.003.

[132] T.P. Schultz, W.G. Glasser, Quantitative structural analysis of lignin by diffuse reflectance Fourier transform infrared spectrometry, Holzforschung. 40 (1986) 37–44.

[133] J. Mao, K.M. Holtman, J.T. Scott, J.F. Kadla, K. Schmidt-Rohr, Differences between lignin in unprocessed wood, milled wood, mutant wood, and extracted lignin detected by 13C solid-state NMR, J. Agric. Food Chem. 54 (2006) 9677–9686.

[134] T. Liitiä, S.L. Maunu, J. Sipilä, B. Hortling, Application of solid-state 13C NMR spectroscopy and dipolar dephasing technique to determine the extent of condensation in technical lignins, Solid State Nucl. Magn. Reson. 21 (2002) 171–186.

[135] K. Lundquist, T. Olsson, NMR studies of lignins. 1. Signals due to protons in formyl groups, Acta Chem. Scand. B. 31 (1977) 788–792.

[136] K. Lundquist, NMR studies of lignins. 4. Investigation of spruce lignin by 1H NMR spectroscopy, Acta Chem. Scand. B. 34 (1980) 21–26.

[137] D.L. Kaplan, Introduction to biopolymers from renewable resources, in: Biopolym. from Renew. Resour., Springer, 1998: pp. 1–29.

[138] K. Lundquist, NMR studies of lignins. 5. Investigation of non-derivatized spruce and birch lignin by 1HNMR spectroscopy, Acta Chem. Scand. B. 35 (1981).

[139] W. Thielemans, R.P. Wool, Lignin esters for use in unsaturated thermosets: Lignin modification and solubility modeling, Biomacromolecules. 6 (2005) 1895–1905.

[140] D. Robert, 5.4 Carbon-13 nuclear magnetic resonance spectrometry, Methods Lignin Chem. (1992) 250–273.

[141] J. Baeza, J. Freer, Chemical characterization of wood and its components, Wood Cellul. Chem. 2 (2000) 275–384.

[142] C.-L. Chen, Characterization of milled wood lignins and dehydrogenative polymerisates from monolignols by carbon-13 NMR spectroscopy, in: ACS Publications, 1998.

[143] L.L. Landucci, Application of Modern Liquid-State NMR to Lignin Characterization. 2. 13C Signal Resolution and Useful Techniques, Holzforschung-International J. Biol. Chem. Phys. Technol. Wood. 45 (1991) 425–432.

[144] D.S. Argyropoulos, S.B. Menachem, Lignin, in: Biopolym. from Renew. Resour., Springer, 1998: pp. 292–322.

[145] D.R. Robert, G. Brunow, Quantitative estimation of hydroxyl groups in milled wood lignin from spruce and in a dehydrogenation polymer from coniferyl alcohol using 13C NMR spectroscopy, Holzforschung-International J. Biol. Chem. Phys. Technol. Wood. 38 (1984) 85–90.

[146] D.S. Argyropoulos, H.I. Bolker, C. Heitner, Y. Archipov, 31P NMR spectroscopy in wood chemistry part V. Qualitative analysis of lignin functional groups, J. Wood Chem. Technol. 13 (1993) 187–212.

[147] P. Malkavaara, R. Alen, E. Kolehmainen, Multivariate correlation between 13C and 31P NMR spectral data on dissolved lignin and the combustion properties of kraft black liquor, Magn. Reson. Chem. 37 (1999) 407–412.

[148] W. Hoareau, W.G. Trindade, B. Siegmund, A. Castellan, E. Frollini, Sugar cane bagasse and curaua lignins oxidized by chlorine dioxide and reacted with furfuryl alcohol: characterization and stability, Polym. Degrad. Stab. 86 (2004) 567–576.

[149] C. Crestini, D.S. Argyropoulos, Structural analysis of wheat straw lignin by quantitative 31P and 2D NMR spectroscopy. The occurrence of ester bonds and α-O-4 substructures, J. Agric. Food Chem. 45 (1997) 1212–1219.

[150] T.M. Liitiä, S.L. Maunu, B. Hortling, M. Toikka, I. Kilpeläinen, Analysis of technical lignins by two-and three-dimensional NMR spectroscopy, J. Agric. Food Chem. 51 (2003) 2136–2143.

[151] M.Y. Balakshin, E.A. Capanema, C.-L. Chen, H.S. Gracz, Elucidation of the structures of

residual and dissolved pine kraft lignins using an HMQC NMR technique, J. Agric. Food Chem. 51 (2003) 6116–6127.

[152] S. Heikkinen, M.M. Toikka, P.T. Karhunen, I.A. Kilpeläinen, Quantitative 2D HSQC (Q-HSQC) via suppression of J-dependence of polarization transfer in NMR spectroscopy: application to wood lignin, J. Am. Chem. Soc. 125 (2003) 4362–4367.

[153] W.G. Glasser, R.A. Northey, T.P. Schultz, Lignin: historical, biological, and materials perspectives, ACS Publications, 1999.

[154] T.Q. Hu, Chemical modification, properties, and usage of lignin, Springer, 2002.

[155] U.P. Agarwal, M. Balakshin, S. Braaten, E. Capanema, R.P. Chandra, H. Chang, Y. Chen, N. Cordeiro, A.R. Esteghlalia, D. Evtuguin, Characterization of lignocellulosic materials, Wiley-Blackwell, Oxford, 2008.

[156] G. Cazacu, M. Capraru, V.I. Popa, Advances concerning lignin utilization in new materials, in: Adv. Nat. Polym., Springer, 2013: pp. 255–312.

[157] F. Bertini, M. Canetti, A. Cacciamani, G. Elegir, M. Orlandi, L. Zoia, Effect of ligno-derivatives on thermal properties and degradation behavior of poly (3-hydroxybutyrate)-based biocomposites, Polym. Degrad. Stab. 97 (2012) 1979–1987.

[158] A. Pinkert, D.F. Goeke, K.N. Marsh, S. Pang, Extracting wood lignin without dissolving or degrading cellulose: investigations on the use of food additive-derived ionic liquids, Green Chem. 13 (2011) 3124–3136.

[159] Y. Uraki, Y. Sugiyama, K. Koda, S. Kubo, T. Kishimoto, J.F. Kadla, Thermal mobility of β-O-4-type artificial lignin, Biomacromolecules. 13 (2012) 867–872.

[160] Z.-W. He, J. Yang, Q.-F. Lu, Q. Lin, Effect of structure on the electrochemical performance of nitrogen-and oxygen-containing carbon micro/nanospheres prepared from lignin-based composites, ACS Sustain. Chem. Eng. 1 (2013) 334–340.

[161] G. Sivasankarapillai, A.G. McDonald, Synthesis and properties of lignin-highly branched poly (ester-amine) polymeric systems, Biomass and Bioenergy. 35 (2011) 919–931. doi:10.1016/j.biombioe.2010.11.002.

[162] J.D. Gargulak, S.E. Lebo, Commercial use of lignin-based materials, in: ACS Publications, 2000.

[163] D.A.I. Goring, Thermal softening of lignin, hemicellulose and cellulose, Pulp Pap. Mag. Canada. 64 (1963) T517–T527.

[164] G.M. Irvine, The glass transitions of lignin and hemicellulose and their measurement by differential thermal analysis, Tappi J. 67 (1984) 118–121.

[165] M.M. Nassar, G.D.M. MacKay, Mechanism of thermal decomposition of lignin, Wood Fiber Sci. 16 (2007) 441–453.

[166] A.R. Mahendran, G. Wuzella, N. Aust, U. Müller, A. Kandelbauer, Processing and characterization of natural fibre reinforced composites using lignin phenolic binder, Polym. Polym. Compos. 21 (2013) 199.

[167] A. Moubarik, N. Grimi, N. Boussetta, A. Pizzi, Isolation and characterization of lignin from Moroccan sugar cane bagasse: Production of lignin–phenol-formaldehyde wood adhesive, Ind. Crops Prod. 45 (2013) 296–302. doi:https://doi.org/10.1016/j.indcrop.2012.12.040.

[168] Y. Jin, X. Cheng, Z. Zheng, Preparation and characterization of phenol–formaldehyde adhesives modified with enzymatic hydrolysis lignin, Bioresour. Technol. 101 (2010) 2046–2048. doi:https://doi.org/10.1016/j.biortech.2009.09.085.

[169] G. Vázquez, G. Antorrena, J. González, S. Freire, The influence of pulping conditions on the structure of acetosolv eucalyptus lignins, J. Wood Chem. Technol. 17 (1997) 147–162.

[170] N. Mosier, C. Wyman, B. Dale, R. Elander, Y.Y. Lee, M. Holtzapple, M. Ladisch, Features of promising technologies for pretreatment of lignocellulosic biomass, Bioresour. Technol. 96 (2005) 673–686.

[171] G.A. Smook, Handbook for pulp & paper technologists, Tappi, 1992.

[172] K. Koljonen, M. Österberg, M. Kleen, A. Fuhrmann, P. Stenius, Precipitation of lignin and extractives on kraft pulp: effect on surface chemistry, surface morphology and paper strength, Cellulose. 11 (2004) 209–224.

[173] J. Marton, T. Marton, Molecular weight of kraft lignin, Tappi J. 47 (1964) 471–476.

[174] F. Monteil-Rivera, M. Phuong, M. Ye, A. Halasz, J. Hawari, Isolation and characterization of herbaceous lignins for applications in biomaterials, Ind. Crops Prod. 41 (2013) 356–364. doi:10.1016/j.indcrop.2012.04.049.

[175] C.E. Courchene, The tried, the true, and the new-getting more pulp from chips modifications to the kraft process for increased yield, (1998).

[176] O. Kordsachia, R. Patt, H. Sixta, Cellulose isolation from different raw materials, Papier. 53 (1999) 96–108.

[177] M. Baucher, C. Halpin, M. Petit-Conil, W. Boerjan, Lignin: genetic engineering and impact on pulping, Crit. Rev. Biochem. Mol. Biol. 38 (2003) 305–350.

[178] A. Sakakibara, H. Takeyama, N. Morohoshi, Untersuchungen über die Hydrolyse von Lignin mit Dioxan und Wasser. IV. Versuch mit methyliertem Lignin und einigen Modellsubstanzen., Holzforschung-International J. Biol. Chem. Phys. Technol. Wood. 20 (1966) 45–47.

[179] B. Saake, R. Lehnen, Lignin, Ullmann's Encycl. Ind. Chem. (2007).

[180] S. Kumar, A.K. Mohanty, L. Erickson, M. Misra, Lignin and its applications with polymers, J. Biobased Mater. Bioenergy. 3 (2009) 1–24.

[181] M. Galbe, G. Zacchi, Pretreatment of lignocellulosic materials for efficient bioethanol production, in: Biofuels, Springer, 2007: pp. 41–65.

[182] X. Pan, N. Gilkes, J. Kadla, K. Pye, S. Saka, D. Gregg, K. Ehara, D. Xie, D. Lam, J. Saddler, Bioconversion of hybrid poplar to ethanol and co-products using an organosolv fractionation process: Optimization of process yields, Biotechnol. Bioeng. 94 (2006) 851–861.

[183] P. Sannigrahi, A.J. Ragauskas, G.A. Tuskan, Poplar as a feedstock for biofuels: a review of compositional characteristics, Biofuels, Bioprod. Biorefining. 4 (2010) 209–226.

[184] X. Pan, D. Xie, K.-Y. Kang, S.-L. Yoon, J.N. Saddler, Effect of organosolv ethanol pretreatment variables on physical characteristics of hybrid poplar substrates, Appl. Biochem. Biotechnol. 137 (2007) 367–377.

[185] A.P. Klein, E.S. Beach, J.W. Emerson, J.B. Zimmerman, Accelerated solvent extraction of lignin from Aleurites moluccana (Candlenut) nutshells., J. Agric. Food Chem. 58 (2010) 10045–8. doi:10.1021/jf1019856.

[186] Q. Lu, W. Liu, L. Yang, Y. Zu, B. Zu, M. Zhu, Y. Zhang, X. Zhang, R. Zhang, Z. Sun, J. Huang, X. Zhang, W. Li, Investigation of the effects of different organosolv pulping methods on antioxidant capacity and extraction efficiency of lignin, Food Chem. 131 (2012) 313–317. doi:10.1016/j.foodchem.2011.07.116.

[187] J. Quesada-Medina, F.J. López-Cremades, P. Olivares-Carrillo, Organosolv extraction of lignin from hydrolyzed almond shells and application of the δ-value theory, Bioresour. Technol. 101 (2010) 8252–8260. doi:10.1016/j.biortech.2010.06.011.

[188] D. Pasquini, M.T.B. Pimenta, L.H. Ferreira, A.A. da S. Curvelo, Extraction of lignin from

sugar cane bagasse and Pinus taeda wood chips using ethanol–water mixtures and carbon dioxide at high pressures, J. Supercrit. Fluids. 36 (2005) 31–39. doi:10.1016/j.supflu.2005.03.004.

[189] M.N.M. Ibrahim, S.B. Chuah, P. Pinang, Characterization of Lignin Precipitated From the Soda Black Liquor of Oil Palm Empty Fruit Bunch Fibers By Various Mineral Acids, ASEAN J. Sci. Technol. Dev. 21 (2004) 57–67.

[190] H. Nadji, P.N. Diouf, a. Benaboura, Y. Bedard, B. Riedl, T. Stevanovic, Comparative study of lignins isolated from Alfa grass (Stipa tenacissima L.), Bioresour. Technol. 100 (2009) 3585–3592. doi:10.1016/j.biortech.2009.01.074.

[191] P. Mousavioun, W.O.S. Doherty, Chemical and thermal properties of fractionated bagasse soda lignin, Ind. Crops Prod. 31 (2010) 52–58.

[192] Z. Li, Y. Ge, Antioxidant activities of lignin extracted from sugarcane bagasse via different chemical procedures, Int. J. Biol. Macromol. 51 (2012) 1116–1120. doi:10.1016/j.ijbiomac.2012.09.004.

[193] E.A.B. da Silva, M. Zabkova, J.D. Araújo, C.A. Cateto, M.F. Barreiro, M.N. Belgacem, A.E. Rodrigues, An integrated process to produce vanillin and lignin-based polyurethanes from Kraft lignin, Chem. Eng. Res. Des. 87 (2009) 1276–1292. doi:10.1016/j.cherd.2009.05.008.

[194] W.G. Glasser, W. De Oliveira, S.S. Kelley, L.S. Nieh, Method of producing star-like polymers from lignin, (1991).

[195] H. Yoshida, R. Mörck, K.P. Kringstad, H. Hatakeyama, Kraft lignin in polyurethanes I. Mechanical properties of polyurethanes from a kraft lignin–polyether triol–polymeric MDI system, J. Appl. Polym. Sci. 34 (1987) 1187–1198.

[196] H. Yoshida, R. Mörck, K.P. Kringstad, H. Hatakeyama, Kraft lignin in polyurethanes. II. Effects of the molecular weight of kraft lignin on the properties of polyurethanes from a kraft lignin–polyether triol–polymeric MDI system, J. Appl. Polym. Sci. 40 (1990) 1819–1832.

[197] X. Luo, A. Mohanty, M. Misra, Lignin as a reactive reinforcing filler for water-blown rigid biofoam composites from soy oil-based polyurethane, Ind. Crops Prod. 47 (2013) 13–19. doi:10.1016/j.indcrop.2013.01.040.

[198] H. Hatakeyama, N. Kato, T. Nanbo, T. Hatakeyama, Water absorbent polyurethane composites derived from molasses and lignin filled with microcrystalline cellulose, J. Mater. Sci. 47 (2012) 7254–7261.

[199] T. Hatakeyama, Y. Asano, H. Hatakeyama, Mechanical and thermal properties of rigid polyurethane foams derived from sodium lignosulfonate mixed with diethylene-, triethylene-and polyethylene glycols, in: Macromol. Symp., Wiley Online Library, 2003: pp. 171–180.

[200] V.P. Saraf, W.G. Glasser, G.L. Wilkes, J.E. McGrath, Engineering plastics from lignin. VI. Structure–property relationships of PEG-containing polyurethane networks, J. Appl. Polym. Sci. 30 (1985) 2207–2224.

[201] C. Ciobanu, M. Ungureanu, L. Ignat, D. Ungureanu, V.I. Popa, Properties of lignin–polyurethane films prepared by casting method, Ind. Crops Prod. 20 (2004) 231–241.

[202] O.S.H. Santos, M. Coelho da Silva, V.R. Silva, W.N. Mussel, M.I. Yoshida, Polyurethane foam impregnated with lignin as a filler for the removal of crude oil from contaminated water, J. Hazard. Mater. 324 (2017) 406–413. doi:https://doi.org/10.1016/j.jhazmat.2016.11.004.

[203] S. Laurichesse, L. Avérous, Chemical modification of lignins: Towards biobased polymers, Prog. Polym. Sci. 39 (2014) 1266–1290. doi:10.1016/j.progpolymsci.2013.11.004.

[204] Y. Tu, P. Kiatsimkul, G. Suppes, F. Hsieh, Physical properties of water-blown rigid polyurethane foams from vegetable oil-based polyols, J. Appl. Polym. Sci. 105 (2007) 453–459.

[205] C.A. Cateto, M.F. Barreiro, A.E. Rodrigues, M.C. Brochier-Salon, W. Thielemans, M.N. Belgacem, Lignins as macromonomers for polyurethane synthesis: A comparative study on hydroxyl group determination, J. Appl. Polym. Sci. 109 (2008) 3008–3017.

[206] S. Fernandes, C.S.R. Freire, C.P. Neto, A. Gandini, The bulk oxypropylation of chitin and chitosan and the characterization of the ensuing polyols, Green Chem. 10 (2008) 93–97.

[207] P. Velazquez-Morales, J.-F. Le Nest, A. Gandini, Polymer electrolytes derived from chitosan/polyether networks, Electrochim. Acta. 43 (1998) 1275–1279.

[208] L.C. Wu, W.G. Glasser, Engineering plastics from lignin. I. Synthesis of hydroxypropyl lignin, J. Appl. Polym. Sci. 29 (1984) 1111–1123.

[209] H. Nadji, C. Bruzzese, M.N. Belgacem, A. Benaboura, A. Gandini, Oxypropylation of

lignins and preparation of rigid polyurethane foams from the ensuing polyols, Macromol. Mater. Eng. 290 (2005) 1009–1016.

[210] A. Gandini, M.N. Belgacem, Z.-X. Guo, S. Montanari, Lignins as macromonomers for polyesters and polyurethanes, in: Chem. Modif. Prop. Usage Lignin, Springer, 2002: pp. 57–80.

[211] M. Evtiouguina, A.M. Barros, J.J. Cruz-Pinto, C.P. Neto, N. Belgacem, C. Pavier, A. Gandini, The oxypropylation of cork residues: preliminary results, Bioresour. Technol. 73 (2000) 187–189.

[212] C. Pavier, A. Gandini, Oxypropylation of sugar beet pulp. 2. Separation of the grafted pulp from the propylene oxide homopolymer, Carbohydr. Polym. 42 (2000) 13–17.

[213] M. Ionescu, Chemistry and technology of polyols for polyurethanes, iSmithers Rapra Publishing, 2005.

[214] A. Gandini, Polymers from renewable resources: a challenge for the future of macromolecular materials, Macromolecules. 41 (2008) 9491–9504.

[215] A. Gandini, M.N. Belgacem, Lignins as components of macromolecular materials, Elsevier, Amsterdam, 2008.

[216] W.G. Glasser, L.C.-F. Wu, J.-F. Selin, Synthesis, structure, and some properties of hydroxypropyl lignins., (1983).

[217] W.G. Glasser, C.A. Barnett, T.G. Rials, V.P. Saraf, Engineering plastics from lignin II. Characterization of hydroxyalkyl lignin derivatives, J. Appl. Polym. Sci. 29 (1984) 1815–1830.

[218] L. Melvin, N. Albert, Process for producing polyoxyalkylene ether-polyols from lignin, (1970).

[219] T. Yamada, H. Ono, Rapid liquefaction of lignocellulosic waste by using ethylene carbonate, Bioresour. Technol. 70 (1999) 61–67.

[220] C.A. Cateto, M.F. Barreiro, A.E. Rodrigues, M.N. Belgacem, Optimization study of lignin oxypropylation in view of the preparation of polyurethane rigid foams, Ind. Eng. Chem. Res. 48 (2009) 2583–2589.

[221] B. Ahvazi, O. Wojciechowicz, T.-M. Ton-That, J. Hawari, Preparation of lignopolyols from wheat straw soda lignin, J. Agric. Food Chem. 59 (2011) 10505–10516.

[222] R. Briones, L. Serrano, R. Ben Younes, I. Mondragon, J. Labidi, Polyol production by chemical modification of date seeds, Ind. Crops Prod. 34 (2011) 1035–1040.

[223] H.B. Staley, D.J. David, Analytical chemistry of the polyurethanes., New York, Robert E. Krieger, 1979.

[224] J.H. Saunders, K.C. Frisch, Polyurethanes: chemistry and technology, (1962).

[225] K. Nakamae, T. Nishino, S. Asaoka, Microphase separation and surface properties of segmented polyurethane—Effect of hard segment content, Int. J. Adhes. Adhes. 16 (1996) 233–239.

[226] M.A. Hood, B. Wang, J.M. Sands, J.J. La Scala, F.L. Beyer, C.Y. Li, Morphology control of segmented polyurethanes by crystallization of hard and soft segments, Polymer (Guildf). 51 (2010) 2191–2198.

[227] M. Xu, W.J. MacKnight, C.H.Y. Chen, E.L. Thomas, Structure and morphology of segmented polyurethanes: 1. Influence of incompatability on hard-segment sequence length, Polymer (Guildf). 24 (1983) 1327–1332.

[228] S. Mondal, D. Martin, Hydrolytic degradation of segmented polyurethane copolymers for biomedical applications, Polym. Degrad. Stab. 97 (2012) 1553–1561.

[229] P.C. Caracciolo, A.A.A. De Queiroz, O.Z. Higa, F. Buffa, G.A. Abraham, Segmented poly (esterurethane urea) s from novel urea–diol chain extenders: Synthesis, characterization and in vitro biological properties, Acta Biomater. 4 (2008) 976–988.

[230] Y. Wang, C. Ruan, J. Sun, M. Zhang, Y. Wu, K. Peng, Degradation studies on segmented polyurethanes prepared with poly (D, L-lactic acid) diol, hexamethylene diisocyanate and different chain extenders, Polym. Degrad. Stab. 96 (2011) 1687–1694.

[231] C. Li, J. Liu, J. Li, F. Shen, Q. Huang, H. Xu, Studies of 4, 4′-diphenylmethane diisocyanate (MDI)/1, 4-butanediol (BDO) based TPUs by in situ and moving-window two-dimensional correlation infrared spectroscopy: understanding of multiple DSC endotherms from intermolecular interactions and motions leve, Polymer (Guildf). 53 (2012) 5423–5435.

[232] M.M. El-Molla, Synthesis of polyurethane acrylate oligomers as aqueous UV-curable binder for inks of ink jet in textile printing and pigment dyeing, Dye. Pigment. 74 (2007) 371–379.

[233] X. Kong, G. Liu, H. Qi, J.M. Curtis, Preparation and characterization of high-solid polyurethane coating systems based on vegetable oil derived polyols, Prog. Org. Coatings. 76 (2013) 1151–1160. doi:10.1016/j.porgcoat.2013.03.019.

[234] C.J. Patel, V. Mannari, Air-drying bio-based polyurethane dispersion from cardanol: Synthesis and characterization of coatings, Prog. Org. Coatings. 77 (2014) 997–1006.

[235] S.D. Rajput, D.G. Hundiwale, P.P. Mahulikar, V. V Gite, Fatty acids based transparent polyurethane films and coatings, Prog. Org. Coatings. 77 (2014) 1360–1368.

[236] B. Ates, S. Koytepe, M.G. Karaaslan, S. Balcioglu, S. Gulgen, Biodegradable non-aromatic adhesive polyurethanes based on disaccharides for medical applications, Int. J. Adhes. Adhes. 49 (2014) 90–96. doi:10.1016/j.ijadhadh.2013.12.012.

[237] D. Ren, C.E. Frazier, Wood/adhesive interactions and the phase morphology of moisture-cure polyurethane wood adhesives, Int. J. Adhes. Adhes. 34 (2012) 55–61.

[238] J.Y. Cherng, T.Y. Hou, M.F. Shih, H. Talsma, W.E. Hennink, Polyurethane-based drug delivery systems, Int. J. Pharm. 450 (2013) 145–162.

[239] A. Mishra, S.K. Singh, D. Dash, V.K. Aswal, B. Maiti, M. Misra, P. Maiti, Self-assembled aliphatic chain extended polyurethane nanobiohybrids: Emerging hemocompatible biomaterials for sustained drug delivery, Acta Biomater. 10 (2014) 2133–2146.

[240] B. Radeleff, L. Grenacher, P. Christoph, C.M. Sommer, U. Stampfl, S. Ramsauer, T. Henn, P. Kurz, R. Lopez-Benitez, I. Berger, Comparison of a Microporous Thermoplastic Polyurethane–covered Stent with a Self-expanding Bare Nitinol Stent in a Porcine Iliac Artery Model, J. Vasc. Interv. Radiol. 20 (2009) 927–935.

[241] A. Severini, S. Mantero, M.C. Tanzi, A. Cigada, M. Salvetti, G. Cozzi, A. Motta, Polyurethane-coated, self-expandable biliary stent: an experimental study, Acad. Radiol. 2 (1995) 1078–1081.

[242] D. Bichon, W. Borloz, A.L. Cassano-Zoppi, In vivo evaluation of a new polyurethane-coated catgut suture, Biomaterials. 5 (1984) 255–263.

[243] P. Slobodian, P. Riha, P. Sáha, A highly-deformable composite composed of an entangled network of electrically-conductive carbon-nanotubes embedded in elastic polyurethane, Carbon N. Y. 50 (2012) 3446–3453.

[244] G. Tetteh, A.S. Khan, R.M. Delaine-Smith, G.C. Reilly, I.U. Rehman, Electrospun polyurethane/hydroxyapatite bioactive Scaffolds for bone tissue engineering: The role of solvent and hydroxyapatite particles, J. Mech. Behav. Biomed. Mater. 39 (2014) 95–110.

[245] H. Xiao, J. Koleske, Polyurethane Coatings, Paint Coat. Test. Man. 15th Ed. Gardner-Sward Handb. (2012) 102–112.

[246] M. Okada, Chemical syntheses of biodegradable polymers, Prog. Polym. Sci. 27 (2002) 87–133.

[247] G.T. Howard, Biodegradation of polyurethane: a review, Int. Biodeterior. Biodegradation.

49 (2002) 245–252.

[248] R. Chandra, R. Rustgi, Biodegradable polymers, Prog. Polym. Sci. 23 (1998) 1273–1335.

[249] M. Pavlova, M. Draganova, Biocompatible and biodegradable polyurethane polymers, Biomaterials. 14 (1993) 1024–1029.

[250] H. Yeganeh, H. Jamshidi, S. Jamshidi, Synthesis and properties of novel biodegradable poly (ε-caprolactone)/poly (ethylene glycol)-based polyurethane elastomers, Polym. Int. 56 (2007) 41–49.

[251] K. Gorna, S. Gogolewski, Biodegradable polyurethanes for implants. II. In vitro degradation and calcification of materials from poly (ϵ-caprolactone)–poly (ethylene oxide) diols and various chain extenders, J. Biomed. Mater. Res. Part A. 60 (2002) 592–606.

[252] J. Guan, M.S. Sacks, E.J. Beckman, W.R. Wagner, Biodegradable poly (ether ester urethane) urea elastomers based on poly (ether ester) triblock copolymers and putrescine: synthesis, characterization and cytocompatibility, Biomaterials. 25 (2004) 85–96.

[253] J. Kylmä, J. V Seppälä, Synthesis and characterization of a biodegradable thermoplastic poly (ester− urethane) elastomer, Macromolecules. 30 (1997) 2876–2882.

[254] S.-I. Lee, S.-C. Yu, Y.-S. Lee, Degradable polyurethanes containing poly (butylene succinate) and poly (ethylene glycol), Polym. Degrad. Stab. 72 (2001) 81–87.

[255] J. Guan, M.S. Sacks, E.J. Beckman, W.R. Wagner, Synthesis, characterization, and cytocompatibility of elastomeric, biodegradable poly (ester-urethane) ureas based on poly (caprolactone) and putrescine, J. Biomed. Mater. Res. Part A. 61 (2002) 493–503.

[256] Y.W. Tang, R.S. Labow, I. Revenko, J.P. Santerre, Influence of surface morphology and chemistry on the enzyme catalyzed biodegradation of polycarbonate-urethanes, J. Biomater. Sci. Polym. Ed. 13 (2002) 463–483.

[257] I. Javni, D.P. Hong, Z.S. Petrović, Soy-based polyurethanes by nonisocyanate route, J. Appl. Polym. Sci. 108 (2008) 3867–3875.

[258] P.G. Parzuchowski, M. Jurczyk-Kowalska, J. Ryszkowska, G. Rokicki, Epoxy resin modified with soybean oil containing cyclic carbonate groups, J. Appl. Polym. Sci. 102 (2006) 2904–2914.

[259] B. Ochiai, S. Inoue, T. Endo, One-pot non-isocyanate synthesis of polyurethanes from bisepoxide, carbon dioxide, and diamine, J. Polym. Sci. Part A Polym. Chem. 43 (2005)

6613–6618.

[260] J. Sun, S. Fujita, M. Arai, Development in the green synthesis of cyclic carbonate from carbon dioxide using ionic liquids, J. Organomet. Chem. 690 (2005) 3490–3497.

[261] P. Król, Generalization of kinetics in the reaction of isocyanates and polyols for modeling a process-yielding linear polyurethane, 1, J. Appl. Polym. Sci. 57 (1995) 739–749.

[262] G. Woods, The ICI polyurethanes book, ICI Polyurethanes. Wiley, 1987.

[263] D.J. Sakhpara, Flexible breathable polyurethane coatings and films, and the prepolymers from which they are made, (1990).

[264] P. Monomers, Composites from Renewable Resources, ed. MN Belgacem and A. Gandini, (2008).

[265] H. Jeong, J. Park, S. Kim, J. Lee, N. Ahn, Compressive viscoelastic properties of softwood kraft lignin-based flexible polyurethane foams, Fibers Polym. 14 (2013) 1301–1310. doi:10.1007/s12221-013-1301-2.

[266] H. Wang, Y. Ni, M.S. Jahan, Z. Liu, T. Schafer, Stability of cross-linked acetic acid lignin-containing polyurethane, J. Therm. Anal. Calorim. 103 (2011) 293–302. doi:10.1007/s10973-010-1052-x.

[267] J.S. Amaral, M. Sepúlveda, C.A. Cateto, I.P. Fernandes, A.E. Rodrigues, M.N. Belgacem, M.F. Barreiro, Fungal degradation of lignin-based rigid polyurethane foams, Polym. Degrad. Stab. 97 (2012) 2069–2076. doi:10.1016/j.polymdegradstab.2012.03.037.

[268] X. Pan, J.N. Saddler, Effect of replacing polyol by organosolv and kraft lignin on the property and structure of rigid polyurethane foam., Biotechnol. Biofuels. 6 (2013) 12. doi:10.1186/1754-6834-6-12.

[269] Z. Peng, F. Chen, Synthesis and Properties of Lignin-Based Polyurethane Hydrogels, Int. J. Polym. Mater. 60 (2011) 674–683. doi:10.1080/00914037.2010.551353.

[270] H. Chung, N.R. Washburn, Improved lignin polyurethane properties with lewis acid treatment, ACS Appl. Mater. Interfaces. 4 (2012) 2840–2846. doi:10.1021/am300425x.

[271] C.A. Cateto, M.F. Barreiro, A.E. Rodrigues, M.N. Belgacem, Kinetic study of the formation of lignin-based polyurethanes in bulk, React. Funct. Polym. 71 (2011) 863–869. doi:10.1016/j.reactfunctpolym.2011.05.007.

[272] Y. Li, A.J. Ragauskas, Kraft Lignin-Based Rigid Polyurethane Foam, J. Wood Chem.

Technol. 32 (2012) 210–224. doi:10.1080/02773813.2011.652795.

[273] H. Hatakeyama, A. Hirogaki, H. Matsumura, T. Hatakeyama, Glass transition temperature of polyurethane foams derived from lignin by controlled reaction rate, J. Therm. Anal. Calorim. 114 (2013) 1075–1082. doi:10.1007/s10973-013-3132-1.

[274] W. Xing, H. Yuan, H. Yang, L. Song, Y. Hu, Functionalized lignin for halogen-free flame retardant rigid polyurethane foam: preparation, thermal stability, fire performance and mechanical properties, J. Polym. Res. 20 (2013) 234.

[275] K. Missoum, M.N. Belgacem, J. Bras, Nanofibrillated cellulose surface modification: a review, Materials (Basel). 6 (2013) 1745–1766.

[276] F.W. Herrick, R.L. Casebier, J.K. Hamilton, K.R. Sandberg, Microfibrillated cellulose: morphology and accessibility, in: J. Appl. Polym. Sci. Appl. Polym. Symp.;(United States), ITT Rayonier Inc., Shelton, WA, 1983.

[277] A.F. Turbak, F.W. Snyder, K.R. Sandberg, Microfibrillated cellulose, a new cellulose product: properties, uses, and commercial potential, in: J. Appl. Polym. Sci. Appl. Polym. Symp.;(United States), ITT Rayonier Inc., Shelton, WA, 1983.

[278] Y. Wang, H. Tian, L. Zhang, Role of starch nanocrystals and cellulose whiskers in synergistic reinforcement of waterborne polyurethane, Carbohydr. Polym. 80 (2010) 665–671.

[279] A. Pei, Q. Zhou, L.A. Berglund, Functionalized cellulose nanocrystals as biobased nucleation agents in poly (l-lactide)(PLLA)–Crystallization and mechanical property effects, Compos. Sci. Technol. 70 (2010) 815–821.

[280] X. Cao, Y. Habibi, L.A. Lucia, One-pot polymerization, surface grafting, and processing of waterborne polyurethane-cellulose nanocrystal nanocomposites, J. Mater. Chem. 19 (2009) 7137–7145.

[281] M. Hasani, E.D. Cranston, G. Westman, D.G. Gray, Cationic surface functionalization of cellulose nanocrystals, Soft Matter. 4 (2008) 2238–2244.

[282] X.M. Dong, T. Kimura, J.-F. Revol, D.G. Gray, Effects of ionic strength on the isotropic− chiral nematic phase transition of suspensions of cellulose crystallites, Langmuir. 12 (1996) 2076–2082.

[283] J. Araki, M. Wada, S. Kuga, T. Okano, Birefringent glassy phase of a cellulose microcrystal suspension, Langmuir. 16 (2000) 2413–2415.

[284] X.M. Dong, J.-F. Revol, D.G. Gray, Effect of microcrystallite preparation conditions on the formation of colloid crystals of cellulose, Cellulose. 5 (1998) 19–32.

[285] J.-F. Revol, L. Godbout, X.-M. Dong, D.G. Gray, H. Chanzy, G. Maret, Chiral nematic suspensions of cellulose crystallites; phase separation and magnetic field orientation, Liq. Cryst. 16 (1994) 127–134.

[286] L. Tang, C. Weder, Cellulose whisker/epoxy resin nanocomposites, ACS Appl. Mater. Interfaces. 2 (2010) 1073–1080.

[287] N.L.G. de Rodriguez, W. Thielemans, A. Dufresne, Sisal cellulose whiskers reinforced polyvinyl acetate nanocomposites, Cellulose. 13 (2006) 261–270.

[288] Y. Habibi, L. Foulon, V. Aguié-Béghin, M. Molinari, R. Douillard, Langmuir–Blodgett films of cellulose nanocrystals: Preparation and characterization, J. Colloid Interface Sci. 316 (2007) 388–397.

[289] Y. Habibi, A. Dufresne, Highly filled bionanocomposites from functionalized polysaccharide nanocrystals, Biomacromolecules. 9 (2008) 1974–1980.

[290] J.O. Zoppe, M.S. Peresin, Y. Habibi, R.A. Venditti, O.J. Rojas, Reinforcing poly (ε-caprolactone) nanofibers with cellulose nanocrystals, ACS Appl. Mater. Interfaces. 1 (2009) 1996–2004.

[291] W. Helbert, J.Y. Cavaille, A. Dufresne, Thermoplastic nanocomposites filled with wheat straw cellulose whiskers. Part I: processing and mechanical behavior, Polym. Compos. 17 (1996) 604–611.

[292] I. Siró, D. Plackett, Microfibrillated cellulose and new nanocomposite materials: a review, Cellulose. 17 (2010) 459–494.

[293] N. Duran, A.P. Lemes, M. Duran, J. Freer, J. Baeza, A minireview of cellulose nanocrystals and its potential integration as co-product in bioethanol production, J. Chil. Chem. Soc. 56 (2011) 672–677.